Annual Report 2012

HELMHOLTZ | ASSOCIATION

Helmholtz Institute Jena

Helmholtz Institute Jena
Fröbelstieg 3
07743 Jena
www.hi-jena.de

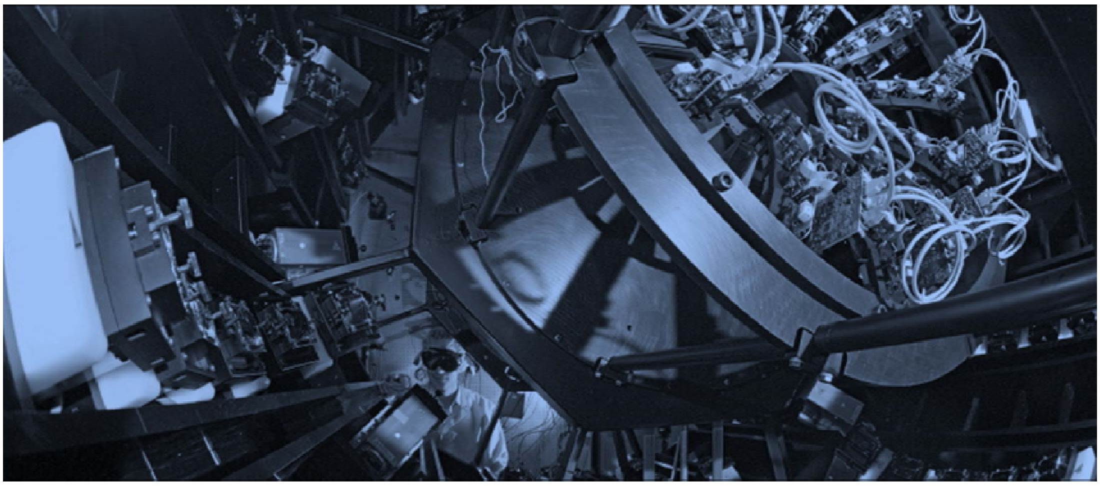

seit 1558

Helmholtz Institute Jena

Annual Report 2012

Contents

Laser particle acceleration

Photon and particle spectroscopy and diagnostics

Theory

Introduction

For the last three years, the Helmholtz Institute Jena (HI-Jena) located at the Campus of the Friedrich-Schiller University of Jena is well recognized for its competence in accelerator, laser and x-ray technology for the exploration of extreme states of matter. Emphasis is on fundamental and applied research at the interface of particle accelerators and lasers to exploit synergies with large discovery potential. For this purpose, the focus is placed on the development of high-power laser systems, x-ray spectroscopy and novel concepts for x-ray generation and particle acceleration. In addition, these experimental efforts are accompanied by theoretical investigations on strong-field quantum electrodynamics, correlated many-body dynamics as well as the physics of hot dense plasmas.

The Helmholtz Institute Jena also has established an important bridge between the Helmholtz Centers in Darmstadt, Dresden and Hamburg, for which it provides and transfers experience at the border between conventional particle-acceleration schemes and the rapidly evolving field of laser-induced particle acceleration. It benefits considerably from the strong involvement of the research groups at the Friedrich-Schiller University Jena working in the fields of high-power laser systems, x-ray spectroscopy techniques and on experiments in the realm of extreme electromagnetic fields. In particular, the HI Jena has been found very valuable for planning and developing research at the two large-scale accelerator projects for electrons and ions, the European XFEL and the International FAIR facilities.

The Scientific Report 2012 presented here demonstrates substantial progress along the various research lines of the institute. As examples we like to mention the work on existing high-power laser systems with peak outputs in the order of petawatts which has been continued successfully, including PHELIX at GSI Darmstadt and the POLARIS laser in Jena. Novel fiber laser systems with high MHz repetition rates will support the seeding of free-electron lasers in the future, such as FLASH at DESY. Today, concepts for the applications of such laser systems for future experiments at the heavy ion storage ring (HESR) of FAIR can be anticipated and are under preparation. Moreover, as a powerful additional tool for future research with heavy ions, an electron beam ion trap has been provided by the Stockholm University and will enable experiments with ions at highest charge states interacting with intense photon fields.

Apart from the progress in experimental research and developments, a further important milestone in the build-up phase of the institute has been achieved by the recruitment of Professor Stephan Fritzsche as head of the theory group. His activities will further strengthen the visibility of the theory on strong-field physics and, especially, on the dynamics of correlated quantum systems and strong-field induced states of matter - in close cooperation with theory groups at the FSU associated with the institute. To enhance the visibility of the theoretical research at the institute, a dedicated theory section has been added to the current Scientific Report.

The Research School for Advanced Photon Science (RS-APS) of the Helmholtz Institute was ceremonially opened on June 28th, 2012 to provide young researchers with a structured PhD program adapted to the scientific goals of the Helmholtz Institute Jena. In this school, PhD students receive a broadly-based, high-level education that is realized together with the partners of the RS-APS: Helmholtz Graduate School HIRe for FAIR (HGS-HIRe) as well as the partners on the campus of the University Jena, namely the Abbe School of Photonics, the Graduate Academy and DFG Training Group „Quantum and Gravitational Fields".

The education program for the next generation of scientists in strong-field physics supports also the final planning and preparation phase of the international research projects FAIR and XFEL and is, hence, ground-laying for further progress in this field.

High power laser development

POLARIS – the high-intensity fully diode pumped laser system commences experimental operation

M. Hornung[1], S. Keppler[2], R. Bödefeld[1], A. Kessler[1], H. Liebetrau[2], M. Hellwing[2], F. Schorcht[1], J. Körner[2], O. Jäckel[1], A. Sävert[2], J. Polz[2], A. K. Arunachalam[2], J. Hein[2], M.C. Kaluza[1,2].

[1] Helmholtz Institute Jena; [2] Institute of Optics and Quantum Electronics, Jena, Germany.

Over the last decade the POLARIS project has been aiming at the development of the required technology and the realization of a fully diode-pumped high-power femtosecond laser system well-suited for triggering laser matter interactions at high intensities. Here, we report on recently achieved improvements of the POLARIS performance parameters which have enabled us to conduct the first successful experimental campaigns with POLARIS in 2012.

At its current stage, the system generates pulses with 4 J pulse energy on target at a central wavelength of 1030 nm. These pulses have a FWHM pulse duration of 164 fs and a repetition rate of 1/40 Hz. POLARIS uses the principle of chirped-pulse amplification with currently five amplification stages (A1-A4 and A 2.5). All amplifiers are using Yb^{3+}-doped fluoride phosphate glass as the active material, which is pumped at 940 nm. Between the first and second amplifier a grating stretcher increases the pulse duration to 2.5 ns. An ultra-fast Pockels cell with a rise time of T_{rise} = 200 ps located before the stretcher and two Pockels cells (with T_{rise} = 6 ns) after the second regenerative amplifier A2 have been installed to suppress amplified spontaneous emission (ASE) and short pre-pulses arriving on a ns-time scale, respectively. The subsequent multi-pass amplifiers A2.5, A3, and A4 increase the pulse energy to the multi-Joule level. After the last amplifier the pulses having peak energies of 6.5 J are recompressed to minimal pulse duration of 164 fs over the full beam profile [2]. Taking into account the compressor transmission of 63%, pulses delivering 4 J onto the target are routinely available for experiments. Pulses of the multi-10-J level will be available after the commissioning of the final amplification stage A5.

To reproducibly deliver laser pulses with POLARIS, which are suitable for high-intensity experiments, the performance of the laser system was optimized, especially regarding the overall laser stability, the temporal intensity contrast and the quality of the focal spot. The temporal intensity contrast was enhanced using a synchronization technique for the regenerative front-end amplifiers as well as a post-pulse suppression technique inside the amplifier chain. Due to the efficient suppression of post-pulses by avoiding transmissive optics in the laser chain as often as possible the nonlinear generation of pre-pulses was significantly reduced. This passive contrast enhancement techniques helped us to achieve a temporal intensity contrast of $<10^8$ at $t \leq -30$ ps before the main pulse. Measurements of the temporal intensity contrast of the fully amplified laser pulses are given in [2,3].

In order to improve the energy content and at the same time to reduce the size of the laser focal spot a closed-loop adaptive optics system has been implemented into the laser system in the end of 2011 [2]. For this purpose a 48-actuator adaptive mirror was installed behind the pulse compressor in combination with a wavefront-sensor. To quantify the quality of the focussed laser pulses the FWHM focal spot area (i.e. the area where the intensity is higher than 50% of the peak intensity) and the fraction of the total pulse energy included in this area (given by the q-factor) were measured with a high-dynamic CCD camera. With a f/3 focussing we currently achieve a focal spot size of 8.7 µm^2 (FWHM) with a q-factor of 0.43. Using this currently available parameters POLARIS is able to generate focused peak intensities in excess of $2x10^{20}$ W/cm^2. To our knowledge, this is the highest peak intensity reported so far which has been achieved with a fully diode-pumped solid-state laser system [1].

As a benchmark experiment for the laser performance the acceleration of protons from thin metal foils via the TNSA-mechanism has been studied. During this campaign more than 1500 high-energy laser shots were delivered onto targets of different materials (Cu, Al, Ag, Ta, Ti) and thicknesses (400 nm - 50 µm). A 2 µm thick tantalum foil leads to a cut-off energy of 17.7 MeV which was reached with 2.3 J pulse energy only [1]. During 2012, a total of more than 7000 high energy shots where delivered into the target area to be used for high-intensity laser matter interaction experiments.

In conclusion, we have significantly improved the performance parameters of the fully diode pumped POLARIS laser system. It now routinely delivers high-contrast, high-intensity laser pulses well suited for experimental applications.

References

[1] M. Hornung, S. Keppler, R. Bödefeld, A. Kessler, M. Hellwing, F. Schorcht, J. Hein, and M. C. Kaluza, “High intensity, high contrast laser pulses generated from the fully diode-pumped Yb:glass laser system POLARIS “ Optics Letters, Vol. 38, Issue 5, pp. 718-720 (2013)

[2] M. Hornung, R. Bödefeld, S. Keppler, A. Kessler, A. Sävert, M. Hellwing, F. Schorcht, J. Hein, M.C. Kaluza, “A closed-loop Adaptive Optics System for POLARIS”, GSI annual report, 2011.

[3] S. Keppler, M. Hornung, R. Bödefeld, A. Kessler, M. Hellwing, M. Kahle, F. Schorcht, J. Hein1 and M.C. Kaluza, “POLARIS contrast improvement by post-pulse suppression”, GSI annual report, 2011.

Current Status of the POLARIS Amplifier A5

A. Kessler[1], S. Keppler[2], M. Hornung[1], H. Liebetrau[1], F. Schorcht[1], M. Hellwing[2], J. Körner[1], J. Hein[1,2] and M. C. Kaluza[1,2]

[1]Helmholtz-Institut-Jena, [2]Friedrich-Schiller-Universität-Jena, Germany

The POLARIS project [1] has the goal to reach laser output energies of 100 J and pulse durations of 150 fs. For this reason the output energy of the POLARIS amplifier A4 (10J) has to be increased at least by a factor of 10. This will be achieved with an additional multipass amplifier named A5, as the last one in the chain. So far, the pump system and the fully motorized beam line have been installed. We have tested and optimized a Yb^{3+}-doped CaF_2 crystal as the amplification medium. Furthermore, A5 was integrated into the existing laser chain between A4 and the vacuum compressor.

Integration of A5 into POLARIS

The setup of A5 is described in more detail in [2]. Currently all nine passes of the multi-pass configuration have been installed. After the amplifier A4 the laser beam diameter is 20 mm (FWHM). To match the beam size to the diameter of the pump region in A5 (currently 35mm FWHM) and to fine tune the beam divergence a vacuum telescope has been installed between A4 and A5. The second vacuum telescope between A5 and the compressor (Fig. 1) further increases the beam diameter by a factor of 4 to be able to use the complete free aperture of the compressor (140 mm).

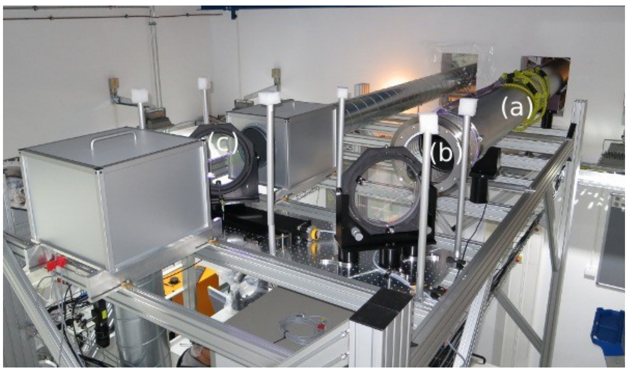

Figure 1: beamline at compressor entrance a) 250mm vacuum telescope tube from A5 b) 5m lens as vacuum window c) motorized mirror for switch between A4 and A5 beamline.

Homogenization of pump profile

To form a homogeneous, super-Gaussian distribution of the pump light, the spots from the 120 individually focused laser diode stacks have to be carefully arranged [2,3]. For this purpose we developed a new algorithm based on in [3] described camera setup. In a first step it generates a pump profile image distribution by summarizing all recorded single pump spots and calculates a gradient image by applying a Sobel operator. In a second step it creates a mask for a pump spot and calculates the average gradient for the masked region of the pump profile. Finally it moves each individual pump spot in the direction of the averaged gradient. This procedure is repeated for each individual pump spot. After moving the spots to

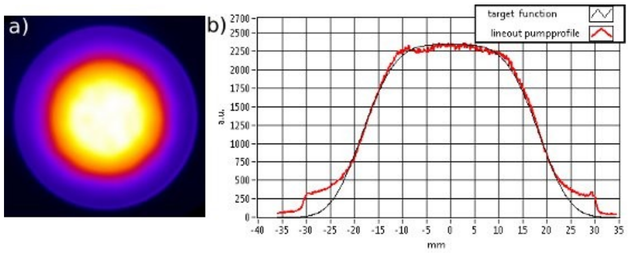

their projected positions the maximum relative intensity deviation from the target function inside its FWHM region is finally less than 4% (Fig.2)

Figure 2. a) A5 pump profile b) comparison of the horizontal lineout and the target function

Laser material and gain measurement

For the last amplifier of POLARIS, we use a 1.7 mol% Yb^{3+}-doped 30 mm thick CaF_2-crystal with a diameter of 65 mm. With nine passes in A5 we have achieved a gain

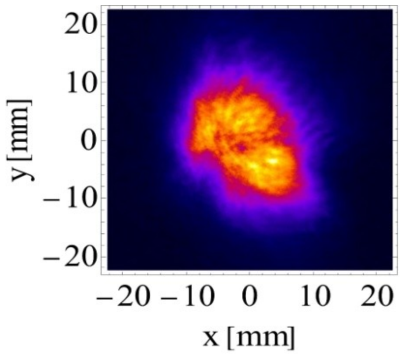

factor of eight in a first gain test using a low energy seed pulse (130mJ) from the amplifier A4. The preliminary beam profile is shown in Fig.3.

Figure 3: A5 output beam profile seeded with 130mJ

[1] M. Hornung *et al.,* Optics Letters **38,** 718 (2013).
[2] A. Kessler *et al.*, HI-Jena annual report 2011
[3] S. Keppler *et al.*, HI-Jena annual report 2011.

Amplifier development with cryogenically cooled $Yb:CaF_2$

J. Körner [1,2], J. Hein[1,2], D. Klöpfel [2], R. Seifert [1], M. C. Kaluza [1,2]

[1]Helmholtz-Institute Jena, Fröbelstieg 3, 07743 Jena

[2] Institute of Optics and Quantum Electronics, Max - Wien - Platz 1, 07743 Jena

Major limitations for the energy scaling of diode pumped high peak power laser systems are heat load within the active medium as well as cost and feasibility of the large scale diode pump engines. Recently, laser systems using Yb:YAG close to liquid nitrogen temperature have demonstrated [1] that the efficiency can be increased significantly in such regimes. The higher efficiency further reduces the thermal load and the complexity of the pump engines for unaltered output parameters.

This arises from the thermal population of the lower laser levels at room temperature in Yb^{3+} doped gain media, which results in a quasi three level operation. At cryogenic temperatures real four level operation is possible, the laser threshold is reduced, and the small signal gain is increased.

The disadvantage of Yb:YAG to realize a high peak power laser is the low bandwidth, which prohibits the direct amplification of ultra short pulses, like for instance in the POLARIS laser system. A promising laser material candidate to achieve direct amplification of femtosecond pulses within an CPA scheme is $Yb:CaF_2$, which maintains its band width also at 80 K [2].

We are developing a laser system producing femtosecond pulses within burst mode, as a test bed for future amplifiers based on cryogenically cooled $Yb:CaF_2$. In this operation mode a burst of pulses is amplified within one laser diode pump pulse. This allows a high extraction fluence together with a low risk for damaging optics.

Furthermore such kind of operation allows for the generation of high peak power pulses at a very high repetition rate, which would not be manageable in a classical operation scheme due to the generated heat load. Such lasers are interesting for a large number of applications such as experiments for laser particle interaction or combustion diagnostics. The technological development of these amplifiers also improves single pulse amplifiers as POLARIS.

The system under investigation consists of a frontend and two cryogenically cooled multi pass $Yb:CaF_2$ amplifiers. The frontend generates pulse trains of 1 ms duration at 10 Hz containing up to 1000 pulses, where each pulse is a 300 fs pulse subsequently stretched to 50 ps.

The mJ level bursts are then amplified to up to 500 mJ in total for a case of 1000 pulses per burst by the first amplifier S1. S1 can be operated from single shot to 10 Hz. As it is shown in figure 1 the single pulse energy can be increased up to 7.5 mJ by reducing the number of pulses per burst.

The final amplifier of the system is designed to deliver up to 5J per burst or 300 mJ single pulse energy within one burst. This corresponds to a peak power of 1TW for the compressed pulses. This amplifier stage is still under development. Nevertheless, energies as high as 2.5 J per burst have been achieved in first tests.

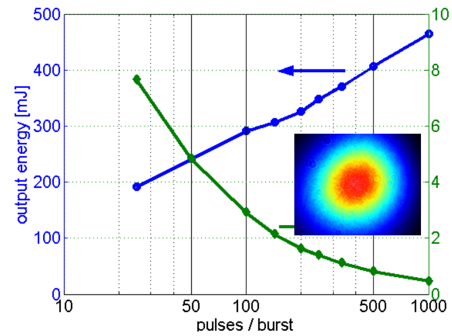

Figure 1: Performance of the first amplifier stage at full power operation (110A diode current for 1.8ms) as a function of the number of pulses within a 1ms seed burst. The inset shows the output beam profile

To get a constant energy for every pulse within the burst the current for the pump diodes is modulated during the pump time. This ensures a constant gain over the burst length as displayed in figure 2. For a burst of 1000 pulses in 1ms this method results in less than 5% pulse to pulse energy variation.

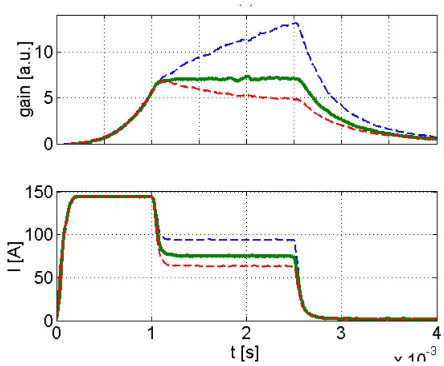

Figure 2: Time resolved gain of the amplifier measured with a cw seed for different step amplitudes of the diode current.

References

[1] S. Banerjee, K. Ertel, P. D. Mason, P. J. Phillips, M. Siebold, M. Loeser, C. Hernandez-Gomez, and J. L. Collier, "High-efficiency 10 J diode pumped cryogenic gas cooled Yb:YAG multislab amplifier," Opt. Lett. 37, 2175-2177 (2012).

[2] S. Ricaud, D. N. Papadopoulos, P. Camy, J. L. Doualan, R. Moncorge, A. Courjaud, E. Mottay, P. Georges, and F. Druon, "Highly efficient, high-power, broadly tunable, cryogenically cooled and diode-pumped $Yb:CaF_2$," Opt Lett 35, 3757-3759 (2010).

Cross section measurements for Yb^{3+}-doped gain media

J. Körner [1,2], J. Hein[1,2], D. Klöpfel [2], R. Seifert [1], M.C. Kaluza [1,2]

[1]Helmholtz Institute Jena, Fröbelstieg 3, 07743 Jena

[2] Institute of Optics and Quantum Electronics, Max - Wien - Platz 1, 07743 Jena

For the development and construction of large scale laser facilities accurate simulations are crucial in order to achieve the desired parameters. Since these simulations strongly depend on the parameters of the laser material, especially the cross sections and the lifetime, the exact knowledge of such parameters is fundamental to ensure correct results of the simulations.

Values found in the literature often vary considerably. In particular, this is the case for the temperature dependence of emission and absorption cross sections, where typically only very few data are available [1,2].

To overcome this lack we developed a setup for highly accurate measurement of cross sections and lifetime. The test samples can be mounted either in a heated mount or a cryostat, enabling us to determine the spectral characteristics of the material at temperatures between 77 K and more than 450 K.

The absorption cross sections are retrieved from the raw data by Lambert-Beer's law. For the emission cross section a combination of the McCumber (MC) relation and the Fuchtbauer Ladenburg (FL) equation is applied. Using these two methods allows to calculate the emission cross sections in two independent ways, where the MC – method has the higher confidence in high absorbing spectral regions, while the FL – method is more reliable in spectral regions with low re-absorption. The combination of both methods ensures an accurate calculation for the whole spectral region of interest and to cross check the validity of the assumptions made for both approaches.

Measurements where performed on several Yb^{3+} doped gain media, especially Yb:YAG, Yb:LuAG, $Yb:CaF_2$ and Yb:glasses. Exemplary results for Yb:YAG which were acquired in a high temperature campaign (between room temperature and 200°C) published in [3], are shown in figures 1 and 2. Measurements were performed in 20 K steps, though only steps of 60K are displayed for the sake of simplicity.

The results from this campaign made clear that even small changes in temperature can have a significant impact on the performance of a laser material. First tests with cross sections from our measurements in simulations have produced results close to real laser amplifier experiments, so that we are confident that the measured values are reliable.

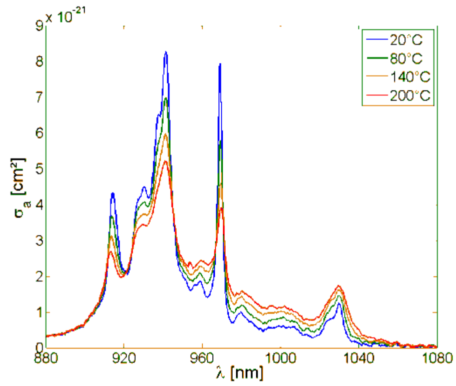

Figure 1: temperature dependent absorption cross sections for Yb:YAG.

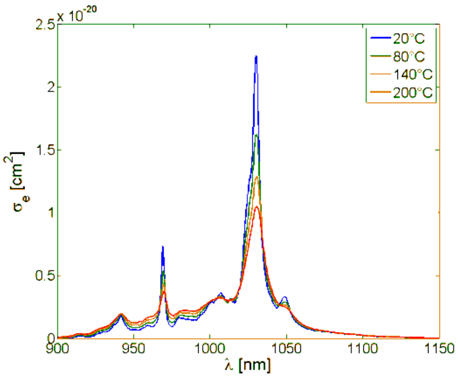

Figure 2: temperature dependent emission cross sections for Yb:YAG.

References

[1] J. Körner, J. Hein, M. Kahle, H. Liebetrau, M. Lenski, M. Kaluza, M. Loeser, and M. Siebold, "Temperature dependent measurement of absorption and emission cross sections for various Yb^{3+} doped laser materials," in (SPIE, 2011), 808003-808007.

[2] D. C. Brown, R. L. Cone, Y. C. Sun, and R. W. Equall, "Yb : YAG absorption at ambient and LF cryogenic temperatures," Ieee J Sel Top Quant 11, 604-612 (2005).

[3] J. Koerner, C. Vorholt, H. Liebetrau, M. Kahle, D. Kloepfel, R. Seifert, J. Hein, and M. C. Kaluza, "Measurement of temperature-dependent absorption and emission spectra of Yb:YAG, Yb:LuAG, and Yb:CaF2 between 20°C and 200°C and predictions on their influence on laser performance," J. Opt. Soc. Am. B 29, 2493-2502 (2012).

Joule-level amplifier development at POLARIS

S. Keppler[1], C. Wandt[2], M. Hornung[1,3], R. Bödefeld[1,3], A. Kessler[3], M. Hellwing[3], F. Schorcht[3], J. Hein[1,3] and M. C. Kaluza[1,3]

[1]Institute of Optics and Quantum Electronics, FSU Jena, Germany; [2]Max-Planck-Institute of Quantum Optics Garching, Germany, [3]Helmholtz-Institute Jena, Germany

The challenging requirements motivated by laser-plasma experiments carried out at POLARIS regarding its energy, pulse duration, focusability and, most important, temporal intensity contrast demand a further progress in the development of laser technology [1]. Moreover, the growing complexity of both the experimental setups and the measurement systems, require an improved stability and accuracy of the diagnostics for the laser pulses.

The principle of relay-imaging and state-of-the-art pump profile homogenization methods are very promising to improve the overall performance of the POLARIS system. Based on these techniques, we have developed a new Joule-level amplifier with a rotationally symmetrical arrangement of the several passes (cf. Fig. 1). The relay imaging of a plane at the amplifying medium to an end mirror was realized by employing curved folding mirrors. Since the successive isometric imaging requires focal spots between subsequent amplifier passes, the amplifier needs to be operated in vacuum. Astigmatism as a result of the slightly tilted curved mirrors is compensated by the innovative three dimensional folding arrangement. Since the tilt angle varies in steps of 30 degrees the astigmatism becomes a defocus with a value of 0.25 µm (PV), which can easily be compensated. For an improved efficiency and a sufficient total gain, the amplifier provides 10 glass passages. Additionally, the number of passes is doubled by using polarization rotation and a polarizing beam splitter. These 20 passes result in a total gain factor of 100 and a designed output energy of 1.5J.

A major part of the amplifier development is devoted to compensating thermal effects. A small fraction of the energy, introduced to the amplifying medium during the pumping, is transferred to heat. This leads to a lensing effect and a depolarization of the abaxial edge regions of the laser pulse. To be able to compensate for the thermal lens, the end mirror is equipped with a ring-shaped piston and a piezo actuator [2]. This allows for a well-controlled spherical deformation of the mirror, which compensates the thermal lens directly after every double-pass and leads to a flat wavefront as shown in Fig. 1. Furthermore, the depolarization is compensated by introducing a quarter waveplate placed close to the end-mirror and aligned with its fast (or slow) axis in the preferred polarization plane defined by the thin film polarizer in front of the amplifier [3]. Due to the orientation of the crystal axes, the on-axis portion of the laser beam that is not influenced by the birefringence experiences no change in polarization state during the transmission. However, the depolarized abaxial edge regions of the laser pulse experience a phase shift by passing the quarter waveplate that counteracts the thermally induced birefringence.

A key issue of the new Joule-level amplifier is the pump source. Here, two pump modules from LASTRONICS GmbH, each delivering a pump power of 19.2kW, provide the pump light at $\lambda_{\mathrm{Pump}} = 940$ nm in a 2.5ms long rectangular pulse. The beam profile of each module is homogenized by a microlens array to a rectangular flat-top profile which is imaged with a telescope into the amplifying medium. The good homogeneity and the high edge steepness ensure a smooth beam profile, cf. Fig1. The two pump modules were coupled into a single beam by rotating the polarization of one module and combining the two beams with a thin film polarizer.

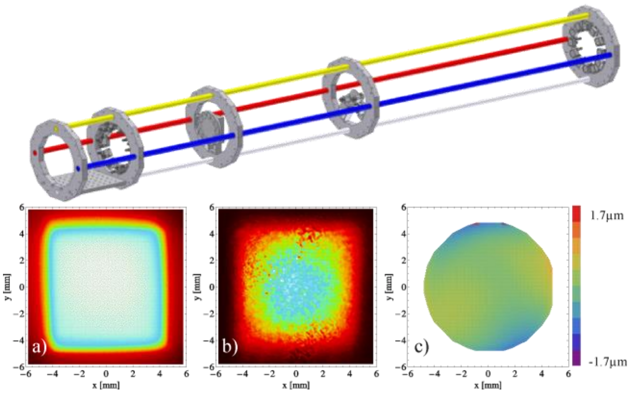

Figure 1: Schematic drawing of the new joule-level amplifier design (top chart) and current results: top-hat shaped pump profile (a) and beam profile (b) as well as the measured wavefront (c) of the amplified laser pulse.

First amplification tests conducted in air delivered very promising results. A total gain factor of 100 and an output energy of 150mJ were achieved in a top-hat shaped output beam profile as depicted in Fig 1. Operation in vacuum will finally provide an energy of 1.5J. The shot-to-shot energy stability was ±3% (RMS) which is equivalent to the energy stability of the seed pulse. Currently, a complete automization as well as a variable motorized intracavity spatial filtering unit for profile cleaning and contrast enhancements are under construction.

References

[1] M. Hornung, S. Keppler, R. Bödefeld, A. Kessler, H. Liebetrau, J. Körner, M. Hellwing, F. Schorcht, O. Jäckel, A. Sävert, J. Polz, A. K. Arunachalam, J. Hein and M. C. Kaluza, Opt. Lett. 38 (2013) 718.

[2] J. Schwarz, M. Ramsey, D. Headley, P. Rambo, I. Smith and J. Porter, Appl. Phys. B 82 (2006) 275.

[3] W. A. Clarkson, N. S. Felgate and D. C. Hann, Opt. Lett. 24, (1999) 820.

A compact temporal contrast-boosting module for the PHELIX laser

F. Wagner[1], C. P. João[2], J. Fils[3], T. Gottschall[4], J. Hein[5,6], J. Körner[5], J. Limpert[4,6], M. Roth[1], T. Stöhlker[3,6] and V. Bagnoud[3,6]

[1]Inst. für Kernphysik, TU Darmstadt, Germany; [2]GoLP, Instituto de Plasmas e Fusao Nuclear – Laboratorio Associado, Instituto Superior Técnico, Portugal; [3]GSI Helmholtzzentrum für Schwerionenforschung GmbH, Germany; [4]Inst. of Applied Physics, Friedrich Schiller University Jena, Germany; [5]Inst. for Optics and Quantum Electronics, Friedrich Schiller University Jena, Germany; [6]Helmholtz-Institute Jena, Germany;

Introduction

The temporal contrast has recently become a very critical parameter of high-power short-pulse laser systems. With intensities exceeding 10^{20} W/cm^2 the pedestal which is typically 6 to 8 orders below the maximum and ranges over a few ns can already ionize the target resulting in very uncontrollable experimental conditions. Morover for many lately proposed experiments such as new mechanisms for laser ion acceleration like BOA or RPA a high contrast is mandatory.

The pedestal originating from amplified spontaneous emission (ASE) in a chirped-pulse amplification system (CPA) can be decreased by increasing the seeding energy of the amplifiers. This can be accomplished with an ultrafast optical parametric amplifier (uOPA) [1]. The only source of noise in the OPA is parametric fluorescence that is confined to the pump pulse duration. Therefore we use a 1 ps pump-laser in our realization [2] to ensure a temporally clean signal-pulse up to 1 ps before the peak as required for many laser-plasma experiments.

Implementation of the contrast-boosting module at PHELIX

The uOPA has been developed for the PHELIX short-pulse laser system. It is located directly behind the short-pulse oscillator (see Fig. 1). Both pump as well as seeding pulse originate from the same oscillator. The uOPA pump-laser is a very compact home-build CPA system using a single chirped-volume Bragg grating for stretching and recompression of the pulses. Amplification is done in two stages with a fiber amplifier and a diode-pumped regenerative ring cavity [3]. Both amplifiers use Ytterbium-doped KGW as an active medium because its bandwidth is large enough to support pulses with sub-picosecond duration. The pump-pulse is overlapped with the signal in a BBO crystal dimensioned to provide amplification factors in excess of 10^5.

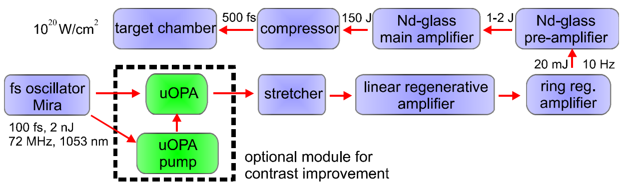

Figure 1: The contrast-boosting module at the PHELIX short-pulse system.

The amplified pulses are sent to the grating stretcher and the following two regenerative amplifiers of the PHELIX short-pulse frontend. Because of the higher seeding energy the gain in the regenerative amplifiers can be reduced to achieve the same energy output level of 20 mJ.

Contrast improvement

To measure the contrast improvement, the beam after the regenerative amplifier of the frontend was sent to a local compressor. The measurement was performed using a scanning high dynamic range third-order cross-correlator (Sequoia, Amplitude Technologies). In figure 2 the resulting contrast is shown for different gain levels in the uOPA. The measurement confirms that the ASE contrast in a CPA system linearly depends on the seeding energy. For a gain of $2*10^4$ the ASE-contrast reaches the detection limit of the cross-correlator which is 10 orders of magnitude below the maximum.

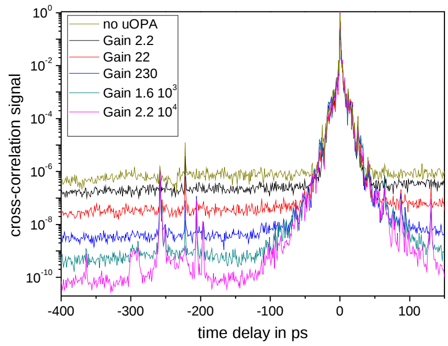

Figure 2: Contrast improvement for different gain levels in the uOPA

Conclusion and Outlook

The new developed module enables an ASE contrast better than 10 orders of magnitude paving the way for numerous new kinds of experiments at PHELIX. The remaining prepulses which are not addressed by the uOPA have been identified and will be removed within the next month.

Reference

[1] C. Dorrer et. al., “High-contrast optical-parametric amplifier as a front end of high-power laser systems,” Opt. Lett. **32** 2143–2145 (2007).

[2] F. Wagner et. al. , “A compact temporal contrast-boosting module for petawatt-class lasers, “ submitted to Optics Express.

[3] C. P. João, F. Wagner et. al, are preparing a manuscript to be called “10 mJ diode-pumped Yb:KYW regenerative amplifier for optical parametric amplifier pumping.”

High repetition rate Optical Parametric Chirped-Pulse Amplifier (OPCPA) system for FEL applications

M. Schulz[2,3], R. Riedel[1,3], A. Hage[3], M. Wiedorn[2,3], A.Willner[1,2], T. Gottschall[1,4], T. Eidaml[1,4], I. Grguraš[6], A. Simoncig[6], T. Dzelzainis[5], H. Höppner[6,7], S. Huber, B. Dromey[6,7], A. L. Cavalieri[6], J. Rothhardt[1,4], J. Limpert[1,4], A. Tünnermann[1,4], M. Zepf[1,5], M. J. Prandolini[1], F. Tavella[1]

[1]HI-Jena, Germany; [2]DESY, Hamburg, Germany; [3]University of Hamburg, Germany; [4]IAP Jena, Germany; [5]Queens University, Belfast, United Kingdom; [6]Max Planck Research Department for Structural Dynamics, University of Hamburg, CFEL, Hamburg, Germany; [7]Carl von Ossietzky University of Oldenburg, Oldenburg, Germany

An OPCPA system is developed for applications at the FLASH free-electron laser (FEL) in Hamburg. This amplifier is designed for a 10 Hz burst repetition rate of 0.1-1 MHz (FLASH repetition rate with an 800 ms long burst). The first application is FEL seeding. A replica of this amplifier will be used as a pump probe laser for FLASH-2. First experimental demonstration of a millijoule level burst mode three-stage OPCPA is demonstrated with the available pump amplifier system (500 W Innoslab) at a reduced repetition rate. Further scaling of the average burst power of the pump amplifier system has been demonstrated with both thin-disk and Innoslab amplifier technologies. The amplifier system and the FEL seed source are developed in a joint collaboration between Helmholtz-Institute Jena groups and the laser development group at DESY Hamburg.

OPCPA pump amplifier and results

As FLASH operates at a high repetition rate (100 kHz to 1 MHz in a burst operation mode), a high average power amplifier is needed. Most applications also require millijoule-level pulse energies. This is particularly demanding on the OPCPA pump amplifier system, which has to deliver pulses with about 20 mJ pulse energy at the above stated operation parameters. Two different types of booster amplifiers are under development. The first type is an Yb:YAG Innoslab amplifier and the second is an Yb:YAG thin-disk amplifier. The thin-disk amplifier has already been tested and operates at the required parameters. We have demonstrated the capabilities of amplification to 2.5 kW of average power during the 100 kHz burst [1]. Further performance scaling towards powers exceeding 10 kW is under investigation. Improvements are under investigation concerning the long term stability in terms of pointing, drift and temporal stability. Having addressed these points, the Innoslab amplifier technique is promising due to its very compact design. A 500 W Innoslab amplifier has been extensively tested as a pump amplifier for the OPCPA system. This Innoslab amplifier was operated at a repetition rate of 27.5 kHz, with output pulse energies of 18.3 mJ. With this amplifier, a three-stage non-collinear OPCPA system has been set up and tested. Frequency-doubled OPCPA pump pulses are used with a pulse duration of about 1 ps and a pulse energy of 7 mJ at a wavelength of 515 nm. The output energy of the OPCPA was 1.39 mJ, leading to conversion efficiency from the pump to the amplified pulses of 19.8%. The setup used for this experiment is shown in Figure 1. The amplified bandwidth of the OPCPA system supports compression of the pulses to the sub-7 fs regime.

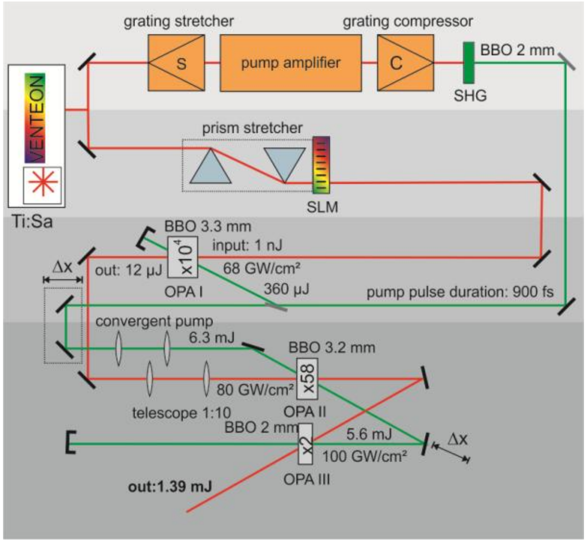

Figure 1: Schematic of the OPCPA system.

To increase the repetition rate of the amplifier output to the demanded 100 kHz, an Innoslab booster system with two additional amplification stages is under development. Output powers of 1.75 kW during the burst could be attained at 100 kHz repetition rate, corresponding to a pulse energy of 17.5 mJ.

OPCPA numerical simulations

A numerical code is being developed to study the critical OPCPA parameters, such as pulse energy, spectral phase and beam quality. Here the focus of the simulations is firstly, the optimisation and the efficient usage of the pump energy for a given spectral bandwidth, and secondly, to ensure sufficient spatial beam quality. In particular, for the generation of high harmonics for FEL seeding, the spatial beam quality not only in the near-field (just after the nonlinear crystal), but in the far-field (at focus) is high important. This model is based on the split-step method and accounts for dispersion and spatial walk-off effects. Furthermore, third-order nonlinear effects (self- and cross-phase modulation) are included, and for high energy OPCPA stages, there are three potentially damaging effects if third order effect become to large: (i) spatially distorted beam profiles resulting in larger M^2-values, (ii) frequency modulation, which may cause problems in re-compressing the signal, and (iii) the phase matching condition becomes time and position dependent. This final effect can reduce the bandwidth and energy of the signal. Additionally, the code can be used to simulate the effects of time jitter and drift.

In summary, it has been show that a three stage OPCPA system can achieve over 20% signal-to-pump with a spectral gain bandwidth that can support a Fourier-limited pulse of 6 fs and with minimal effect on the beam spatial quality. The spatial beam quality is largely dependent on the quality of the pump intensity within the nonlinear crystal and not on the spatial phase of the pump. It now becomes interesting to analyse what happens to various pulse parameters if the time delay (Δt – the time between the pump and signal pulse) is allowed to vary about the optimal value of zero. This variation can be caused by a time jitter from pulse to pulse or a slow drift. Figure 2 shows the dependence of pulse energy (red line) after the first stage on Δt. Clearly any time jitter or drift of the order of ±0.2 ps will reduce to energy output by ~40%. In contrast, the bandwidth (black squares) would appear to be relatively constant over a delay of ±0.2 ps. Therefore pulse energy is more sensitive to time jitter or drift compared to the spectral parameters that affect the pulse duration. These results are being prepared for publication.

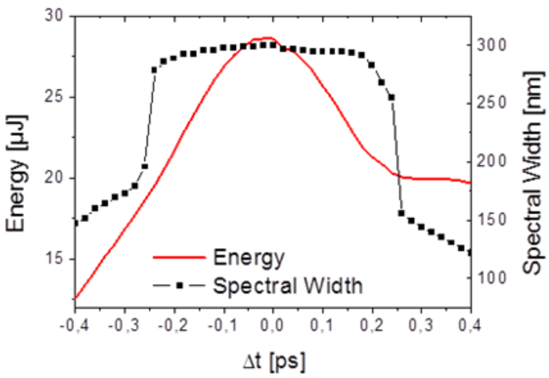

Figure 2: Effects of timing drift and jitter on parametric amplification for a signal pulse: (i) the dependence of output pulse energy of the first OPCPA stage on time delay Δt, where the time delay is between signal and pump pulses (red curve); (ii) the dependence of bandwidth of the first OPCPA stage on time delay Δt.

XUV seed source development

A dual-gas high-harmonic generation (HHG) method developed for FLASH-2 was further tested. The HHG conversion efficiency at wavelengths around 10 nm could be enhanced via quasi-phase-matching (QPM) [2]. The principle of this HHG method is the enhancement of the XUV signal using hydrogen jets for phase tuning between multiple QPM HHG sources. A versatile XUV spectrometer was specially designed for various applications. The HHG spatial beam properties were investigated using the SWORD-method. Theoretically, numerical simulations of dual-gas HHG indicate that the output in the cut-off spectral region can be selectively enhanced without disturbing the single-atom gating mechanism [2]. Figure 3(a) shows the harmonic yield from a single-jet source (black) compared to a dual-gas target. In this particular example, a Gaussian spectral region of 15 eV (FWHM) is filtered from the on-axis spectrum at ~160 eV. The Fourier transform of the filtered component could potentially yield an isolated attosecond pulse of 137 as (FWHM); thus achieving a selective enhancement of ~2.5 at ~160 eV when using the dual-gas target (Figure 3(b)). These results constitute a promising step towards more powerful table-top attosecond sources.

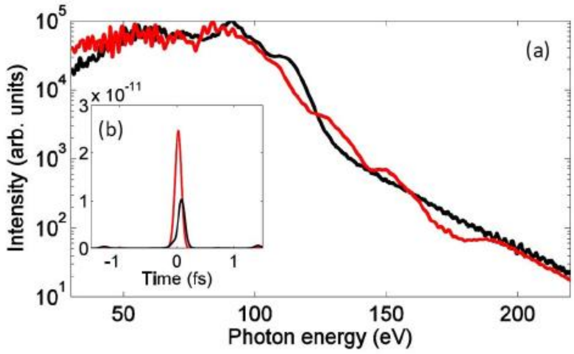

Figure 3: (a) Simulated angularly integrated spectra for single neon jet (black) and the dual-gas target (red). (b) Attosecond pulse revealed from the on-axis spectrum at 160 eV with a window of 15 eV (FWHM).

References

[1] M. Schulz *et al.* Pulsed operation of a high average power Yb:YAG thin-disk multipass amplifier. *Opt. Express* **20**: 5038-5043 (2012)

[2] A. Willner *et al.* Coherent spectral enhancement of carrier-envelope-phase stable continua with dual-gas high harmonic generation. *Opt. Letters* **37**: 3672-3674 (2012)

Dual-channel fiber amplifier for FEL seeding

T. Gottschall[1,2], T. Eidam[1,2], M. Schulz[3,4], R. Riedel[1,4], M. J. Prandolini[1], F. Tavella[1], J. Limpert[1,2], A. Tünnermann[1,2]

[1]Helmholtz Institute Jena, Germany; [2]Institute of Applied Physics, Friedrich-Schiller-Universität Jena, Germany; [3]DESY, Hamburg, Germany; [4]University of Hamburg

In cooperation with the laser development group at DESY in Hamburg a long-term stable light source is developed at the HIJ Jena capable of producing energetic few-cycle pulses. In the near future, it is planned to employ the output of such a system converted to the XUV spectral region for seeding a free-electron laser (FEL) and, therewith, to improve the spectral and spatial properties of its emitted radiation [1].

The generation of the required energetic few-cycle pulses bases on optical-parametric chirped pulse amplification (OPCPA [2]). The system (shown in Fig. 1 and Fig. 2) is designed for different modes of operation and possesses two input ports for different types of seed sources. Additionally, it consists of two amplification channels, the so-called burst amplifier and the white-light seeder, which are split behind a common pre-amplifier stage.

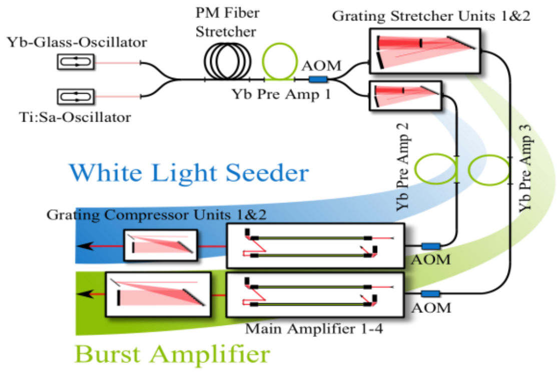

Figure 1: Schematic setup of the fiber amplifier system.

Titanium-sapphire seed source

In a first mode of operation, only the burst amplifier is employed. Therefore, the long-wavelength tail of a broadband few-cycle titanium-sapphire oscillator is launched into the system. By using two acousto-optic modulators the pulse repetition frequency is reduced and, additionally, trains of an arbitrary number of pulses (i.e. bursts) are formed in order to adapt the laser pulses to the electron bursts of the FEL. In this amplification channel an Offner-type stretcher with a large dielectric reflection grating is used to stretch the pulses to 4 ns pulse duration. In the following two amplification stages the pulses are amplified to energies of up to 50 µJ employing rod-type large-pitch fibers [3] and finally compressed to pulse durations <1 ps. Nevertheless, the large stretching in this channel basically allows for amplification and compression of much higher pulse energies in the multi-mJ range, which will be achieved in future experiments by including additional amplifiers based on thin-disk or Innoslab technology.

Finally, in the subsequent OPCPA stage, which will be developed at DESY, the laser pulses can be used as pump for the initial broadband oscillator pulses.

Ytterbium-glass seed source

In a second mode of operation pulses from an Ytterbium-based seed source with a central wavelength at 1030 nm can be launched into the system. Comparable to the previous case, these pulses are amplified in the burst-amplifier. Additionally, in the second channel, the white-light seeder), these pulses are amplified to a few microjoules of pulse energy and a compressed to a comparatively short duration of only <400 fs. This is achieved by employing a smaller foot print stretcher/compressor unit with a lower stretching ratio, but with a broader spectral bandwidth of 20 nm.

Furthermore, these re-compressed pulses are spectrally broadened exploiting white-light generation in an undoped YAG crystal and further compressed in time.

Contrary to the previous mode of operation, here this signal is sent together with pump pulses from the burst-amplifier in the OPCPA stage.

Figure 2: Picture of a) amplifier module, b) all-fiber pre-amp stage and c) 4 ns stretcher/compressor.

References

[1] L.-H. Yu et al., Science 11 2000: 289 (5481), 932.
[2] J. Rothhardt et al., Opt. Express 17, 24130 (2009)
[3] J. Limpert et al., Nature Light: Science & Applications (2012) 1, e8

A Megahertz Level Repetition Rate Source for Attoscience

Manuel Krebs[1,], Steffen Hädrich[1,2], Stefan Demmler[1], Jan Rothhardt[1,2], Amelle Zaïr[3], Luke Chipperfield[4], Jens Limpert[1,2], Andreas Tünnermann[1,2]*

[1]Helmholtz-Institute, Jena, Germany
[2]Friedrich-Schiller-Universität Jena, Institute of Applied Physics, Jena, Germany
[3]Imperial College, London, UK
[4]Max-Born Institute for Nonlinear Optics and Short Pulse Spectroscopy, Berlin, Germany

Recently, physics has experienced completely new opportunities due to the availability of light pulses of attosecond pulse durations. For the first time, these pulses enable experimental access to the motion of electrons in atoms and molecules. However, the generation of such hyper-fast events comes at the cost of low repetition rates in the kilohertz range, resulting in noisy signals and weak statistics, which hamper the further evolution of this exciting field. Based on our expertise on high repetition rate optical parametric amplification, we developed a megahertz level source of isolated attosecond pulses which is expected to significantly advance attosecond physics.

Experimental Setup

The pulses are generated using High Harmonic Generation (HHG) in a gas jet. A state-of-the-art fibre laser pumped optical parametric amplifier (OPA) [1] delivering 14 µJ pulses at up to 0.6 MHz repetition rate is used as driving laser system. To reach the shortest possible pulses, active spectral phase compensation is employed in order to control the occurrence of nonlinear phase during amplification in the OPA [2]. Therefore, pulse durations of only two optical cycles are achieved, which enable the usage of amplitude gating for the generation of isolated attosecond pulses. This technique requires excellent CEP stability. An active stabilisation of the pump laser timing is employed to improve the CEP stability of the system to below 100 mrad (RMS) [3]. An adjustable wedge pair allows for shifting the carrier envelope phase of the driver pulses, which are subsequently focused by an off-axis parabola onto an argon gas jet to an intensity of $4.0 \cdot 10^{14}$ W/cm².After filtering the fundamental radiation and low order harmonics by an aluminium and a zirconium foil of 200 nm thickness, the XUV radiation is characterized by a flat-field grating based XUV spectrometer.

Experimental Results

The XUV spectra have been measured for different CEPs. According to theory, the spectra show periodic behaviour with changing CEP (Fig. 1). For certain phases, the resulting spectra exhibit strong modulations, while for others, the radiation forms a spectral continuum. The latter case corresponds to the generation of isolated attosecond pulses.

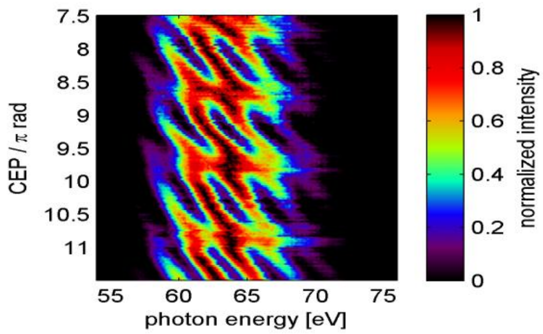

Figure 1: HHG spectra for different carrier envelope phases measured at 150 kHz. For certain values, a continuous spectrum is acquired, corresponding to an isolated attosecond pulse.

Simulation

A simulation based on solving the time-dependent Schrödinger equation and the Maxwell wave equation has been carried out. It excellently reproduces the measured CEP dependent spectra. This allows an estimation of the pulse parameters of the generated pulses. The simulated pulses have a duration of 314 as and exhibit a contrast ratio of 1:8 with respect to the neighbouring pulses.

Conclusion

A state-of-the-art optical parametric amplifier system delivering nearly transform-limited two-cycle pulses with excellent CEP stability of 86 mrad at repetition rates up to 0.6 MHz has been employed for isolated attosecond pulse generation. The production of a single isolated attosecond pulses with a duration of ~300 as is confirmed by excellent agreement with numerical simulations. The presented megahertz level repetition rate source for isolated attosecond pulses will enormously advance attoscience in future.

References

[1] J. Rothhardt, S. Demmler, S. Hädrich, J. Limpert, and A. Tünnermann, Optics Express, vol. 20, no. 10, pp. 10870–8, May 2012.
[2] S. Demmler, J. Rothhardt, S. Hädrich, J. Bromage, J. Limpert, and A. Tünnermann, Optics Letters, vol. 37, no. 19, p. 3933, Sept. 2012.
[3] S. Hädrich, J. Rothhardt, M. Krebs, S. Demmler, J. Limpert, and A. Tünnermann, Optics Letters, vol. 37, no. 23, p. 4910, Nov. 2012.

Thulium-doped large-pitch fibers: High potential for pulsed fiber sources at 2 µm

F, Stutzki[1], F. Jansen[1], C. Jauregui[1], J. Limpert[1,2] and A. Tünnermann[1,2]

[1] Institute of Applied Physics, Jena, Germany; [2] Helmholtz-Institute Jena, Germany;

Introduction

Ytterbium-doped fiber laser systems have been widely developed in recent years. Systems with more than 10 kW of output power in cw-operation and diffraction-limited beam quality are commercially available. Furthermore, ultra-short-pulse systems (with sub-ps pulse duration) have reached almost 1 kW of average power. These fiber-based chirped-pulse-amplification (CPA) systems at 1 µm are nowadays routinely operated at pulse peak powers exceeding 1 GW and average output powers of about 100 W.

These impressive results have been obtained with Ytterbium as active material (emission wavelength around 1 µm), while many applications (medical, biological, spectroscopic) and processes (e.g. high-harmonic generation) benefit from longer wavelengths around 2 µm. A very promising rare-earth ion for 2 µm lasers is Thulium [1]. Thulium-based cw-fiber laser systems have shown average output powers in excess of 1 kW. However, the performance of pulsed fiber lasers around 2 µm is limited by the development of fibers with larger mode-field areas, which can dramatically reduce parasitic nonlinear effects induced by high peak powers.

Large-pitch fibers

Fiber designs allowing for mode-field diameters beyond 50 µm are the key component for high-peak-power and high-energy pulsed fiber laser sources around 1 µm. The large-pitch fiber concept, developed in Jena with the support by HIJ since 2010, follows a new design principle: the delocalization of higher-order modes [2]. This concept ensures effective single-mode operation at very large mode areas (demonstrated beyond 100 µm) with high average powers in the 100 W regime.

In 2012 a Thulium-doped large-pitch fiber has been designed and tested in different laser configurations. A first proof-of-principle experiment has been performed in a cw-oscillator configuration. This large-pitch fiber allowed for a new record mode-field diameter of more than 60 µm at an average output power of 52 W [3].

Thulium-based Q-switched fiber laser

Based on these first experimental observations an actively Q-switched large-pitch-fiber oscillator has been developed. The schematic setup is shown in Fig. 1. This system employs a dual-pump scheme to homogenize and minimize the thermal load produced by the laser process. The resonator, formed by an HR mirror and the Fresnel reflection of the fiber end facet, is Q-switched by an acousto-optic modulator.

This configuration allows generating 2.4 mJ pulse energy at a repetition rate of 13.9 kHz, corresponding to an average output power of 33 W [4]. In combination with a measured pulse duration of 15 ns this leads to a new record power of more than 150 kW for a Q-switched Thulium-base fiber oscillator. The beam quality has been measured to be $M^2 < 1.3$ (Fig. 2).

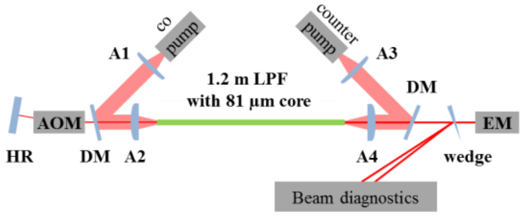

Fig. 1: Experimental setup of the Q-switched fiber laser

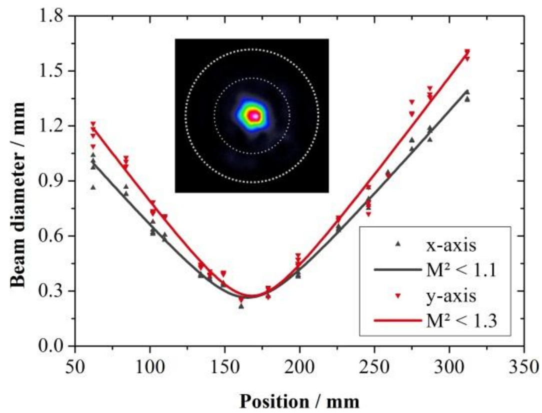

Fig. 2: Beam propagation factor M^2 measurement and near-field beam profile

In conclusion, these proof-of-principle experiments with Thulium-based large-pitch fibers have demonstrated the potential for ultra-short pulse amplification. Future iterations of the fiber will allow for mode-field areas beyond 100 µm and, therefore, enable GW-peak power fiber CPA systems.

References

[1] S. D. Jackson, Nature Photonics 6, 423-431 (2012)

[2] J. Limpert, F. Stutzki, F. Jansen, H.-J. Otto, T. Eidam, C. Jauregui, and A. Tünnermann, Light Sci. Appl. 1, e8 (2012)

[3] F. Jansen, F. Stutzki, C. Jauregui, J. Limpert, and A. Tünnermann, Opt. Lett. 37, 4546-4548 (2012)

[4] F. Stutzki, F. Jansen, C. Jauregui, J. Limpert, and A. Tünnermann, Opt. Lett. 38, 97-99 (2013)

Enhancing the peak and average power of fiber laser systems via coherent combination and shorter pulse durations

A. Klenke, T. Eidam, J. Limpert, A. Tünnermann

[1]Helmholtz Institute Jena, Germany; [2]Institute of Applied Physics, Friedrich-Schiller-University Jena, Germany

In the last decade, a lot of progress has been made in developing technologies to amplify high energy/high peak-power ultrashort pulses at high repetition rates and, consequently, to high average powers. However, independently from the laser architecture, there are issues such as thermal effects, nonlinearities or damage threshold that limit the maximum achievable performance. Therefore, coherent combination of amplifiers is an interesting concept to overcome these limitations.

Coherent combination

In earlier experiments we could already demonstrate that with two coherently combined Ytterbium-doped rod-type fibers in a state-of-the-art chirped-pulse amplification (CPA) system it is possible to generate compressed pulse energies of up to 3 mJ [1] at high repetition rates. Thus, the pulse energy and peak-power is larger than what has so far been shown with a single fiber-amplifier system. Now, we have scaled up this approach in a new CPA system with four combined amplifiers (Fig. 1). We employ the large-pitch-fiber (LPF) technology developed in our group, which provides superior mode stability especially at high average powers. The fibers are arranged in a cascaded splitting/combination configuration. The stabilization of the path lengths in the amplifiers is realized by measuring the phase errors with Hänsch-Couillaud (HC) detectors and by using piezo-based delay lines. With this system, we were able to show an average power of 532 W at 400 kHz [2]. This corresponds to a pulse energy of 1.3 mJ at a pulse duration of 670 fs. The efficiency of the combination was estimated to be 93%, therefore confirming previous theoretical investigations [3] about the combination efficiency with increasing number of channels. Additionally, the system provides an excellent beam quality of M^2 smaller than 1.2x1.1. To our knowledge, this is the Gigawatt peak-power laser with the highest average power worldwide.

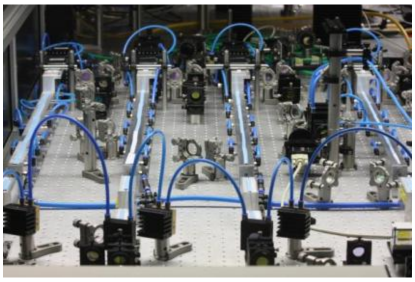

Figure 1: Four coherently combined fs fiber amplifiers.

High bandwidth stretcher and compressor design

Another approach to increase the peak-power of a femtosecond laser system is to shorten the pulse durations while keeping the pulse energy constant. We have developed and are currently working on integrating a new stretcher (Fig. 2) and compressor design into the new CPA system mentioned above. This supports a larger spectral bandwidth and, therefore, shorter compressed pulse durations. Additionally, a spectral-amplitude shaper has been included into the laser. With this system, we could already demonstrate an increase of the peak power by a factor of two compared to the previous design with pulse durations below 300 fs.

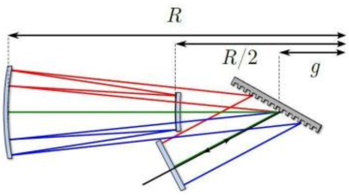

Figure 2: Schematic setup of an Offner-type stretcher.

The next step will be to use this CPA system as a driving laser for high-harmonics generation and optical parametric chirped-pulse amplification. The peak power can be further scaled by expanding the coherent-combination technique from spatial domain (parallel amplification) into time domain (serial amplification). This architecture will also be investigated as the basis for the ICAN project, e.g. for laser driven particle acceleration.

References

[1] A. Klenke, E. Seise, S. Demmler, J. Rothhardt, S. Breitkopf, J. Limpert, and A. Tünnermann, "Coherently-combined two channel femtosecond fiber CPA system producing 3 mJ pulse energy," Opt. Express **19**, 24280-24285 (2011).

[2] A. Klenke, S. Breitkopf, M. Kienel, T. Gottschall, T. Eidam, S. Hädrich, J. Rothhardt, J. Limpert, and A. Tünnermann, "532W, 1.3mJ, 4-channel coherently combined femtosecond fiber CPA system," submitted to Optics Letters.

[3] A. Klenke, E. Seise, J. Limpert, and A. Tünnermann, "Basic considerations on coherent combining of ultrashort laser pulses," Opt. Express **19**, 25379-25387 (2011).

Laser particle acceleration

Ultra-thin foils for laser ion acceleration in the radiation-pressure regime

B. Aurand[1,2], L.-O. Heim[3], B. Elkin[4], B. Lommel[1], B. Kindler[1], O. Jäckel[2,5], S. Kuschel[2,5], C. Rödel[2,5] and T. Kuehl[1,2,6]

[1] GSI , Darmstadt, Germany; [2] Helmholtz Institute Jena, Jena, Germany; [3] Center for Smart Interfaces, Darmstadt, Germany; [4] Fraunhofer Institute for Interfacial Engineering and Biotechnology, Stuttgart, Germany; [5] Institute for Optic and Quantum Electronics, Jena, Germany; [6] Johannes Gutenberg University, Mainz, Germany;

Introduction

Recent developments by our and other groups on the mechanism of radiation-pressure driven acceleration of protons and heavy ions [1,2,3,4] emphasizes the strong dependence of the results on a very high laser contrast of $> 10^9$, as well as the development of suitable targets. Since a few years diamond-like-carbon (DLC) foils are an appropriate choice. The drawback is the low mechanical stability for foils having a thickness of just a few. We developed an alternative process using a polymer based film which is produced by vapor deposition. Test of the surface roughness as well as the mechanical stability show great advantage for this kind of material compared to normal DLC foil.

Setup

We use parylene, an industrial coating material which is hydrophobic and optical transparent [5]. Starting from a glass substrate which is wiped with a hydrophilic barrier layer (detergent) the polymer is attached by pyrolytic chemical vapor deposition (p-CVD) forming a homogeneous layer on all surfaces within the deposition chamber, see fig, 1

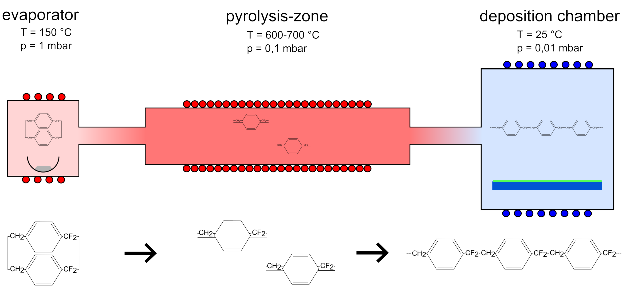

Fig.1 : Process of pyrolytic chemical vapour deposition (p-CVD) of parylene onto the glass substrates.

After deposition the glass substrate is removed and stored in inert gas, allowing storage times of more than one year before mounting as a target.

The foil can be flooded of the substrate by slowly casting in a bath of water and being attached to a target mount by adhesion, afterwards. For laser-acceleration experiments we used in previous experiments a 15nm thick foil attached on a special target mount (fig. 2a) creating more than 400 targets which can be used without opening the chamber in between shots. It was also possible to attach the foils self-supporting on very large apertures, up to 20mm, see fig. 2b

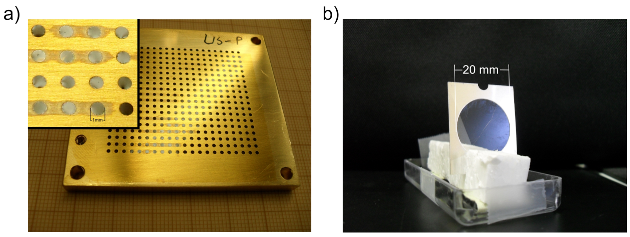

Fig.2 : a) Parylene foil attached to target mount used for laser-acceleration experiments. B) Self-supporting 15 nm foil freestanding on 20 mm aperture.

Characterization

For a proper characterization we measured the thickness of each processed foil by ellipsometry, resulting in a thickness derivation of not more than 1nm at different positions of a large (150 x 100 mm) foil sample and a average thickness of 15nm.

The mechanical stability of the parylene foil was compared to the stability of a DLC foil of the same thickness Here 30 nm thick foils were used. For this purpose both foils were attached on TEM-grids creating small self-supporting samples. The force-distance relation was measured via nanoindentation using an atomic-force microscpe (AFM). The measured elasticity of the parylene is 5 times higher than the one of the DLC, which explains the higher resistance against mechanical shock and temperature variation observed during hadling. Using AFM topography mode, we measured the surface roughness in addition. Both samples hade more or less the same average roughness of $R_{DLC}= 5.7 \pm 0.9$ nm and $R_{Parylen}= 8.6 \pm 2.3$ nm.

References

[1] B. Aurand et al. , in CLEO: QELS-Fundamental Science, OSA Techn. Digest (2012), paper JTh3I.2.
[2] A. Henig *et al.*, PRL 103, 245003 (2009)
[3] S. Kar *et al.*, PRL 109, 185006 (2012)
[4] B. Qiao et al., PRL 105, 155002 (2010)
[5] A. Greiner *et al.*, Acta Polymer 48, 1 (1997)

Ion Acceleration in Multispecies Targets Driven by Laser Radiation Pressure

M. Zepf[1,2], S. Kar[2], K. F. Kakolee[2], B. Qiao[2], A. Macchi[3,4], M. Cerchez[5], D. Doria[2], M. Geissler[2], P. McKenna[6], D. Neely[7], J. Osterholz[5], R. Prasad[2], G. Sarri[2], O.Willi[5], X.Y. Yuan[6], M. Borghesi[2,7]

[1]Helmholtz Institut Jena, D-07743 Jena, Germany; [2]Centre for Plasma Physics, Queen's University Belfast, Belfast BT7 1NN, United Kingdom;[3]Istituto Nazionale di Ottica, CNR, Pisa, Italy;[4]Department of Physics ''Enrico Fermi,'' Largo B. Pontecorvo 3, 56127 Pisa, Italy; [5]Institut für Laser-und Plasmaphysik, Heinrich-Heine-Universität, Düsseldorf, Germany; Department of Physics, SUPA, University of Strathclyde, Glasgow G4 0NG, United Kingdom
[7]Central Laser Facility, Rutherford Appleton Laboratory, Didcot, Oxfordshire OX11 0QX, United Kingdom; [8]Institute of Physics of the ASCR, ELI-Beamlines Project, Na Slovance 2, 18221 Prague, Czech Republic.

The acceleration of ions from ultrathin foils has been investigated by using 250 TW, subpicosecond laser pulses, focused to intensities of > 10^{20} Wcm^{-2} and the results published in Physical Review Letters[1]. The ion spectra show the appearance of narrow-band features for protons and carbon ions peaked at higher energies (in the 5–10 MeV/nucleon range) and with significantly higher flux than previously reported. The spectral features and their scaling with laser and target parameters provide evidence of a multispecies scenario of radiation pressure acceleration in the light sail mode, as confirmed by analytical estimates and 2D particlein-cell simulations. The scaling indicates that monoenergetic peaks with more than 100 MeV/nucleon are obtainable with moderate improvements of the target and laser characteristics, which are within reach of ongoing technical developments. The experiment was carried out employing the Petawatt arm of the VULCAN laser system at the Rutherford Appleton Laboratory, STFC, United Kingdom. A schematic of the experimental setup is shown in Fig. 1. The laser delivered ~200 of energy on target in pulses of 700–900 fs FWHM duration after being reflected off a plasma mirror (PM), resulting in an intensity contrast ratio of 10^9 between the main pulse and the nanosecond-long amplified spontaneous emission. The laser was focused on a target at normal incidence by an f/3 of-axis parabolic mirror. While exponential spectra were always observed from 5–10 μm thick foil targets, narrow-band features in proton and heavier ion spectra were obtained from submicron-thick targets irradiated at high intensities. For example, the spectra in Fig. 1(b), from a 100 nm thick Cu target irradiated by a LP (p polarization) laser pulse at a peak intensity of 3 10^{20} Wcm^{-2}, show narrow-band peaked features in the proton (charge to mass ratio Z/A = 1) and carbon (Z/A = 0.5) spectra, clearly separated from a lower energy component (as usual in standard interaction conditions, protons and carbon ions observed in the spectrum originate from surface contaminant layers).

The appearance and position of distinct peaks in the ion spectrum could be controlled by varying laser and target-parameters as shown in Figs. 2(a) and 2(b). Peaks were observed only in the limit of thin foils and high intensity [Fig. 2(a)] with the peaks shifting towards higher energy as either the intensity was increased or the target thickness was reduced [Fig. 2(b)]. In order to assess the possible influence of radiation pressure effects on the spectral profiles observed, a simple analytical model was developed taking into account the hole-boring (HB) and light-sail (LS) phases of the RPA mechanism. The position of the peak energy is reproduced well by the model and shows the characteristic scaling for RPA with E_{ion}~$(a_0{}^2\tau/\chi)^2$.

In conclusion, we have reported on the observation of narrow-band features in the spectra of laser-accelerated ions, which appear to be consistent with radiation pressure acceleration, in a regime where LS overcomes sheath acceleration.

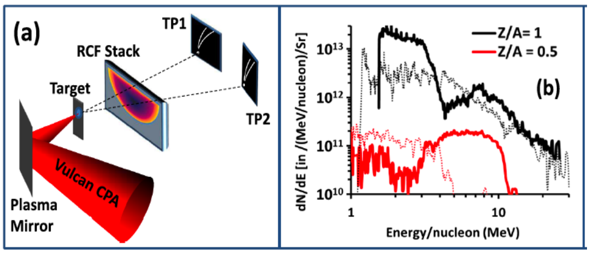

Figure 1: (a) Schematic of the Experimental set-up and (b) Ion spectra obtained from 100 nm Cu target irradiated by a LP laser pulse at I_0 =3 10^{20} Wcm^{-2}. Different line colors correspond to different ion species (see the figure legend); solid and dotted lines represent spectra obtained on TP1 and TP2, respectively.

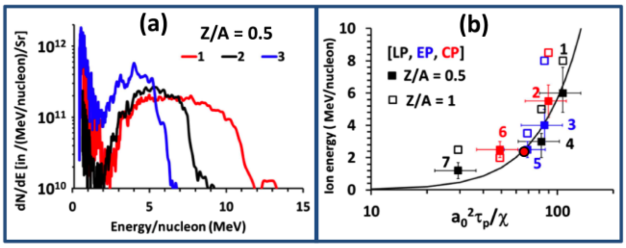

Figure 2: FIG. 2 (color online). (a) Graph showing comparison between three ion (Z/A= 0:5) spectra, where the position of the spectral peaks is plotted in (b) as a function of $a_0{}^2\tau/\chi$.

The experimental parameter set [a_0, target material, target thickness μm)] for the data points 1–7 is [15.5, Cu, 0.1], [10, Cu, 0.05], [13.8, Cu, 0.1], [7.5, Al, 0.1], [6.9, Al, 0.1], [13.6, Al, 0.5], and [14.1, Al, 0.8], respectively. The analytical estimate is shown by black solid line in (b).

References

[1] S. Kar et al., Phys. Rev. Lett., 109, 185006 (2012).

Target Thickness Scan in Laser Ion Acceleration Experiments

O. Jäckel[1,2], J. Polz[1,2], A. K. Arunachalam[1,2], A. Sävert[1,2], R. Brüning[2], M. Hornung[1,2], S. Keppler[1,2], J. Hein[1,2], R. Bödefeld[1,2], M. Hellwing[1,2], A. Kessler[1,2], and M.C. Kaluza[1,2]

[1]Helmholtz-Institute Jena, Jena, Germany; [2]Institute for Optics und Quantumelectronics, Jena, Germany

Target normal sheath acceleration (TNSA) is the most extensively investigated laser driven ion acceleration scheme so far, but several aspects of the acceleration process are still not fully understood. An extensive experimental study investigating the influence of the parameters target material and target material thickness on the produced ion spectra provides a dedicated data set to contribute to the further understanding of the TNSA mechanism.

TNSA Process

The physical picture behind TNSA is the following [1,2]. A laser pulse is focused onto the front surface of a several µm thick target foil applying relativistic light intensities. The produced hot electron distribution expands within the target foil predominantly towards the target back surface. The hotter the distribution the more it extends beyond the residual ion distribution formed by the initial foil. Within this unscreened potential field strengths in the range of TV/m are generated and cause the foil ions' and the surface contaminants' field ionisation and subsequent acceleration. TNSA produces ion beams with exponential energy spectra extending up to a certain cut-off energy which denotes the maximum ion energy.

Experimental Setup

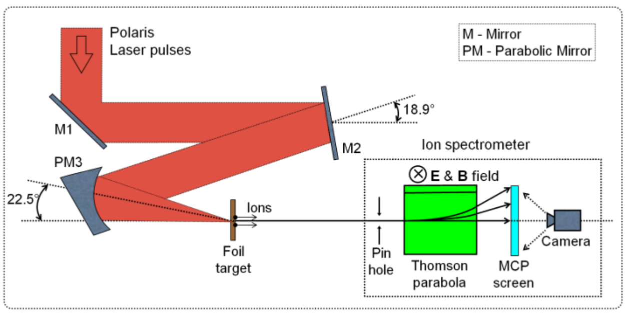

Figure 1: Setup to study ion acceleration at POLARIS

Fig. 1 shows the setup during the experimental campaign at POLARIS. The POLARIS pulses contained about 2.5 J within 230 fs (FWHM) at a central wavelength of 1030 nm. Focusing with an f/2 off-axis parabolic mirror led to focal intensities of about $4{\cdot}10^{19}$ W/cm² on the target front surface. Thin metal foils were stretched in frames to provide 40 × 40 mm² targets sufficient for a series of 200 shots. A Thomson parabola ion spectrometer was equipped with a microchannel-plate based detector to record the spectrum of the produced ion beam online.

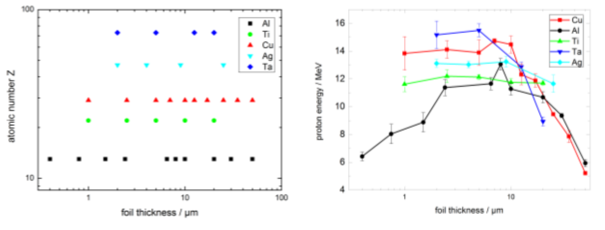

Figure 2: Left: Target's overview. Right: Maximum proton energy as a function of the target thickness for different materials.

Results

Aluminum, titanium, copper, silver, and tantalum were used as target materials in thicknesses varying from 400 nm to 50 µm. For each target material we found a similar behavior for decreasing thickness. The average maximum proton energies increase up to an optimal target thickness until they decrease again for a further reduction of the thicknesses. Less clear but nevertheless visible is the increase of the maximum ion energy for optimal target thickness with the atomic number of the target material.

For a more detailed understanding of the described behavior an extension to the analytical model of Mora [3] was investigated [4]. It is based on the implementation of a certain back surface ion density gradient depending on the target thickness and the electron density. Therefore numerical simulations with the hydrodynamic code MULTI-fs are currently performed to support the findings concerning the ion density gradient for the experimental data of the POLARIS measurements.

References

[1] S.C. Wilks et al. "Energetic proton generation in ultra-intense laser-solid interactions", PRL **82** (2001)

[2] O. Jäckel et al. "All-optical measurement of the hot electron sheath driving laser ion acceleration from thin foils", NJP **12** 103027 (2010)

[3] P. Mora, "Plasma Expansion into a Vacuum", PRL **90** (2003)

[4] T. Kiefer et al., in preparation

Focusing and energy selection of laser-accelerated protons

I. Hofmann[1], *J. Meyer-ter-Vehn*[2], *X. Yan*[2], *and H. AlOmari*[1]
[1]GSI, Darmstadt, Germany; [2]MPQ Garching, Germany

Laser accelerated protons are characterized by relatively large energy and angular spreads. For practical applications - like bio-medical, therapy or fast imaging of dense plasmas - efficient collection at the source and energy selection to a required energy window are crucial issues. We suggest a method for combined focusing and energy selection, which is an effective alternative to the usually pursued dispersive energy selection by magnetic dipoles. Our method is based on the chromatic effect - the dependence of focal length on energy - of a magnetic solenoid or quadrupole triplet in combination with an aperture [1]. The latter selects a certain energy width, which is found proportional to the aperture radius. This method is specific to laser accelerated particles, where the beam size at a focus is dominated by the energy spread and not the intrinsic emittance of the beam as in conventional accelerators.

The main difference between quadrupoles and a solenoid is the first order focusing property of quadrupoles; solenoids instead only focus in second order, which makes them less effective at higher energies. Below 10 MeV a pulsed solenoid [2] or permanent magnet quadrupoles [3] have been employed so far. A useful guidance to decide between solenoids or a doublet/triplet at higher energies can be obtained through a scaling expression of their focusing properties based on thin lens approximations for the focal length f_s of a solenoid and F_d of a quadrupole doublet [4]. Comparing a solenoid with a doublet of the same overall length L and equal field B, we obtain for the ratio T_d of focusing strengths (here defined as inverse focal lengths) in terms of only geometrical quantities:

$$T_d \equiv \frac{1/F_d}{1/f_s} = \frac{4sl^2}{a^2L}, \tag{1}$$

where l is the individual quadrupole length, s the separation of quadrupoles (from center to center) and a the maximum beam radius. Hence the focusing strength of a doublet is superior to that of a solenoid, if a is sufficiently small relative to the length. As an example, consider a doublet with a gap between magnets equal to their length, in which case we have $T_d = (2/3)^3(L/a)^2$ and the transition occurs for $L/a > (3/2)^{3/2}$. This may enforce super-conducting or pulsed power technologies for the solenoid at higher energies when the rigidity demands for a longer solenoid at fixed aperture. For laser protons this transition occurs in practice between 1-10 MeV (for details see Ref. [5].

The chromatic focusing effect can be used for an effective energy selection, as only particles with focal spot sufficiently close to the aperture plane are transmitted effectively. This is demonstrated in a TRACEWIN computer simulation of size-equivalent solenoid and triplet systems. As initial distribution the output spectrum of a radiation pressure acceleration model to create a proton energy spectrum extending up to 250 MeV is used [6]. Resulting orbits of a TRACEWIN simulation with 3000 rays are shown in Fig. 1. Note that both lens systems are about 1 m long, but the solenoid field has to be at 6.3 T, whereas the quadrupoles are at 1.5 T. An important outcome is that the solenoid transmission is 47%, but the triplet transmission with 35% is not significantly lower. The rays also indicate the energy selection principle of particles with focal spot close to the apertures, which works equally well for the triplet as for the solenoid.

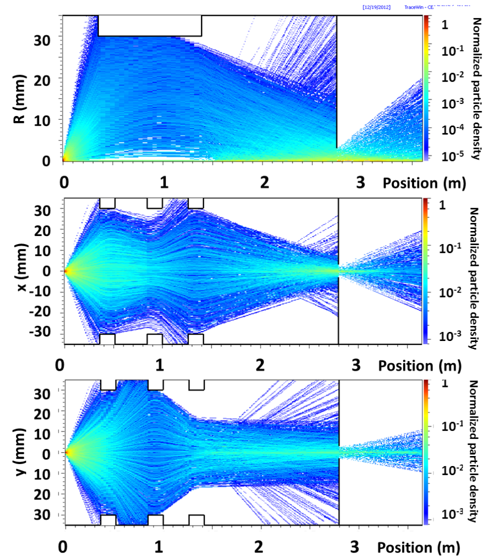

Figure 1: Transverse density plots for RPA-distribution in equivalent solenoid (top) and triplet (center: x-plane, bottom: y-plane) systems adjusted to 220 MeV.

References

[1] I. Hofmann, J. Meyer-ter-Vehn, X. Yan and H. Al-Omari, Nucl. Instr. Methods A 681, 44-54 (2012); I. Hofmann, "Chromatic energy filter", WIPO Patent Application WO/2012/080118.

[2] T. Burris-Mog *et al.*, Phys. Rev. ST Accel. Beams **14**, 121301 (2011).

[3] M. Schollmeier *et al.*, Phys. Rev. Lett. 101, 055004 (2008)

[4] M. Reiser, "Theory and Design of Particle Particle Beams", Wiley-VCH, Weinheim, 2008, p. 102ff.

[5] I. Hofmann, Phys. Rev. ST Accel. Beams **16**, 041302 (2013).

[6] X.Q. Yan et al., Phys. Rev. Lett. **103**, 135001-1 (2009).

Few-cycle optical probe-pulse for the investigation of relativistic laser-plasma interactions*

M. B. Schwab[1,#], O. Jäckel[1,2], A. Sävert[1], J. Polz[1], and M. C. Kaluza[1,2,]

[1]Institut für Optik und Quantenelektronik, Jena, Germany; [2]Helmholtz-Institut Jena, Jena, Germany

Introduction

We present a few-cycle probe-beam system implemented on the JETI 40 TW laser for the investigation of relativistic laser-plasma interactions. Using a pump-probe configuration, a shadowgraphic image of the plasma wave [1] in electron acceleration experiments was recorded.

The creation of few-cycle optical pulses is well-established and has been implemented on femtosecond Ti:sapphire laser systems for quite some time [2]. These pulses can be created via spectral broadening via self-phase modulation (SPM) in a gas-filled hollow-core fiber (HCF) followed by temporal compression by chirped mirrors (CMs). Depending on the filling-gas and the incident intensity, a spectrum spanning several hundred nm is achievable. The created spectrum is modulated due to interference effects; however, the technique is capable of supporting few-cycle pulse durations.

Optical probing of laser-plasma interactions is also a well-established practice. Both transverse probing and longitudinal probing techniques are frequently used [3-4]. Due to the femtosecond timescale of laser-plasma phenomena, a primary trend of probing techniques is the improvement of their temporal resolution, for which a few-cycle probe is well tailored.

Experimental Setup

Figure 1. shows a diagram of the probe's setup. 1% of the pump-pulse's energy is picked off by a 1:99 beamsplitter (BS) creating a probe-pulse that is synchronized with the pump-pulse. After the probe's beam diameter is reduced in size by an apodized-aperture (AA), two CMs temporally compress the probe and a one-meter focal length lens (L) focuses it through a Brewster window (BW) and into a gas-filled HCF. The probe's quadratic dispersion is controlled such that its shortest pulse duration, i.e. highest intensity, is realized at the entrance to the HCF. The resulting SPM broadens the probe's spectrum enough to support sub-5 fs pulse durations. Upon exiting the HCF, the probe is collimated and a group of 8 CMs once again temporally compress the probe so that its shortest duration will be achieved in the evacuated target chamber.

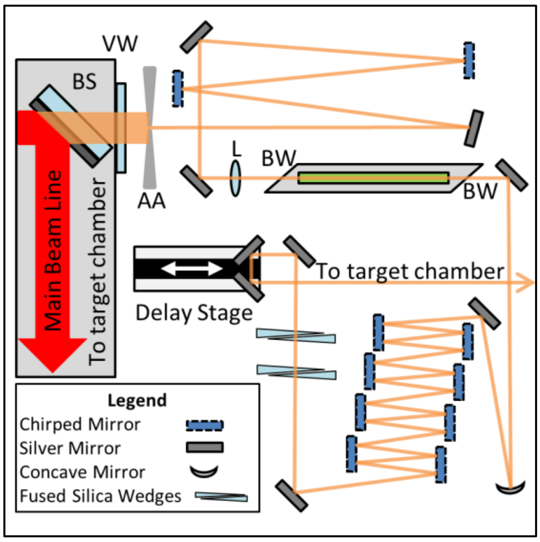

Figure 1: Few-Cycle Probe Diagram

A delay stage enables the relative timing between the pump and probe to be adjusted in 33 fs steps. Additionally, fused silica wedges allow fine-tuning of the probe's quadratic dispersion.

Results

The probe setup was characterized using neon and argon gas in the HCF with argon showing the best results for the available input pulse energy. The resulting broadened spectrum supported a Fourier-limited Full Width Half Maximum (FWHM) pulse duration of 4.4 fs. Measured FWHM probe durations fell within 5.9 ± 0.4 fs with a pulse energy of 300 ± 15 µJ exiting the HCF.

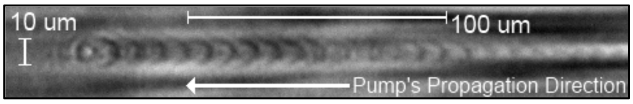

Figure 2: Shadowgraphic image of a plasma wave

Figure 2. shows a shadowgraphic image of a plasma wave driven by the ponderomotive force of the pump-pulse in ionized H_2 gas. The fine details seen in the image prove that the few-cycle probe will be a valuable tool for femtosecond laser-plasma diagnostics.

References

[1] T. Tajima, et al., Phys. Rev. Lett. **43**, 267–270 (1979).
[2] M. Nisoli, et al., Appl. Phys. Lett. **68**, 2793 (1996).
[3] A. Buck, et al., Nat. Phys. **7**, 543–548 (2011).
[4] N. H. Matlis, et al., Nat. Phys. **2**, 749–753 (2006).

* Work supported by the DFG, EC, BMBF, and EFRE.
# matthew.schwab@uni-jena.de

Probing laser-driven electron acceleration with a few cycle probe beam

A. Sävert[1,2,#], M. Nicolai[2], M. Reuter[1], O. Jäckel[1,2], M. Schwab[2], M. Möller[1], T. Rinck[2], M. Schnell[2] and M.C. Kaluza[1,2]

[1]Helmholtz Institute Jena, Jena, Germany; [2]Friedrich Schiller Universtiy , Jena, Germany.

With the 40TW JETI laser system at IOQ and HI-Jena ultra-short electron bunches with kinetic energies up to 200 MeV can be generated routinely. These electron bunches are generated during the interaction of the high intensity laser pulse with an under dense plasma. Here, the laser beam is focused by an off axis parabolic mirror to a spot of 13 µm diameter (FWHM) with a peak intensity of $8x10^{18}$ Wcm^{-2} into the leading edge of a super sonic helium gas jet. The electron bunches are self injected into the plasma wave and then accelerated in the blow out regime. The electron density is optimized by varying the background pressure of the valve of the gas jet to get well collimated electron bunches with a good shot to shot stability. Additionally we transversely image the interaction region to follow the acceleration process.

The pulse duration of the JETI laser is 27 fs, which is not short enough to resolve the accelerating structure, i.e. the plasma wave, within our parameter space of plasma frequencies. Therefore, a new synchronized probe beam has been developed capable of producing sub 6 fs laser pulses with a Gaussian like beam profile [1].

During the second half of 2012 we used this new probe beam on the JETI laser to study the electron acceleration process with under dense plasma targets. The probe beam was characterized with a few cycle SPIDER from APE to optimize the dispersion caused by the fiber, the chirped mirrors, the entrance window into the target chamber and the path through air since for sub 10 fs laser pulses even the dispersion of air cannot be neglected anymore.

Due to the broad bandwidth of the probe pulse spanning over 300 nm, a new imaging system comprising a large working distance microscope objective and an achromatic lens was installed. The magnification factor is determined by the focal length of the two optics and was as high as 12.5. The resolution of the imaging system is of the order of 1 µm. This new probe beam setup fulfills the temporal and spatial requirements to resolve characteristic structures during an electron acceleration experiment.

While the recorded data is still under evaluation preliminary results show that it is possible to observe periodic structures (Figure 1a), which can be identified with the plasma wave. In the snapshots, the main laser pulse has propagated from the right over a distance of 0.8 mm into the plasma. The peaks of the plasma wave already exhibit a strong curvature due to the relativistic motion of the electrons. The profile along the y=0 position is shown in Figure 1b. The position of the main laser pulse is estimated to be at z=0. The first oscillation period (on the left) shows a remarkable modulation which is an indication of high electron density gradients. A continuous wavelet transformation was applied to the profile in Figure 1b. This transforms the 1D profile into a 2D plot with gives the spatial wavelength for every position (Figure 1c). The first 10 cycles of the wave show a strong modulation with a wavelength of 9.1±1.6 µm.

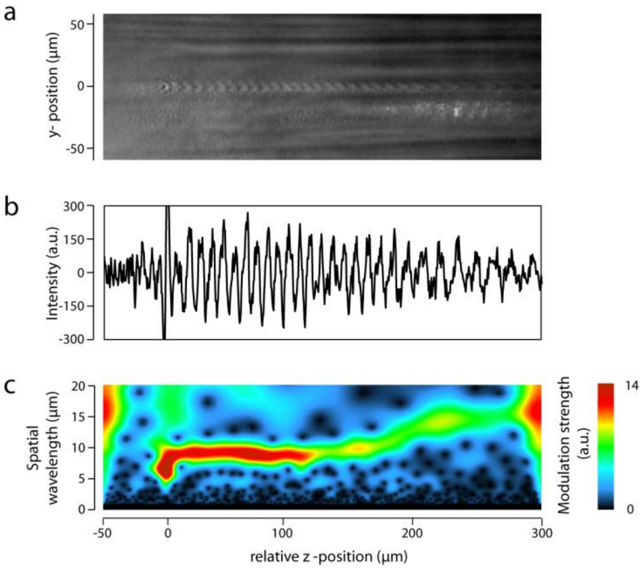

Figure 1: Shadowgraph of the plasma wave (a) and profile along the y=0 position (b) and corresponding continuous wavelet transform (c). The laser is propagating from the right to the left.

At later times during the interaction the amplitude of the plasma wave decreases and the wavelength increases which can be attributed to wave breaking.

Additionally PIC simulations for our experimental conditions are under way and are benchmarked against our results.

The new probe beam has proven to be a reliable light source with unique features offering the unique possibility at IOQ and HI-Jena to design a number of new experiments, e.g., to use polarimetry to visualize the electron bunch within the plasma wave and observe the point of injection.

References

[1] M. B. Schwab, O. Jäckel, A. Sävert, J. Polz and M.C. Kaluza, „ Few-cycle optical probe- pulse for the investigation of relativistic laser- plasma interaction", GSI Scientific Report (2012)

alexander.saevert2@uni-jena.de

Photon and particle spectroscopy and diagnostics

Research School of Advanced Photon Science of the Helmholtz Institute Jena

R. Märtin [*1,2], *H. Gies*[1,4], *C. Spielmann*[1,3], *and Th. Stöhlker*[1,2,3]

[1]HI-Jena, Jena, Germany; [2]GSI, Darmstadt, Germany; [3]IOQ, FSU, Jena, Germany; [4]ITP, FSU, Jena, Germany

One of the essential goals of the Helmholtz Institute Jena (HI Jena) is the graduate education of young scientists in the field of fundamental and applied physics by means of high-power lasers, accelerated particles, and x-ray science. It focus on future research opportunities as provided by the international FAIR facility in Darmstadt and the European XFEL in Hamburg as well as other large scale projects related to strong-field physics and the investigation of extreme states of matter. To ensure the best educational and training possibilities for the doctoral students associated to the HI Jena, the Research School of Advanced Photon Science (RS-APS) has been founded in summer 2012 [1].

The Research School provides structured PhD education which is in close connection to main scientific objectives of the HI Jena. The RS-APS supports up to 20 students through funding and its educational training program. Even

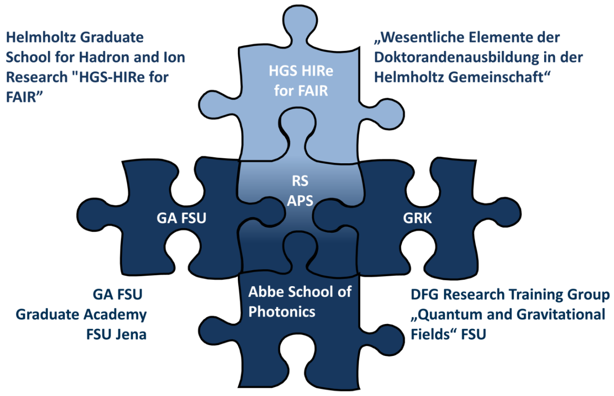

Figure 1: Illustration of the already existing cooperating graduate programs and their connection to the RS-APS.

though there are already existing graduate programs at the University of Jena and the different Helmholtz centers there is the need to to provide professional education adapted on the research profile of the HI Jena. Moreover the geographical separation of the different partner centers requires a research school and its management located directly at the HI Jena. In addition to the professors and junior research leaders directly associated to the HI Jena about ten professors of different institutes of the University Jena are responsibly involved in the realization of the RS-APS:

- Helmholtz Institute Jena (HI-Jena): Prof. Th. Kühl, PD. Dr. W. Quint, PD. Dr. A. Surzhykov, Dr. F. Tavella, Prof. M. Zepf
- Institute of Applied Physics (IAP): Jun. Prof. J. Limpert, Prof. A. Tünnermann
- Institute of Condensed Matter Theory and Optics (IFTO): Jun. Prof. S. Skupin
- Institute of Optics and Quantum Electronics (IOQ): Prof. M. Kaluza, Prof. G. Paulus, Prof. C. Spielmann, Prof. Th. Stöthlker
- Institute of Theoretical Physics (ITP): Prof. S. Fritzsche, Prof. H. Gies, Prof. A. Wipf

The organizational structure of the RS-APS is depicted in Fig. 1. To comply with the structure of the University Jena, RS-APS applied for admittance to the university's graduate academy [3] and was accepted on June 25th, 2012. Additionally, the school is in close cooperation with both the Abbe School of Photonics [2], which resides at the Department for Physics and Astronomy, and the DFG graduate college Quantum and Gravitational Fields [4]. Moreover the RS-APS is member of the Helmholtz Graduate School for Hadron and Ion Research (HGS-HIRe) for FAIR [5] and grants its supported students access to graduate programs of the Helmholtz Association. The school is headed by a three-person committee. The RS-APS is chaired by the spokesman Prof. C. Spielmann, while the coordinator Dr. R. Märtin performs organizational tasks with support by the administration of the HI Jena.

Apart from the scientific work conducted within the research projects pursued at the HI Jena, doctoral students are being offered training courses to consolidate their understanding of the various research fields of HI-Jena, as well as to broaden the students soft skills. Through the integration of the RS-APS to the educational program of its partners the school provides the students with a great variety of different academic courses, e.g. dedicated soft skills programs are offered by the partners HGS-HIRe and the Graduate Academy. In summer 2013 the first Lecture Week devoted to the physics of the HI Jena will be conducted by the RS-APS in cooperation with HGS-HIRe. Furthermore the seminars of the Institute are of great relevance. The seminars provides a platform for exchange and discussion for the scientists from different research fields present at the HI Jena.

References

[1] `http://www.hi-jena.de/en/helmholtz_institute_jena/rs_aps/`

[2] `http://www.asp.uni-jena.de/doctoral.html`

[3] `http://www.jga.uni-jena.de/`

[4] `http://cms.rz.uni-jena.de/gk_quanten/Homepage.html`

[5] `http://hgs-hire.de/`

* r.maertin@gsi.de

X-ray Laser Developments at PHELIX

B. Ecker[1,2], B. Aurand[2,3,4], D. C. Hochhaus[3,7], P. Neumayer[3], B. Zielbauer[1,4], K. Cassou[5], S. Daboussi[5], O. Guilbaud[5], S. Kazamias[5], T. T. T. Le[6], E. Oliva[6], L. Li[6], H. Zhao[8], Q. Jin[8], D. Ros[5], P. Zeitoun[6], and T. Kühl[2,4]

[1]Helmholtz Institute Jena , [2]Johannes-Gutenberg Universität Mainz, [3]ExtreMe Matter Institute EMMI, [4]GSI Helmholtzzentrum fuer Schwerionenforschung, [5]LASERIX-CLUPS / Université Paris-Sud 11 [6]Laboratoire d'Optique Appliquée, [7]Goethe-Universität Frankfurt, [8]Institute of Modern Physics, CAS

Introduction

We report on results of a double-stage molybdenum x-ray laser experiment. The two targets were pumped using the double-pulse grazing incidence pumping technique, which includes travelling wave excitation for both the seed- and the amplifier-target..

The main motivation for X-ray laser (XRL) research at GSI is to perform spectroscopy experiments on highly-charged heavy-ions stored in the experimental storage ring (ESR) of the GSI accelerator facility[1]. The first experiment of this kind will aim at measuring the 2s1/2 – 2p1/2 transition in Li-like ions. For ions of an atomic number between 50 (Sn) and 92 (Ur), this transition energy lies between 100 eV and 300 eV [1], which corresponds to wavelengths between 12 nm and 4 nm. Setting up the experiment in a way, where the XRL is counter propagating to the ion bunch, one can exploit the relativistic Doppler effect. The use of laser-pumped plasma XRL's, with typical photon energy up to 100 eV [2,3,3] can address the whole range of lithium-like ions for the lowest lying transitions The perspective for FAIR, given by the even higher ion velocities at HESR , opens a completely new range of experiments.

Experiment

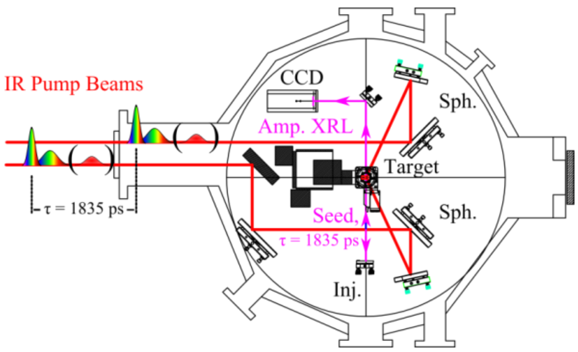

Fig. 1. Sketch of the experimental setup. A more detailed description is given in the text.

A Mach-Zehnder like interferometer, which was implemented in the short-pulse frontend of the PHELIX laser, was used to create the chirped double-pulse structure required for the DGRIP scheme [2]. After compression, the pulse duration of the two pulses was 200 ps (prepulse) and 2 ps (main pulse). Using the PHELIX pre-amplifier section, the total pump energy on the target amounted to 600 mJ, equally distributed between two individual pumping beams. Inside the target chamber, the two beams were focused in opposite direction onto the Mo slab target by two spherical mirrors, as illustrated in Fig. 1. The line foci were vertically separated by ~ 3 mm. The output of the lower XRL – the seed pulse - was focused into the upper – amplifying- medium by a spherical XUV mirror.

Results

Seeded x-ray laser operation has been demonstrated, resulting in x-ray laser pulses of up to 240 nJ and 2 mrad × 2 mrad divergence. The peak brilliance of the amplified x-ray laser of 4×10^{23} photons /s /mm² /mrad² in 5×10^{-5} relative bandwidth was more than two orders of magnitude larger compared to the original seed pulses.Figure 1 shows the typical beam patterns of the HH observed (filters: Zr and Ti) under (a) only He gas jet (valve stagnation pressure: 4000 mbar), (b) Ne 400 mbar jet, and (c) both gas jets for Ne 400-He 4000 mbar.

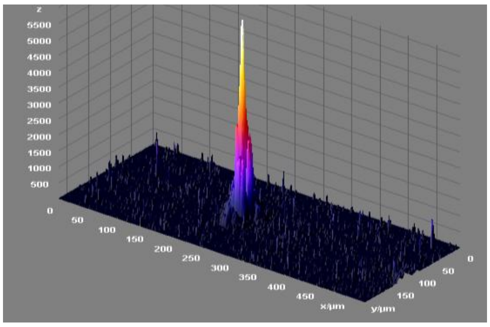

Fig. 2: Beam quality of the seeded XRL. showing 2 mrad × 2 mrad divergence.

References

1. D.Winters et al., GSI Annual report 2012
2. B. Ecker et al., Opt. Express **20**(23), 25391 (2012).
3. D. Zimmer et al., Optics Express, 13, 2403, 2008
4.D. Ros et al., NIM A, 653,, 76, 2011

Amplification of high harmonic generation signal by double gas jet scheme

J. Seres[1], E. Seres[1], B. Aurand[2,3], S. Namba[4], B. Landgraf[1,2], C. Spielmann[1,2], and T. Kühl[2,3,5,6]

[1] Institute for Optic and Quantum Electronics, Jena, Germany; [2] GSI , Darmstadt, Germany; [3] Helmholtz Institute Jena, Jena, Germany; [4] Hiroshima University, Japan; [5] Johannes Gutenberg University, Mainz, Germany; [6] EMMI Extreme Matter Institute, Darmstadt, Germany

Introduction

High-harmonic (HH) radiation due to nonlinear interaction of rare gas with an ultrashort, high intensity laser pulse has attracted a great deal of interest for various applications, such as, attosecond pulses [1] and a seeding light for an X-ray free electron laser (XFEL) [2]. On the other hand, we have observed X-ray parametric stimulated amplification of the HH emission for the first time [3]. However, the output of the HH in high photon energy regime is still weak, so that practical applications are limited in some particular physical and chemical research. In order to increase the output energy and obtain much shorter wavelength radiation, a double gas jet method was used in this study. As a result, we succeeded in a significant enhancement of the HH output. Moreover, the appearance of a high intensity, hot spot emission was observed.

Experiment

The experiment was carried out at the JETI laser-system, delivering pulses of 200 mJ, 10 Hz in 26 fs, with a pulse contrast in the range of better than 10^6. The beam was focused by a spherical mirror to an intensity of $< 5\times10^{15}$ W/cm^2. In order to enhance the HH lights, we employed a double gas jet scheme, in which the first gas was Ne as a seeder and the second jet (He) served as an amplifier. Both gases were supplied by electro-magnetic pulsed gas valves. An extreme ultraviolet (EUV) spectrometer was used to measure the HH spectra and their intensity distribution. The beam pattern of the HH was observed by a back-illuminated soft X-ray CCD camera, at which some appropriate filters (Ti and Zr) were inserted to select wavelength region and block the fundamental laser light.

Results

Fig. 1 shows the typical beam patterns of the HH observed under (a) only He gas jet (valve stagnation pressure: 4000 mbar), (b) Ne jet 400 mbar, and (c) both gas jets for Ne 400-He 4000 mbar.

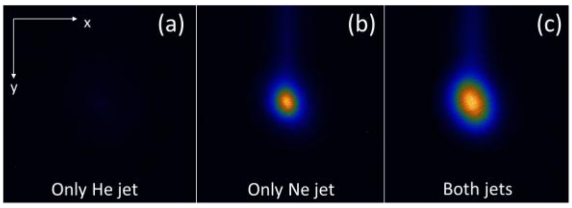

Fig. 1: Two dimensional image of the high harmonic radiations for (a) only He jet (4000 mbar), (b) Ne (400 mbar), and (c) both jets operated. For comparison, the graphs are shown in the same color scale. Significant enhancement of the HH signal was obtained.

The distance of the jets was set to d=0 mm. The figures are shown in the same color scale. As clearly seen, no HH was observed for only He gas jet, whereas by operating both jets the HH signal becomes higher by two times than that by only the Ne jet.

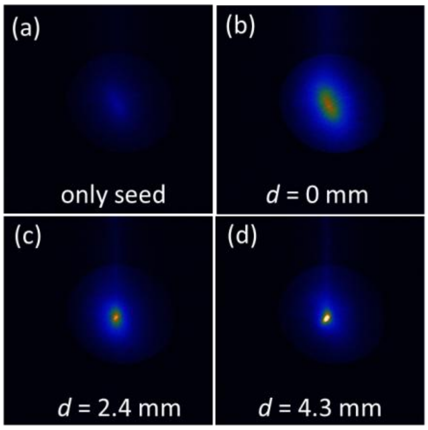

Fig. 2: Variation of the HH image on the gas jet distance. Above d~2mm, the hot spot appeared, where the gain coefficient increased by ~20 times.

On the other hand, the hot spot where the HH intensity is locally enhanced is obtained as shown in Fig. 2. The experimental conditions are as follows: stagnation pressures of Ne 250 mbar, He 4000 mbar, Zr-Ti filters, for various jet distances were used. The seed lights generated in Ne gas jet were amplified significantly at d=0 mm, which is similar with that in Fig. 1. However, in the case of the jet distances above d~2 mm, we obtain the intense spot radiation near the beam center. At optimal condition, we demonstrate that the gain coefficient at the hot spot, which is defined by the ratio of HH intensity with both gas jets to that of Ne one, is around 20.

References

[1] M. Hentschel *et al*., "Attosecond metrology", Nature 414, 509 (2001).

[2] T. Togashi *et al*., "Extreme ultraviolet free electron laser seeded with high-order harmonic of Ti:sapphire laser", Opt. Express, 19, 317 (2011).

[3] J. Seres *et al*.," Laser-driven amplification of soft X-rays by parametric stimulated emission in neutral gases", Nature Phys. 6, 455 (2010).

Phase matching and quantum path interference in high-order harmonic generation up to photon energy of 1 keV

J. Seres[1], E. Seres[1,2], B. Landgraf[1,2], B. Ecker[2,3], B. Aurand[2,3], T. Kühl[2,3], S. Namba[4], C. Spielmann[1,2]

[1]IOQ, Friedrich Schiller University, Jena, Germany; [2]Helmholtz Institute Jena, Jena, Germany; [3]GSI, Darmstadt, Germany, [4] Hiroshima University, Japan

Phase matching is indispensable for the efficient generation of high-order harmonic radiation (HHG), especially in the range of several-100-eV. Recently it has been theoretically predicted that perfect pressure induced phase matching cannot be realized in helium in the 0.2-1 keV spectral range using 800 nm light pulses [1]. In this report we present a detailed experimental study of the phase mismatch for the first time and derive guidelines for maximizing the short wavelength signal without perfect phase matching.

Measurement results

The high harmonic spectra at a series of different He gas pressures have been measured using the 26-fs-long pulses of the JETI Ti:sapphire laser system, which can deliver pulses up to 1 J pulse energy at 800 nm central wavelength and with 10 Hz repetition rate. The laser pulses were loosely focused into a He gas target with interaction length of 1 mm and the peak intensity was about $5x10^{15}$ W/cm². After blocking the fundamental laser light with thin Al (200 nm) and Ti (100 nm) foils, the spectra were measured with an x-ray scanning spectrograph (McPherson 248/310G) equipped with a photomultiplier (Channeltron 4751G). Using a 1200 grooves/mm grating, it is possible to record soft x-ray spectra in the spectral range of 0.2-2 keV with high spectral resolution.

Low frequency modulation

In the recorded spectra, we can observe a low frequency modulation of the harmonic amplitudes as it can be seen in Fig. 1 for a backing pressure 0.3 bar. The low frequency modulation is attributed to the constructive and destructive interference of the phase mismatching contribution between the driving laser pulse and the generated harmonics. The observed near 100% modulation depth caused by phase-matching provides evidence that the measured spectra are built up from coherent radiation in the full measured spectral range. According to the theory, this low frequency spectral modulation can be described with a

$$I_{HHG}(q) \propto \mathrm{sinc}^2(\pi p_0^{-1} q p) \quad (1)$$

function, where p is the gas pressure; q is the harmonic order and p_0^{-1} is the phase matching parameter. The sinc² modulation periods have been determined by the Fourier transform of the harmonic spectra in the spectral range of 270-880 eV. In all spectra, we observe two dominant distinguishable peaks (inset of Fig. 1). In Fig. 2, we summarize the position of these two peaks as a function of the pressure. As predicted by the phase matching theory, the obtained periods scale linearly with the pressure and we can estimate p_0^{-1} as the slope of the lines.

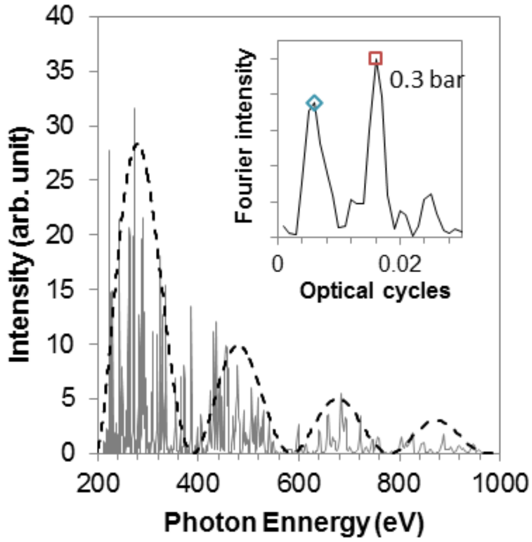

Figure 1: Measured HHG spectrum at 0.3 bar backing pressure with its Fourier transform in the inset.

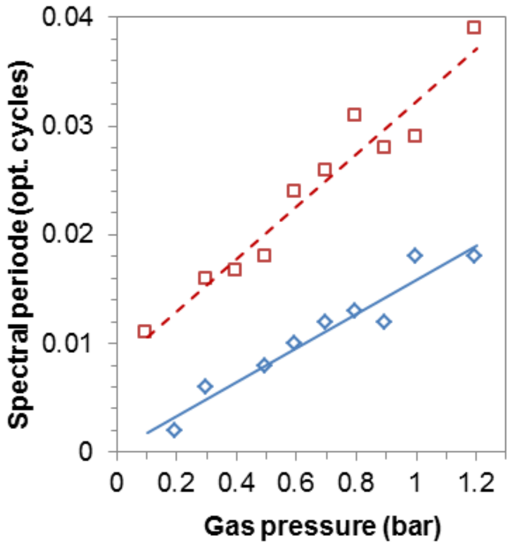

Figure 2: Pressure dependence of the peak positions of the Fourier transform from the inset of Fig. 1.

Both curves in Fig. 2 reveals that the modulation period will become zero only for a negative or zero pressure, i.e. perfect phase matching cannot be realized in He by pressure-tuning in the few-100-eV spectral range in agreement with recently published results predicting pressure phase matched HHG above 100 eV only for longer wavelength driving laser pulses [1]. However, the lower (blue curve) of the two modulation period curves indicates more favorable phase matching condition. The extrapolated curve will cross the x-axis near zero pressure, which is the optimum for stimulated recombination of x-ray parametric amplification (XPA) [2, 3]. Based on these findings we are now able to predict the optimum parameters for achieving phase-matching and XPA at the same time.

High frequency modulation

A recorded x-ray spectrum is shown in the inset of Fig. 1, in the 0.2-1 keV spectral range and a part of the spectrum is highlighted in Fig. 3 for the range of the 200th to 360th harmonics corresponding to energy range of about 300 to 600 eV, respectively. The resolution of the x-ray spectrograph has made possible to resolve individual harmonic lines in this range. The harmonic lines are especially very well resolved in the range of harmonic order of 201-221 and 269-289. In the range of 221st to 261st harmonics and near the upper end, the signal is much weaker because of a lack of phase matching. Above harmonic order 321 the visibility of the harmonic lines is weaker as a consequence of the decreasing spectral resolution of the spectrograph and the limited sampling rate. The small anomaly in the range of harmonic order 293 (450 eV) is attributed to the L absorption edge of the thin Ti-filter in the beam path.

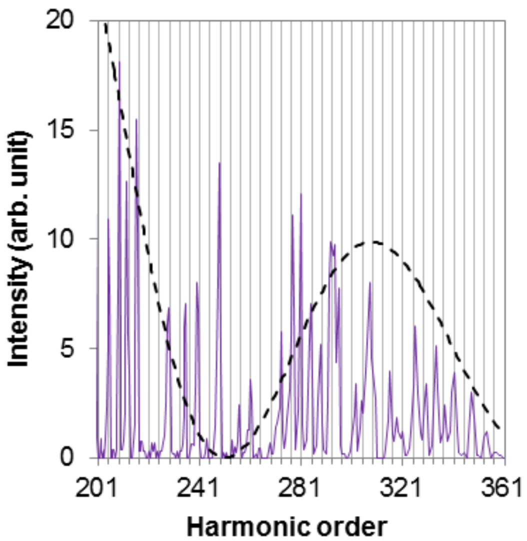

Figure 3: Harmonic lines in the measured spectra are sitting in the 4i+1 harmonic position, which is the consequence of the quantum path interference of two dominating electron trajectories.

We can find an unexpected behavior of the harmonic line structure in Fig. 3. No every odd (2i+1) harmonics are in the spectrum, as would be expected for standard high harmonic generation. Only every second harmonics lines appear at harmonic orders of 4i+1. We attribute this phenomenon to the quantum path interference of two dominating electron trajectories. These trajectories are extended long trajectories with acceleration times of about 15/8 and 17/8 optical cycles between the ionization and recombination events. From these trajectories, four x-ray pulses are generated in every optical cycle in contrary to standard high harmonic generation from short trajectories, where two pulses are generated in every optical cycle. Fourier transform of this temporal behavior gives the lack of every second harmonic order. The two dominating trajectories are selected by x-ray parametric amplification, because for these two trajectories the necessary condition for resonance enhancement is fulfilled.

Summary

From the presented measurements we can draw the following major conclusions. For laser intensities in the range of 10^{15}-10^{16} W/cm², high order harmonics can be generated and stimulated emission of x-rays can be realized from extended long electron trajectories. For these extended trajectories, the time between ionization and recombination is about two optical cycles and in every optical cycle four x-ray pulses are generated. The determination of phase matching conditions from the measured spectra further supports the essential contribution of x-ray parametric amplification in the harmonic generation process. These results help to better understand high-order harmonic generation and x-ray parametric amplification at higher laser intensities and provide guidelines to extend the generated spectrum to higher photon energies at increased efficiency; paving the way for attosecond science far beyond 100 eV photon energies.

The authors acknowledge for the contributions of the JETI laser team.

References

[1] T. Popmintchev, M.-C. Chen, A. Bahabad, M. Gerrity, P. Sidorenko, O. Cohen, I. P. Christov, M. M. Murnane, and H. C. Kapteyn, "Phase matching of high harmonic generation in the soft and hard X-ray regions of the spectrum", PNAS **106**, 10516 (2009).

[2] J. Seres, E. Seres, D. Hochhaus, B. Ecker, D. Zimmer, V. Bagnoud, T. Kuehl, and C. Spielmann, "Laser-driven amplification of soft X-rays by parametric stimulated emission in neutral gases", Nature Phys. **6**, 455 (2010).

[3] J. Seres, E. Seres, C. Spielmann, "Classical model of strong-field parametric amplification of soft x rays", Phys. Rev. A **86**, 013822 (2012).

Efficient near-monochromatic high harmonic radiation from surface plasmas

C. Rödel[1,2], J. Bierbach[1,2], M. Yeung[1,4], B. Dromey[4], M. Wünsche[1,2], T. Hahn[3], D. Hemmers[3], G. Pretzler[3], M. Zepf[1,4], and G.G. Paulus[1,2]

[1]Helmholtz Institute Jena, Helmholtzweg 4, D-07743 Jena, Germany; [2]Institut of Optics and Quantum Electronics, Friedrich Schiller University Jena, D-07743 Jena, Germany; [3]Institut für Laser- und Plasmaphysik, Heinrich-Heine-Universität Düsseldorf, D-40225, Düsseldorf, Germany; [4]Centre for Plasma Physics, Queen's University Belfast, BT7 1NN, United Kingdom

Ultrashort coherent XUV and soft x-ray pulses of high brilliance are required for the seeding of planned free-electron laser (FEL) facilities such as FLASH II or XFEL. Research in the project "Surface High Harmonic Generation (SHHG)" is focused on the generation of intense XUV pulses from solid density plasmas with a focus on the particular demands for seeding an FEL. First, the efficiency of SHHG in the "Relativistic Oscillating Mirror" (ROM) mode has been investigated and was optimized utilizing elongated plasma density ramps. A plasma scale length of the order of $\approx \lambda/10$ has been found to lead to the highest efficiencies. The resulting optimized pulse energies of several μJ per harmonic (at $32.5\,\mathrm{eV}$) could already be exploited for seeding. Second, we have studied SHHG on blazed grating surfaces. It was shown that particular harmonic frequencies can be enhanced as compared to the adjacent harmonics. This leads to a spatial filtering of the harmonic radiation which could also be useful for seeding.

Harmonic generation from relativistic plasma surfaces in ultrasteep plasma density gradients

Harmonic harmonic generation in the ROM mode has been studied in the limit of ultrasteep plasma density gradient by experiments and simulations. Our observations reveal that the absolute efficiency of the harmonics declines for the steepest plasma scale length $L_p \to 0$ in contradiction to the wide-spread belief. The shortest plasma density gradients have been realized using laser pulses with the highest possible contrast. Absolute photon yields have been recorded using a calibrated spectrometer system [2]. The pulse energies E_{XUV} for individual harmonics are on the order of $3-24\,\mu$J for the 17th harmonic and $0.3-2.7\,\mu$J for the 21st depending on different contrast and preplasma settings. The efficiency of harmonics reflected from the laser driven plasma surface in the ROM mode was estimated to be in the range of $10^{-4} - 10^{-6}$ of the laser pulse energy for photon energies ranging from $20 - 40$ eV. The best results have been obtained for an intermediate density scale length of the order of $\lambda/10 - \lambda/5$.

Laser-plasma simulation support the experimental result, see Ref. 1. The observed dependence of the efficiency on the plasma scale length can be understood in terms of the plasma dynamics as follows. First, the denser the plasma and the steeper the gradient, the more the electric field $\vec{E}_{crit}$ at the critical density is reduced where the harmonics are generated. Second, the "spring constant" of the electron plasma becomes larger for denser and steeper plasmas, making the "relativistic oscillating mirror" harder to drive to high values of the Lorentz factor γ associated with a more efficient production of higher harmonic orders.

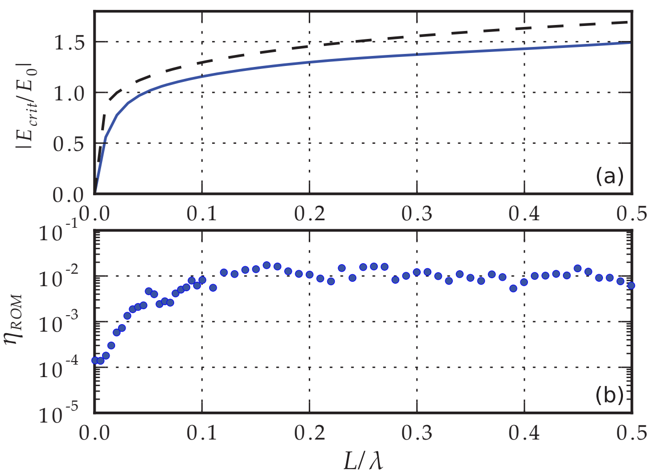

Figure 1: (a) Surface field $\vec{E}_{crit}$ at the critical density in units of the incident field $\vec{E_0}$, as estimated from the equation in the textbook of Kruer (black dashed line) and computed exactly by numerical integration for an exponential gradient (blue line). (b) Efficiency of SHHG above the 14th order $\eta_{ROM} = \int_{14\omega_0}^{\infty} I(\omega)d\omega/P_0$ for $a_0 = 3.5$ at different plasma scale lengths from a set of 1D PIC simulations. Incidence was p-polarized, the plasma ramp is exponential up to a maximum density of $n_e = 200n_c$.

Near-monochromatic high-harmonic radiation from relativistic laser plasma interactions with blazed grating surfaces

Intense, femtosecond laser interactions with blazed grating targets are studied through experiment and laser plasma simulations. The high harmonic spectrum produced by the nonrelativistic harmonic generation prozess ”CWE” (Coherent Wake Emission) is angularly dispersed by the grating leading to near-monochromatic spectra emitted at different angles, each dominated by a single harmonic and its integer multiples. The spectrum emitted in the direction of the third-harmonic diffraction order is measured to contain distinct peaks at the 9th and 12th harmonics which agree well with two-dimensional PIC simulations using the same grating geometry. This scheme appears to be a viable method of producing near-monochromatic, short-pulsed extreme-ultraviolet radiation.

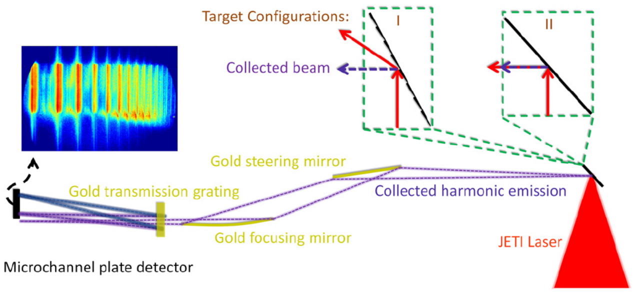

Figure 2: Experimental setup: JETI laser pulses are focused on (I) a blazed grating target with the third harmonic's first diffraction order directed to the spectrometer or (II) a fused silica target reflecting the beam to the spectrometer in specular direction. The XUV radiation is collected by a steering and focusing mirror. The harmonic spectrum is recorded using a transmission grating and a CCD.

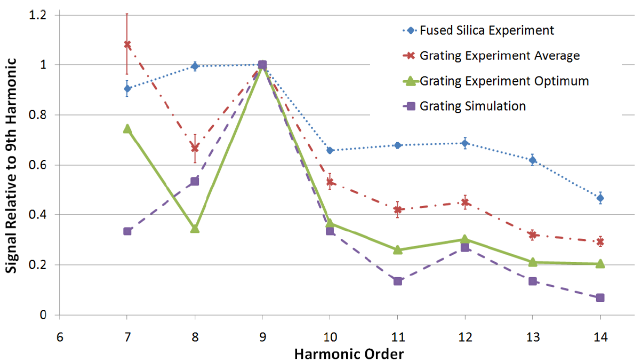

Figure 3: Comparison of harmonic spectra obtained from the experiment and simulations: While the harmonic spectrum is decaying for higher orders for the fused silica target (case II), an enhancement of the 9th harmonic (slightly also the 12th) is found when the blazed grating configuration (case I) is used. The experimental results agree well with the harmonic spectrum obtained by a laser plasma simulation

References

[1] C. Rödel, D. an der Brügge, J. Bierbach, M. Yeung, T. Hahn, B. Dromey, S. Herzer, S. Fuchs, A. Galestian Pour, E. Eckner, M. Behmke, M. Cerchez, O. Jäckel, D. Hemmers, T. Toncian, M.C. Kaluza, A. Belyanin, G. Pretzler, O. Willi, A. Pukhov, M. Zepf, and G. G. Paulus, *Harmonic Generation from Relativistic Plasma Surfaces in Ultrasteep Plasma Density Gradients*, Physical Review Letters **109**, 125002, 2012

[2] S. Fuchs, C. Rödel, M. Krebs, S. Hädrich, J. Bierbach, A. E. Paz, S. Kuschel, M. Wünsche, V. Hilbert, U. Zastrau, E. Förster, J. Limpert, and G. G. Paulus, *Sensitivity calibration of an imaging extreme ultraviolet spectrometer-detector system for determining the efficiency of broadband extreme ultraviolet sources*, Review of Scientific Instruments **84**, 023101, 2013

[3] M. Yeung, B. Dromey, C. Rödel, J. Bierbach, M. Wünsche, G. Paulus, T. Hahn, D. Hemmers, C. Stelzmann, G. Pretzler, and M. Zepf, *Near-monochromatic high-harmonic radiation from relativistic laser-plasma interactions with blazed grating surfaces*, New Journal of Physics **15**, 025042, 2013

Near-monochromatic high-harmonic radiation from relativistic laser–plasma interactions with blazed grating surfaces

M. Zepf[1,2]*, M. Yeung*[2]*, B. Dromey*[2]*, C. Rödel*[1,3]*, J. Bierbach*[1,3]*, M. Wünsche*[3]*,G. G. Paulus*[1,3]*, T. Hahn*[4]*, D. Hemmers*[4]*, C Stelzmann*[4]*, G Pretzler*[4]

[1]Helmholtz Institut Jena, D-07743 Jena, Germany; [2]Centre for Plasma Physics, Queen's University Belfast, Belfast BT7 1NN, United Kingdom; [3]Institut für Optik und Quantenelektronik, FSU Jena, D-07743 Jena, Germany; 4 Institut für Laser- und Plasmaphysik, Heinrich-Heine-Universität Düsseldorf

Intense, femtosecond laser interactions with blazed grating targets are studied through experiment and particle-in-cell (PIC) simulations. The high harmonic spectrum produced by the laser is angularly dispersed by the grating leading to near-monochromatic spectra emitted at different angles, each dominated by a single harmonic and its integer-multiples. The spectrum emitted in the direction of the third-harmonic diffraction order is measured to contain distinct peaks at the 9th and 12th harmonics which agree well with two dimensional PIC simulations using the same grating geometry. This confirms that surface smoothing effects do not dominate the far-field distributions for surface features with sizes on the order of the grating grooves whilst also showing this to be a viable method of producing near-monochromatic, short-pulsed extreme ultraviolet radiation.

The petawatt arm of the VULCAN laser system at the Rutherford Appleton Laboratory, STFC, United Kingdom. A schematicof the experimental setup is shown in Fig. 1. Thelaser delivered ~200 of energy on target in pulses of 700–900 fs FWHM duration after being reflected off a plasma mirror (PM), resulting in an intensity contrast ratio of 10^9 between the main pulse and the nanosecond-long amplified spontaneous emission. The laser was focused on a target at normal incidence by an f/3 of-axis parabolic mirror. While exponential spectra were always observed from 5–10 µm thick foil targets, narrow-band features in proton and heavier ion spectra were obtained from submicrometer-thick targets irradiated at high intensities. For example, the spectra in Fig. 1(b), from a 100 nm thick Cu target irradiated by a LP (p polarization) laser pulse at a peak intensity of 3 10^{20} Wcm^{-2}, show narrow-band peaked features in the proton (charge to mass ratio Z/A = 1) and carbon (Z/A = 0.5) spectra, clearly separated from a lower energy component (as usual in standard interaction conditions, protons and carbon ions observed in the spectrum originate from surface contaminant layers).

The appearance and position of distinct peaks in the ion spectrum could be controlled by varying laser and target-parameters as shown in Figs. 2(a) and 2(b). Peaks were observed only in the limit of thin foils and high intensity [Fig. 2(a)] with the peaks shifting towards higher energy as either the intensity was increased or the target thickness was reduced [Fig. 2(b)]. In order to assess the possible influence of radiation pressure effects on the spectral profiles observed, a simple analytical model was developed taking into account the hole boring (HB) and LS phases of the RPA mechanism. The position of the peak energy is reproduced well by the model and shows the characteristic scaling for RPA with $E_{ion} \sim (a_0{}^2\tau/\chi)^2$.

In conclusion, we have reported on the observation ofnarrow-band features in the spectra of laser-accelerated ions, which appear to be consistent with radiation pressure acceleration, in a regime where LS overcomes sheath acceleration. This work has been published in New Journal of Physics [1].

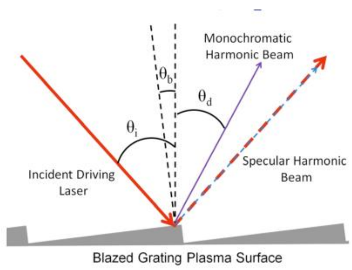

Figure 1: (a) Schematic Schematic of harmonic generation from blazed grating surfaces. The high intensity laser pulse ionizes the grating surface and subsequently generates a harmonic spectrum, which is spectrally dispersed due to the grating structure. Matching the blaze condition $\Theta_i - \Theta_d = 2\Theta_b$ or when the diffraction order corresponds to a specular reflection from the groove surface) allows efficient diffraction into a particular diffraction order yielding a near-monochromatic beam consisting of a single harmonic.

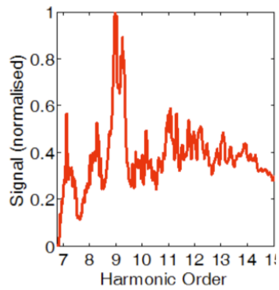

Figure 2: Spectrum showing an enhanced 9th harmonic as expected from PIC simulations. The small number of grooves illuminated in this experiment limits the rejection of neighbouring orders and could be improved with larger spots/higher line density gratings

References

[1] S. Kar et al., Phys. Rev. Lett., 109, 185006 (2012).

Coherent synchrotron emission from electron nanobunches formed in relativistic laser–plasma interactions.

M. Zepf[1,2], B. Dromey[2], S. Rykovanov[3], M. Yeung[2], R. Hörlein[3,4], D. Jung[4,5], D. C. Gautier[5], T. Dzelzainis[2], D. Kiefer[3,4], S. Palaniyppan[5], R. Shah[5], J. Schreiber[3,4], H. Ruhl[3], J. C. Fernandez[5], C. L. S. Lewis[2], B. M. Hegelich[5]

[1]Helmholtz Institut Jena, D-07743 Jena, Germany; [2]Queen's University Belfast, Belfast BT7 1NN, United Kingdom;[3] Ludwig-Maximilians-Universität, Am Coulombwall 1, D-85748 Garching, Germany, [4]Max-Planck-Institut für Quantenoptik, D-85748 Garching, Germany, [5]Los Alamos National Laboratory, New Mexico 87545, USA,

Harmonic radiation produced by intense laser–solid interactions above the plasma frequency have, so far, been consistent with Doppler upshifted reflection from collective relativistic plasma oscillations—the relativistically oscillating mirror mechanism. Recent theoretical work, however, has identified a new interaction regime in which dense electron nanobunches are formed at the plasma–vacuum boundary resulting in coherent XUV radiation by coherent synchrotron emission[1] (CSE). Our experiments enable the isolation of CSE from competing processes, demonstrating that electron nanobunch formation does indeed occur. We observe spectra with the characteristic spectral signature of CSE—a slow decay of intensity, I, with high-harmonic order, n, as $I(n) = n^{-1.62}$ before a rapid efficiency rollover. Particle-in-cell code simulations reveal how dense nanobunches of electrons are periodically formed and accelerated during normal-incidenc interactions with ultrathin foils and result in CSE in the transmitted direction. This observation of CSE presents a route to high-energy XUV pulses and offers a new window on understanding ultrafast energy coupling during intense laser–solid density interactions. our work has recently been published in Nature Physics [2].

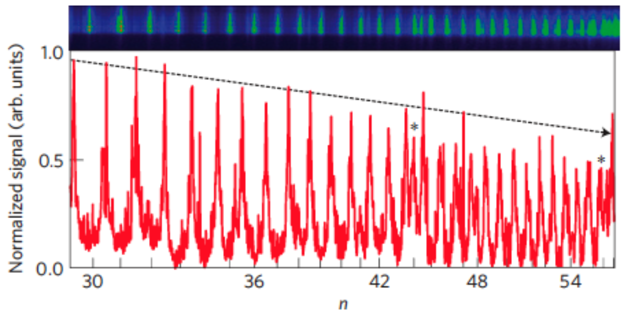

Figure 1: Harmonic spectra in transmission from 200-nm DLC foils. A typical CCD image and spectrum obtained in transmission along the laser propagation axis from 200nm foils (0 mrad to 53 mrad half-cone angle, spectral lines marked with asterisks) collected using an adjustable gold focusing optic.

The experiment was performed on the Trident laser using at Los Alamos National Lab. delivering laser pulses with 80 J in 500 fs at 1053nm. The laser was focused to a near-diffraction-limited focal spot using an F/3 off-axis parabolic mirror. The system has pulse contrast of $1{:}10^{-10}$ at 1 ns and $1{:}10^{-7}$ at 10 ps prior to the peak of the pulse. Figure 1 shows a spectrum taken with an XUV spectrometer. The slow decay to higher orders n with a slope $\sim n^{-1.6}$ is notably shallower from other harmonic sources (such as Relativistic Oscillating Mirror harmonics which decay with $n^{-8/3}$ or faster). Such slow decay is consistent with coherent synchrotron radiation, which is expected under our conditions [1]. Since competing sources can be ruled out under the current conditions [2], the slope and the beamed nature of the harmonics allow us to conclude that coherent synchrotron emission from laser driven foil interactions has been observed for the first time, giving rise to a new, coherent mechanism producing XUV radiation.

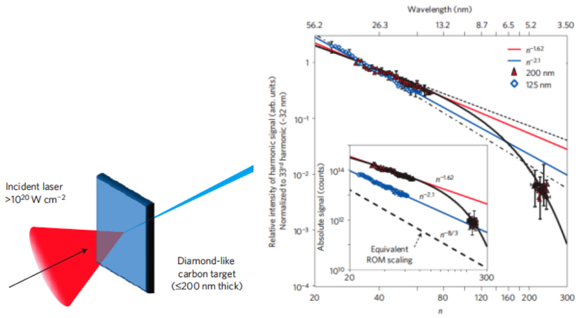

Figure 2: Schematic of the experimental set-up (left) and Harmonic spectra from DLC foils. Harmonics from 200nm (red triangles) and 125nm (open blue diamonds) foils are spatially and spectrally integrated and corrected for system transmission giving best fits of $n^{-1.62}$) and $n^{-2.1}$ respectively, for n<70. The gap in the spectrum is due to spectrometer transmission. The bars represent uncertainty due to shot-to-shot fluctuations and propagation of errors from spectral deconvolution. The dashed ($n^{-1.49}$)) and dot–dashed ($n^{-2.25}$) lines correspond to maxima (for 200 nm) and minima (for 125 nm) fits to the uncertainty for n<70, respectively, and essentially represent the extrema of the total uncertainty for this experiment. The curved solid black line serves as a guide to the spectral shape of the emission from the 200nm foils. The inset shows the absolute count levels for 125nm and 200nm DLC targets and compares these with the relative signal strength expected from a corresponding ROM ($n^{-8/3}$) source. The observed absolute energy in a single harmonic can be estimated as ~200µJ at 20nm (58th harmonic) for 200nm DLC foils and can be considered a lower bound due to the limited detection aperture in our experiment.

References

[1] An der Brügge, D. & Pukhov, Phys. Plasmas 17, 033110 (2010)
[2] B. Dromey et al. Nature Physics, **8**, 804 (2012)

Thomson backscattering from laser-generated, relativistically moving high-density electron layers

A. Paz[1,2], S. Kuschel[1,2], C. Rödel[1,2], M. Schnell[1], O. Jäckel[2], M.C. Kaluza[1,2], and G.G. Paulus[1,2]

[1]Institute of Optik and Quantumelectronics, Friedrich-Schiller-University Jena, Max-Wien-Platz 1, 07743 Jena, Germany; [2]Helmholtz Institut Jena, Fröbelstieg 3, 07743 Jena, Germany

We have implemented an all-optical setup using the Jena Titanium:Sapphire TW laser system (JETI) for Thomson backscattering from a relativistic electron bunch. The main pulse is split into two pulses: one to accelerate electrons from thin aluminium foil targets to energies of the order of some MeV and the other, counterpropagating probe pulse is Thomson-backscattered off these electrons when they exit the target rear side. The highest scattering intensity is observed when the probe pulse arrives at the target rear surface 100 fs after the irradiation of the target front side by the pump pulse, corresponding to the maximum flux of hot electrons at the interaction region. These results can provide time-resolved information about the evolution of the rear-surface electron sheath and hence about the dynamics of the electric fields responsible for the acceleration of ions from the rear surface of thin, laser-irradiated foils.

Introduction

Thomson backscattering involves the collision of laser photons with a relativistic electron beam. The approaching laser pulse and its wavelength appear length contracted by the initial relativistic factor of the electron beam in its frame of reference. Upon interaction, the electrons undergo oscillations in the field of the laser pulse leading to the emission of radiation which is Doppler upshifted when measured in the laboratory frame [1].

By its upshifted frequency the backscattered photons also carry important characteristics of the electron beam such as its energy distribution and effective temperature. Thus, an all-optical Thomson backscattering setup can also be used as an in-situ time-resolved diagnostic for the electron acceleration process [2]. Obtaining a deeper understanding of electron acceleration dynamics is essential to the study of ion acceleration mechanisms.

Experiment

The main JETI pulse is split into two pulses by a dielectric-coated 90/10 beam splitter. 90% of the main pulse energy is used as the pump pulse which accelerates electrons from thin aluminium foil targets to energies of the order of some MeV. The remaining 10% of the main pulse energy is utilised as the counter-propagating probe pulse that scatters off the relativistic electrons as they emerge from the target rear side. The temporal delay between the arrival of the two pulses at the target position is varied by translating the beam splitter normal to its surface. A scan of the pump-probe delay allows for the probing of the temporal evolution of the rear-surface electron sheath produced by the ponderomotive electron acceleration mechanism.

The results show a strong dependence of the scattering yield on the difference between the arrival time of the pump and the probe pulses at the target position, see Fig. 1. The XUV photon yield is at its maximum when the pump pulse interacted with the target front side 100 fs before the arrival of the probe pulse at the target rear surface. At this particular pump-probe delay, the flux and temperature of the electrons accelerated to the target rear side are also at their peak. At longer pump-probe delays, the rear-surface electron sheath has already expanded and cooled down leaving a small number of scatterers to interact with the probe pulse [3]. This is seen as a steady decrease in the signal for increasing positive delays.

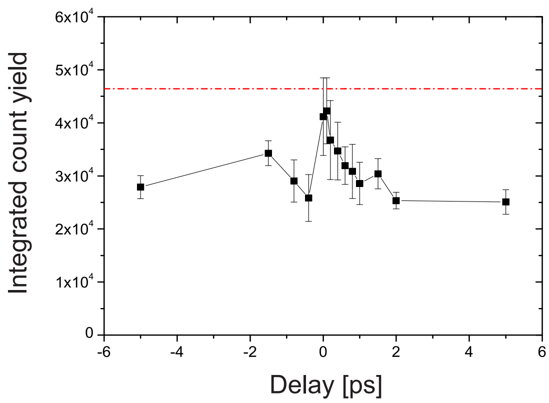

Figure 1: Dependence of the integrated count yield of the XUV signal on the pump-probe delay. A positive delay indicates that the pump pulse hits the target before the probe pulse while the opposite is true for a negative delay. The red dashed line indicates the sum of the XUV count yield due to the pump and the probe pulse.

Furthermore, the energy distribution of the accelerated electrons is also deduced from the Thomson backscattered spectrum. Since for our experimental conditions the escaping hot electron population is generated primarily by the ponderomotive electron acceleration mechanism, the electron energy distribution is expected to be broad with a mean

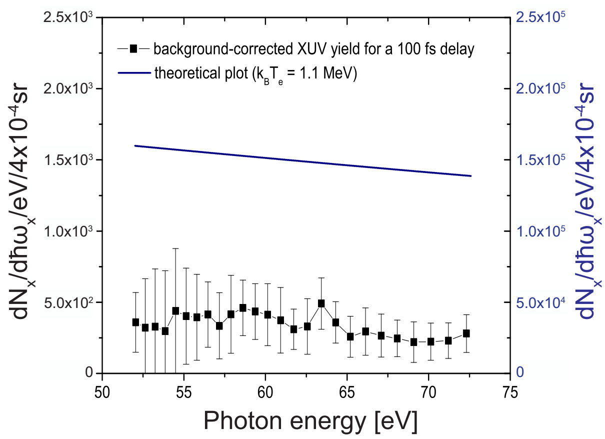

Figure 2: The experimentally obtained XUV spectrum for the case when the pump arrived at the target 100 fs before the probe pulse (black square) superimposed with the theoretical plot for an electron distribution with a mean kinetic energy of 1.1 MeV (blue line). The difference of the photon yield between the two plots can be attributed to the imperfect overlap of the electron beam with the laser pulse in the experiment.

kinetic energy of 1.1 MeV. Consequently, backscattering from this hot electron population produces a broad XUV photon spectrum with Doppler upshifted energies that are greater than 52 eV as seen in Fig. 2 [4].

Conclusion

These results indicate that Thomson backscattering is a powerful diagnostic tool to probe the temporal evolution of the rear-surface electron sheath and hence the ion-acceleration fields.

References

[1] E. Esarey, S. Ride and P. Sprangle, "Nonlinear Thomson scattering of intense laser pulses from beams and plasmas", *Physical Review E* **48** 3003–3021 (1993).

[2] Liesfeld B., "A photon collider at relativistic intensity", *PhD thesis, University of Jena* (2006)

[3] O. Jäckel, J. Polz, S. M. Pfotenhauer, H-P. Schlenvoigt, H. Schwoerer and M.C. Kaluza, "All-optical measurement of the hot electron sheath driving laser ion acceleration from thin foils", *New Journal of Physics* **12** 103027 (2010).

[4] A. Paz, S. Kuschel, C. Rödel, M. Schnell, O. Jäckel, M. C. Kaluza and G. G. Paulus, "Thomson backscattering from laser-generated, relativistically moving high-density electron layers", *New Journal of Physics* **14** 093018 (2012).

Spatially resolved x-ray spectroscopy of laser-heated Titanium at POLARIS

T. Kämpfer[1,2], R. Loetzsch[1,2], I. Uschmann[1,2], O. Jäckel[1,2], J. Polz[2], M. Hornung[1], R. Bödefeld[1], M. Hellwing[2], S. Keppler[2], J. Hein[1,2], M. C. Kaluza[1,2], E. Förster[1]

[1] Helmholtz-Institut Jena, Fröbelstieg 3, D-07743 Jena, Germany; [2] Institut für Optik und Quantenelektronik, Friedrich-Schiller-Universität Jena, Max-Wien-Platz 1, D-07743 Jena, Germany

The interaction of a subpicosecond, high-intensity laser pulse with a solid target produces a high-density plasma on its surface that emits characteristic x-rays of the target material. The spectroscopic analysis of the K-shell emission, in combination with spatial resolution, is a powerful tool to characterize properties of such highly coupled plasmas in the "warm dense matter" (WDM) regime [1, 2]. Furthermore, at relativistic laser intensities electrons are accelerated to high kinetic energies and strong electric and magnetic fields are produced, especially at the interfaces of thin foils. In particular, protons and other ion species are accelerated to MeV energies at the rear side of a thin target due to the so called 'target normal sheet acceleration' mechanism (TNSA). A spectroscopic analysis of the rear side x-ray emission with spatial resolution provides insight into important properties at the rear surface such as temperature, temperature gradients, strong fields, correlations e.g. to proton emission etc..

First experiments, conducted at the POLARIS laser facility in 2012, had the goal of performing K-shell spectroscopy from such thin foil targets (5µm Titanium), combined with a 1-d spatial resolution. To achieve this, $K_{\alpha 1}$ and $K_{\alpha 2}$ emission of Titanium was imaged from the rear side onto an x-ray CCD, which provides a spectral window of 25eV and a 1-dimensional spatial resolution of 7.5 µm. The toroidally bent GaAs crystal spectrometer employed in these experiments is described in [3]. To gain understanding of the acceleration process, ion spectra were simultaneously recorded. In order to separate the x-ray emission from front and rear side, layered foils (front: 2µm Aluminum, rear: 5µm Titanium) were used.

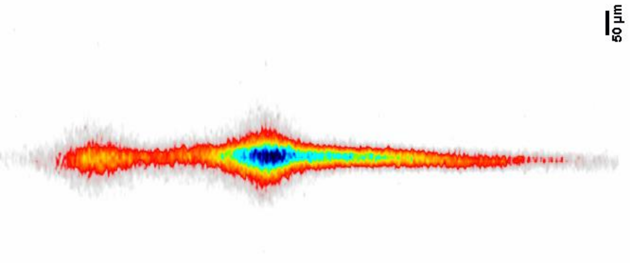

Figure 1: Single-shot K_α emission spectrum of a 5µm Titanium foil, recorded at the POLARIS laser. Strong blue shifted satellite lines are visible in the emission centre (increasing photon energy from left to right, spatial resolution in the vertical direction).

A typical 'single-shot' emission spectrum of a 5µm Ti foil, illuminated with relativistic intensities is shown in Figure 1. The centre of the excited region shows a strong emission of broad and blue shifted satellite lines, indicating high temperatures and densities (WDM). With increasing vertical distance, the emission spectrum reduces to the well known Ti-K_α doublet lines. In order to reconstruct emission spectra as a function of the radial distance, one has to perform an Abel-inversion of the spatially mapped emission profiles (inset of figure 2), since the spectrometer always integrates in the horizontal direction. These measurements indicate electron temperatures of several tens of eV [1, 2] in a region of few tens of microns. With the help of state of the art line-shape calculations one may in the future infer more accurate temperature distributions and may also identify different effects arising from strong electric and magnetic fields.

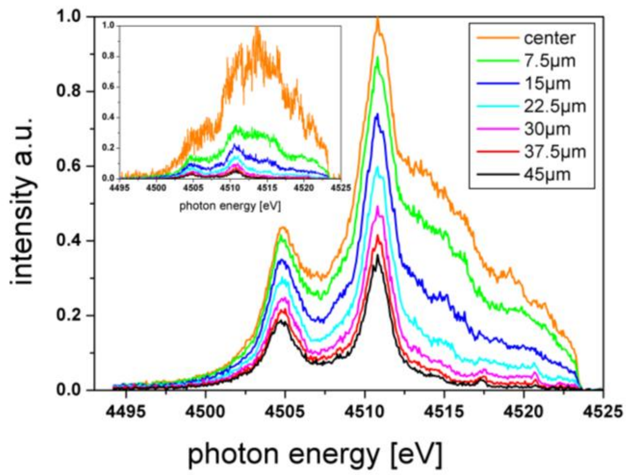

Figure 2: Horizontal line-outs of the recorded K_α emission from a 5µm thin laser heated Titanium foil. Inset: K-shell emission as a function of the radial distance generated by Abel-inversion of the spatially mapped emission profiles.

References

[1] U. Zastrau, P. Audebert, V. Bernshtam, E. Bambrink, T. Kämpfer, E. Kroupp, R. Lötzsch, Y. Maron, Yu. Ralchenko, H. Reinholz, G. Röpke, A. Sengebusch, E. Stambulchik, I. Uschmann, L. Weingarten, E. Förster, Physical Review E 81 (2010), 026406 1-4
[2] E. Stambulchik, *et al.*, J. Phys. A 42 (2009), 214056
[3] F. Zamponi, Dissertation, Friedrich-Schiller Universität Jena, (2007)

A beamline for x-ray laser spectroscopy at the experimental storage ring at GSI

D F A Winters[1], V Bagnoud[1], B Ecker[1,2,] U Eisenbarth[1],

S Gotte[1], Th Küh1[1,2,3,4], P Neumayer[4,5], C. Spielmann[3,6],

T Stöhlker[1,3,6], B Zielbauer[1,3]

1 GSI Helmholtzzentrum für Schwerionenforschung GmbH, Darmstadt, Germany

2 Johannes Gutenberg-Universität, Mainz, Germany

3 Helmholtz Institut Jena, Germany

4 Extreme Matter Institute (EMMI), Darmstadt, Germany

5 Goethe-Universit¨at, Frankfurt am Main, Germany

6 Friedrich-Schiller-Universität, Jena, Germany

1. Introduction

Heavy highly charged ions are unique 'few electron systems' (1-4 electrons) and therefore ideal candidates for a direct comparison between state-of-the-art atomic structure calculations and high-precision measurements. The ground state hyperfine structure of heavy hydrogen-like ions has already been measured directly by means of laser spectroscopy at the Experimental Storage Ring (ESR) at GSI [1]. In summer 2011,also the first direct measurement of the ground state hyperfine structure in a heavy lithium-like ion (Bi80+) has been performed at the ESR [2] (this volume). The fine structure splitting in heavy Li-like ions could, due to the large transition energies, never be studied with available laser systems. Calculations [3] show that the 2s1/2 - 2p1/2 transitions for Li-like elements, with Z between 50 and 95, roughly span the wavelength range between 4 and 12 nm (or 100 and 300 eV). However, with the aid of an X-Ray Laser (XRL), and exploiting the large Doppler shift of the transition wavelength in the ESR, such a laser spectroscopy experiment will be possible. As an example, the Doppler shift due to the relativistic velocities (70% of c) of the stored ions can be _100 eV, which is very large. Since an XRL can produce _65 eV photons (see below), the combination of both yields a photon energy of _165 eV. With this technique also other ground state properties of atomic nuclei, such as masses (or binding energies), charge radii, spins, and nuclear magnetic moments can be inferred [4].

2. Experimental aspects

Since several years x-ray lasers at different wavelengths have been operated successfully at the PHELIX facility at GSI [5]. Here, a set of high-intensity laser pulses is used to create a plasma in a solid target and excite electrons in the ionic states to create a population inversion sufficient for laser operation. The wavelength at which lasing occurs can be varied via the target material. Experimental results from four different targets (period 5 elements): Ag, Pd, Mo, and Zr span the wavelength range between 12 and 24 nm (or 50 and 100 eV), over which they produce rather similar intensities. But more importantly, the laser wavelength is very narrow and known to about one part in 10^4. This is the main reason why such an XRL, and not a much brighter light source (such as an FEL), is most suitable for the proposed studies. Ongoing XRL development focusses on further optimization of high and stable XRL photon numbers. In addition, it is planned to increase the repetition rate of the PHELIX pre-amplifier from 1 shot per 2 minutes, to about 1 shot per 10 seconds.

For an experiment at the ESR, a compact XRL setup needs to be developed, which can be placed directly underneath the ESR beamline in order to minimize XRL beam losses [5]. The IR-light (1 J, 1053 nm) needed to pump the target will come from the PHELIX pre-amplifier and will be transported through a dedicated laser beamline to the ESR hall. This long (ca. 60 m) beamline will be made out of stainless steel tubing and vacuum flanges so that it can be pumped to about 10^{-2} mbar. After transport to the ESR hall, the pump light will be compressed to a short (few ps) pulse in a dedicated double-pass compressor. Another short (5 m) beamline will then transport the compressed IR-beam to the XRL chamber. This setup will contain the target material, which will be irradiated in the so-called butterfly configuration [7], and the required diagnostics (e.g. a CCD camera). One technical challenge is to couple in as much of the XRL-light as possible and still maintain the excellent UHV conditions (10^{-11} mbar) inside the ESR. Therefore, a system of shutter valves, equipped with thin metal filters, and differential pumping through small apertures are being considered.

In addition, a set of rapid shutter valves, equipped with glass windows, allows for a prealignment of the beamline with a visible auxiliary laser, as well as for maintaining the vacuum integrity in case of metal filter damage [8]. The conversion efficiency, i.e. the ratio of ‘energy out’ and ‘energy in’, is about 10^{-6} for this type of XRL. For a pump IR-beam of about 1 J, the emerging ‘spectroscopy beam’ will thus have an energy of about 1 μJ (10^{11} photons). Coupling in and collimation of the XRL-light into the ESR can be achieved with only one 90° off-axis parabola and one flat mirror, both XUV multilayer coated. The overlap between laser and ion beam will be in the middle of the straight section of the ESR. At the end of this straight section an in vacuo XUV-CCD camera will be installed for alignment and diagnostic purposes.

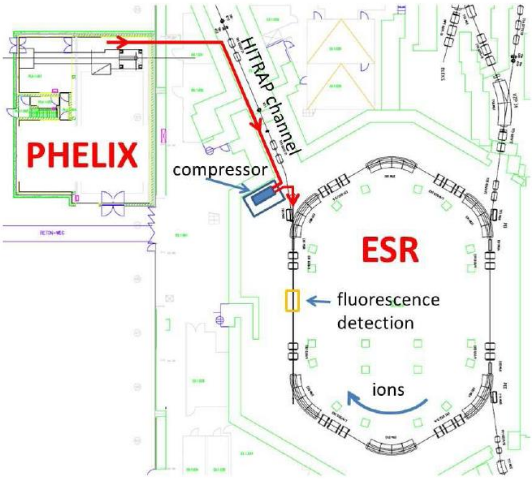

Figure 1 Overview of the two facilities at GSI: PHELIX and ESR. The red line indicates the path of the laser, the blue line that of the ions.

Since the wavelength of the XRL is fixed by the choice of the target, the ion velocity will be scanned such that the transition is probed in small steps, while recording the fluorescence. The results will be a measurement of the central wavelength, its width, and the strength of the resonance (peak height).

Due to the ion’s relativistic velocity, the fluorescence of the laser excited Li-like ions will be emitted in a forward cone (searchlight), which renders the need for a dedicated detection system. Since the 2p - 2s decay is very fast (E1 transition), the fluorescence immediately follows excitation. The best spectroscopy scheme is then to create only a few meter long ion bunches (14 ns long), which will be timely excited by the XRL pulses, and to detect the fluorescence directly afterwards, i.e. within the interaction region of about 1 m length. Detection will therefore be done in vacuo in the middle of the ESR’s straight section, using a metal collector, extraction and focussing electrodes, and a micro-channel plate (MCP) detector. The fluorescence is in the XUV domain and will release low energy electrons from the metal, which will then be guided by electrodes onto the MCP. Simulations have shown that the collection efficiency is about 5%, and the detection efficiency about 70%. An important aspect here is that the ion beam can be stored in the ESR for several tens of minutes, but then a new injection is required. During the ‘loading’ cycle of the ESR, the detection system must be retracted. Therefore, the whole detection system must be able to move (linearly) in and out of the path of the ion beam.

This new and technically challenging project will be carried out in close collaboration with the Helmholtz Institut Jena. There are also good collaborations with the universities of Münster (detection system), Darmstadt (data acquisition), and Jena (laser development).

References

[1] P. Seelig, Th. Kühl et al., Phys. Rev. Lett. 81, 4824 (1998).
[2] W. Nörtershäuser, D.F.A. Winters, Th. Kühl et al., GSI beamtime application (2008).
[3] W.R. Johnson et al., At. Data. Nucl. Data. Tables 64, 279 (1996).
[4] E.W. Otten, Treatise on Heavy-ion Sciences, D.A. Bromley ed. Vol. 8 (1988), p.515-638 Plenum Press, New York.
[5] V. Bagnoud et al., Appl. Phys. B 100, 137 (2010)
[6] D. Winters et al., Physics Scripta to be published
[7] B. Ecker et al., ICXRL 2012 - Paris, France, conference proceeding (2012), Springer-Verlag, Berlin Heidelberg New York.
[8] B. Zielbauer et al., ICXRL 2012 - Paris, France, conference proceeding (2012), Springer-Verlag,Berlin Heidelberg New York.

Compact cryogenic liquid droplet beam source for relativistic laser-plasma generation

R. A. Costa Fraga[1], *A. Kalinin*[1], *M. Kühnel*[1], *D. C. Hochhaus*[2,3], *A. Schottelius*[1], *J. Polz*[4], *M. C. Kaluza*[4,5], *P. Neumayer*[2,3], *and R. E. Grisenti*[1,6]

[1]Institut für Kernphysik, J. W. Goethe-Universität, Max-von-Laue-Str. 1, 60438 Frankfurt am Main, Germany; [2]ExtreMe Matter Institute EMMI and Research Division, GSI Helmholtzzentrum für Schwerionenforschung, Planckstr. 1, 64291 Darmstadt, Germany; [3]Frankfurt Institute for Advanced Studies, J. W. Goethe-Universität, Ruth-Moufang-Str. 1, 60438 Frankfurt am Main, Germany; [4]Institut für Optik und Quantenelektronik, Max-Wien-Platz 1, 07743 Jena, Germany; [5]Helmholtz-Institut Jena, Helmholtzweg 4, 07743 Jena, Germany; [6]GSI Helmholtzzentrum für Schwerionenforschung, Planckstr. 1, 64291 Darmstadt, Germany

The interaction of ultrashort laser pulses with solid targets allows producing extreme conditions that are relevant to tabletop particle accelerators and laboratory astrophysics. Here, the laser energy is initially transferred to the target via the generation of relativistic electrons. However, the usually large dimensions of the employed targets, flat thin foils of mm^2 to cm^2 size, allow the hot electrons to spread transversely leading to a significant reduction of the energy density in the target, thus precluding the efficient heating of the target material. Rayleigh droplet beams, produced by expanding a liquid through a micrometer-sized orifice into vacuum, are extremely attractive with respect to the above applications because, when the Rayleigh instability is induced by an intentionally applied excitation, the triggered breakup process delivers a perfectly periodic stream of identical, isolated droplets at rates of up to several MHz, thereby enabling detailed scaling studies under highly reproducible conditions.

However, the stable generation of periodic droplet beams of cryogenic elements such as hydrogen and argon, which represent the most scientifically relevant target systems for many potential applications, proves challenging. The high vapor pressure at the triple point of liquid argon and hydrogen results in very efficient evaporative cooling upon vacuum expansion. The expanding liquid filament thus rapidly cools below its normal melting point and freezes well before Rayleigh breakup can take place[1].

We have developed a compact injection source that addresses the above drawbacks delivering stable, periodic droplet beams of the cryogenic gases hydrogen and argon ideally suited for novel studies on relativistic laser-plasma generation[2]. At the heart of our droplet injector, shown in Fig. 1a, is the use of a glass capillary that is inserted into an outer glass capillary tube. As the liquid jet emerges from the inner capillary it expands in an axially co-flowing gas plenum that suppresses evaporative cooling. An important aspect of the source described here is the challenge of working at cryogenic temperatures. In our design the typical distance between the inner capillary orifice and the outer tube exit hole is adjusted down to ~ 1 mm (Fig. 1a). This feature allows significantly reducing the interaction time of the droplets with the co-flowing gas, which is held responsible for the degradation of the droplet spatial stability observed in previous studies. Figures 1b,c show periodic beams of monodisperse argon and hydrogen droplets of diameter ≈ 21 μm and ≈ 13 μm, respectively, jetting from the outer tube exit hole in vacuum. We have shown that our triggered droplet beams exhibit the necessary spatial stability, with a mean relative displacement that ensures a nearly ideal overlap between the laser pulse and the droplet[2, 3].

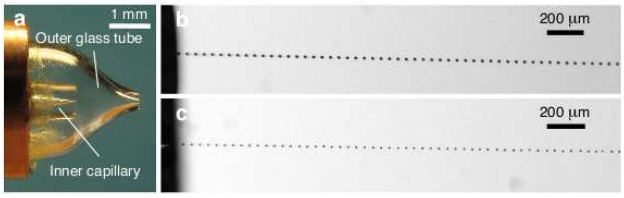

Figure 1: (a) Enlarged view of the exit end of our cryogenic droplet injector evidencing the outer glass tube and the central inner capillary. (b), (c) Stroboscopic images of periodic argon (b) and (c) hydrogen droplet beams propagating in vacuum.

The capability of our droplet injector has been recently demonstrated at the PHELIX laser facility by employing an argon droplet beam as target[3]. In particular, the K-shell spectra obtained from the argon droplets irradiated with energetic laser pulses provide evidence for extensive ionization of the M-shell with the creation of charge states of up to 14+, indicating an elevated bulk temperature. A more in-deep analysis of the x-ray spectra hints to a heating mechanisms beyond the pure collisional heating, with an additional, ultra-fast contribution resulting from ohmic dissipation effects in the mass-limited droplet[3]. These results thus clearly demonstrate the potential of our cryogenic droplet injector to open up new exciting studies of matter under extreme conditions.

References

[1] M. Kühnel *et al.*, Phys. Rev. Lett. **106**, 234501 (2011).

[2] R. A. Costa Fraga, *et al.*, Rev. Sci. Instrum. **83**, 025102 (2012)

[3] P. Neumayer, *et al.*, Phys. Plasmas **19**, 122708 (2012)

Experiments at FLASH: temporal diagnostic tool

R. Riedel[1,2]*, A. Al-Shemmary*[3]*, M. Gensch*[4]*, T. Golz*[3]*, M. Harmand*[3]*, N. Medvedev*[6]*, M. J. Prandolini*[1]*, K. Sokolowski-Tinten*[5]*, S. Toleikis*[3]*, U. Wegner*[3]*, B. Ziaja*[6,7]*, N. Stojanovic*[3]*, F. Tavella*[1]

[1]Helmholtz-Insitut Jena, Germany; [2]University of Hamburg, Germany; [3]DESY, Hamburg, Germany; [4]Helmholtz-Zentrum Dresden-Rossendorf, Germany; [5]Faculty of Physics and Center for Nanointegration Duisburg-Essen (CENIDE), Germany; [6]Center for Free-Electron Laser Science Hamburg, Germany; [6]Center for Free-Electron Laser Science Hamburg, Germany; [7]Institute of Nuclear Physics, Kraków, Poland.

The development of temporal diagnostic techniques for free-electron lasers is a very active field of research. Pulse duration measurement methods for XUV free-electron lasers (FEL), such as XUV autocorrelation or THz streaking are difficult experiments to perform (see references in [1]). A simple technique for the characterization of temporal properties of the pulses would be highly desirable. SASE FELs also suffer from large shot-to-shot pulse arrival time fluctuations at the experiment. Thus, the temporal resolution and the reproducibility of pump-probe experiments are limited. Temporal properties of a SASE FEL need to be fully monitored to perform precise pump probe experiments.

Plasma switch for temporal diagnostics at free-electron lasers

To overcome this limitation, we have developed a single-shot temporal diagnostic tool that utilizes a solid-state plasma switch as optical cross-correlator [1]. This technique is based on a technique used to find the temporal overlap between an optical laser and the FEL for pump probe experiments [2]. An intense XUV pulse is incident under a shallow angle on a solid-state target and generates a high electron density within the conduction band via photo-absorption. This changes the optical properties within the sample surface. Due to the shallow angle, different temporal parts of the FEL wavefront are mapped to different spatial positions on the target. The target surface is probed with an ultrashort optical laser pulse. The measured temporally (and hence spatially) varying change of optical transmission is related to the cross-correlation between the optical pulse, $I_{\mathrm{laser}}(t)$, and the integrated XUV pulse,

$$S(\Delta t) = \int_{-\infty}^{+\infty} I_{\mathrm{Laser}}(t)\; G(t-\Delta t, I_{FEL}(t-\Delta t))\; \mathrm{d}t, \qquad (1)$$

where $G(t) = G(I_{\mathrm{FEL}}(t))$ is the transmission function of the plasma. Detailed theoretical simulations allow us to understand the ionization dynamics within the target material. For our experimental conditions the plasma density, $n_{\mathrm{e}}(t)$, follows almost instantaneously the integrated FEL intensity,

$$n_{\mathrm{e}}(t) \propto \int_{t_0}^{t} I_{\mathrm{FEL}}(t', y)\mathrm{d}t', \qquad (2)$$

which enables us to retrieve the intensity envelope of the FEL pulse. Our experiment was performed on the FEL FLASH at DESY in Hamburg, using two distinct wavelengths, 5.5 nm and 41.5 nm, to demonstrate the versatility of the method. A measurement at 41.5 nm is shown in Figure 1. The measurement is fitted with a calculated cross-correlation curve assuming an FEL pulse with Gaussian temporal distribution of about 184 fs. Furthermore, we showed the possibility to implement the technique as an online tool. This allows carrying out a pump-probe experiment and measuring simultaneously the pulse duration and arrival time of the XUV pulses on a single-shot basis. The temporal resolution of the measurement will be further improved by using shorter probe pulses. Future experimental campaigns at FLASH and at FERMI will determine the robustness of this method for future implementation at the FLASH-2 FEL as an online tool.

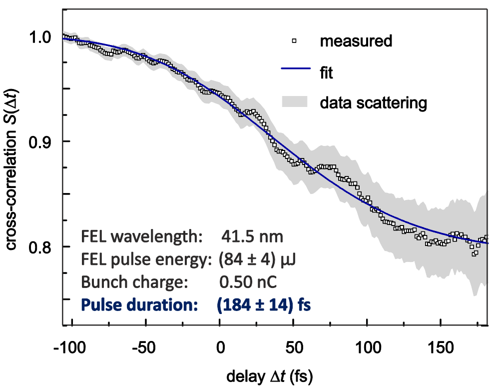

Figure 1: Cross-correlation on a fused silica target. Measured (white dots) and fitted (blue line) curve at 41.5 nm FEL wavelength. The obtained FEL pulse duration is (184 ± 14) fs. The grey data scattering originates from small fluctuations in spatial beam profile (optical laser and FEL).

References

[1] R. Riedel *et al.*, *Nature Comm.* DOI: 10.1038 (2013).

[2] M. Harmand *et al.*. *J. of Instr.* DOI: 10.1088/1748-0221/7/08/ P08007 (2012).

Controlled interaction of ions with high-intensity laser light

M. Vogel[1,2], *W. Quint*[2,3], *G. Paulus*[4], *and Th. Stöhlker*[2,4,5]

[1]TU Darmstadt; [2]GSI, Darmstadt; [3]Ruprecht Karls-Universität Heidelberg; [5]Helmholtz-Institut Jena; [4]Universität Jena

We are currently preparing an experimental setup which features a Penning trap for preparation and control of suitable ion targets for irradiation with high-intensity laser light and study of subsequent reactions. Of particular interest is the detailed investigation of multiphoton-ionisation of confined particles by highly intense laser light. One important aspect is control over the confined particles' mass, charge, density, localization and optimized overlap with the laser light by Penning trap techniques like the use of trap electrodes as 'electrostatic tweezers' and by application of a 'rotating wall', respectively. Also, the non-destructive detection of reaction products is a central property. The Penning trap setup is designed in a portable fashion, such that it can be attached to existing laser systems easily [1].

The interaction of highly intense radiation with matter and the corresponding non-linear effects have been subject of lively research, both theoretical and experimental, especially in the infrared and visible photon energy regimes. Laser systems capable of producing high intensities also at photon energies in the extreme ultra-violet (EUV) and (soft) X-ray regime open access to novel effects like non-linear Compton effects or simultaneous elastic and inelastic photon scattering, and allow multiphoton-ionisation experiments in a new domain. However, experiments have so far not been able to prepare and investigate well-defined particle ensembles and to non-destructively analyse the reaction products with high accuracy, nor were they able to select or prepare products for further studies in a well-defined way.

The particles (atomic or molecular ions) are confined in the Penning trap following in-trap production or capture of externally produced ions. Confined ions can be cooled, compressed, positioned and selected with respect to their mass and charge prior to laser irradiation. The reaction products are analysed by non-destructive methods and hence remain confined for further studies. Such measurements are, for example, able to determine cross sections for multiphoton-ionisation in an energy- and intensity- regime so far not or not sufficiently examined. Additionally, the created electrons may be extracted from the trap and analysed externally. Hence, the reaction energetics may be reconstructed as completely as possible.

Figure 1 shows an example of a multiphoton ionization study using these techniques: ions are dynamically loaded into the trap from external sources or produced in the trap by electron impact or laser ionization (A). One or more specific ion species are selected (B), these ions are then cooled, compressed by a rotating wall and positioned. Thus, the ion target is well-prepared for interaction with the high-intensity laser. During and following the laser interaction, the charge state evolution of the confined ions is monitored

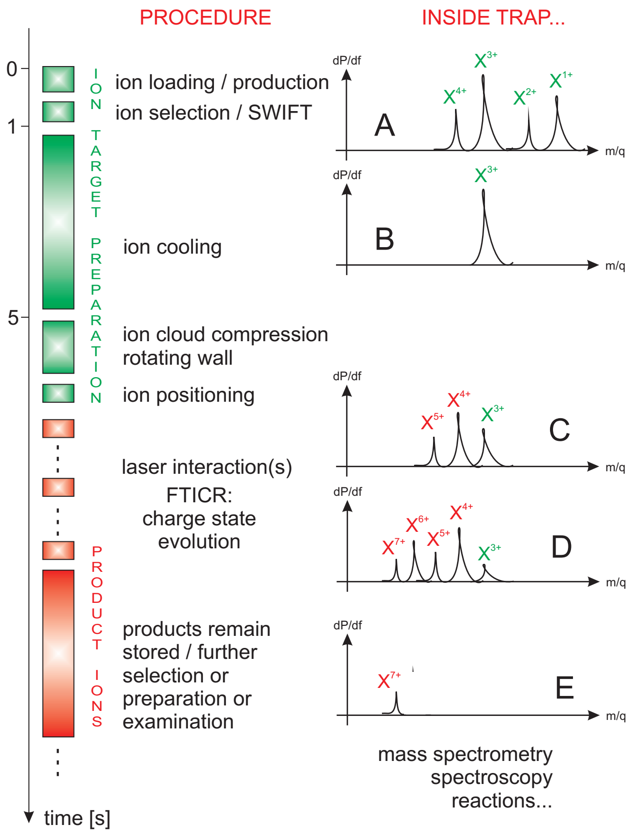

Figure 1: Example of an experimental timing scheme for a study of multiphoton ionization. The individual durations are meant to reflect the typical order of magnitude. The right hand side shows the corresponding mass-to-charge spectra of the trap content, for details see text.

by FT-ICR-spectrometry (C and D). Specific product ions can be selected and remain stored for further use (E).

Ion positioning along the experimental axis has some interesting features when a focused laser is considered since it allows to determine the position of the focus with high resolution. At the same time, especially for strongly focused lasers, ion positions can be chosen such that the reaction takes place at different field intensities and thus allows a study of the reaction as a function of laser field intensity without the need to change laser parameters.

References

[1] M. Vogel, W. Quint, Th. Stöhlker and G.G. Paulus, Nucl. Inst. Meth. B **285**, 65 (2012).

Ion momentum distributions from strong-field ionization of atomic ions using linearly and elliptically polarized laser light

P. Wustelt[1,2], M.Möller[1,2], T. Rathje[1,2], A.M. Sayler[1,2], D. Hoff[1,2], S. Trotsenko[1], T. Stöhlker[2,3], G.G.Paulus[1,2]

[1]Helmholtz Institute Jena, Germany, [2]Institute of Optics and Quantum Electronics, Jena, Germany, [3]GSI, Darmstadt, Germany

Strong-field ionization of atoms is of central importance for many phenomena like laser-based electron or ion acceleration by ultra-intense laser pulses. At relativistic intensities laser pulses ionize the target atoms or molecules to high charge states in a multi-photon multi-electron process. We have performed a series of experiments where the multi-electron dynamics during the strong-field ionization of atomic ions in linearly and elliptically polarized laser fields is probed by measuring the momentum distribution and charge state of the ions that result from the multi-photon ionization.

Experimentally, we use the newly developed ion beam apparatus, see Fig. 1, together with a high-power laser system that delivers 10 mJ, 35 fs at a repetition rate of 1 kHz. The ion beam is produced by a duoplasmatron ion source or an EBIT (electron beam ion trap). The duoplasmatron produces a dense ion beam with ion currents up to several µA, but low charge states. The EBIT provides the option to start from different initial charge states of the same atom and to isolate the effects of each ionization step. From the ion source, the ion beam with a kinetic energy of several keV is guided through a series of Einzel lenses, a Wien filter, deflectors and pinholes in order to produce a dense and collimated beam at the interaction point with the laser. After photo ionization, the full three dimensional momentum distribution and charge state of the ions are measured using a position- and time-sensitive detector together with external electric fields that separate the initial and final charge states in space and time.

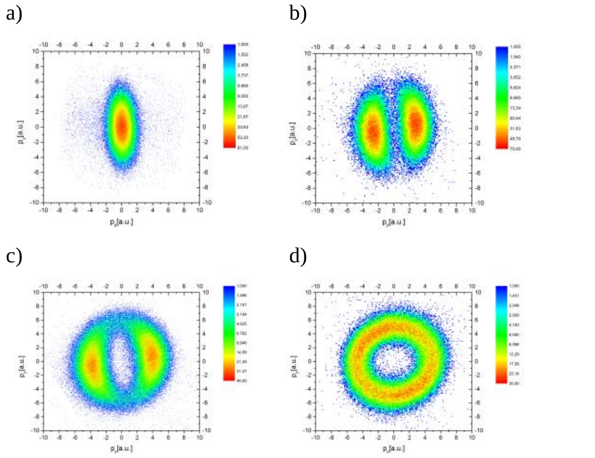

Figure 2: Ion momentum distribution of single ionization of Ne^+. for different ellipticities ε from linear to nearly circular: a) linear, b) ε=0.5 c) ε=0.75 d) ε=0.95

Status of the project: The ion beam setup is routinely operated during dedicated beam times of the laser system. In 2012, momentum and charge state distributions of ions resulting from the ionization of singly charged Xenon, Neon and Helium are studied as a function of intensity and ellipticity of the laser pulses. With a new focusing geometry, peak intensities up to $5{\cdot}10^{16}$ W/cm² are reached such that highly charged ions up to Xe^{8+}, Ne^{5+} and He^{2+} can be observed. From the measured ion momentum distributions, the multi-photon multi-electron dynamics is reconstructed and compared to classical trajectory Monte-Carlo simulations that are performed and compared with the experimental results

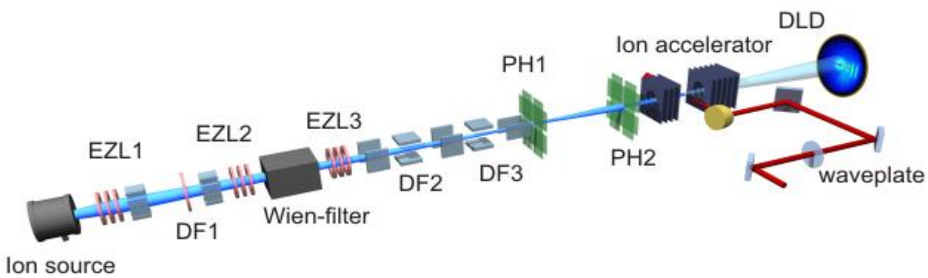

Figure 1: Experimental setup of the ion beam apparatus, which includes a duoplasmatron ion source, Einzel lenses (EL1-2), a Wien filter (WF), deflector plates (DF1-3), pinholes (AP1-2), an ion accelerator for ion separation in time and a delay-line detector (DLD). The laser pulses are focused perpendicular to the ion beam in the apparatus after the polarization is modified by wave plates.

Two-electron one-photon transition in Li-like Bi

S.Trotsenko[1,2], *A. Gumberidze*[3], *K. Sosnova*[4], *E. Rozenbaum*[4], *M. Lestinsky*[2], *and Th. Stöhlker*[1,2,5]

[1]Helmholtz-Institut Jena, Jena, Germany; [2]GSI, Darmstadt, Germany; [3]ExtreMe Matter Institute/GSI, Darmstadt, Germany; [4]Sankt-Petersburg University, Sankt-Petersburg, Russia; [5]Friedrich-Schiller-University Jena, Germany

We report on experimental study of the decay properties of $1s(2s^2)$ state in Li-like bismuth (Z=83), adopting a state selective K-shell ionization technique [1]. This state is expected to undergo predominantly an exotic $1s(2s)^2 \rightarrow (1s)^2 2p_{1/2}$ two-electron one-photon decay (TEOP) [2, 3], which is interesting because of its sensitivity to electron correlation effects. In the high-Z ions the $1s(2s^2)$ state can also decay to the ground $(1s)^2 2s$ state via a radiative magnetic dipole M1-transition. The strong variation of the decay properties of the states along the isoelectronic sequence is an ideal testing ground for our understanding of the interplay of electron correlation and relativistic effects in a few-electron ions.

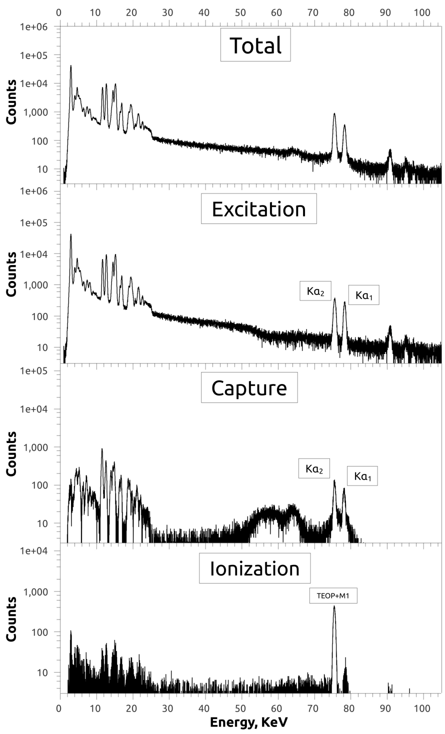

Figure 1: Preliminary x-ray spectra recorded for $Bi^{79+} \rightarrow N_2$ (see text for details).

The experiment was performed at the ESR (GSI) with 98 MeV/u Be-like bismuth ions colliding with a gas jet target (N_2). The x-rays produced in this process (see Fig. 1) were measured under an angle of 35° with respect to the propagation direction of the ion beam (for details concerning the setup see [1]). By the coincident registration of x-rays with the charge state of the ions after the collision, few different radiative processes can be separated: K-shell excitation of the Be-like ions, the radiative electron capture and the formation of excited states of the Li-like ions produced by K-shell ionization. As can be seen in the ionization spectrum (Fig 1:Ionization), K-shell ionization appears to be a very selective population process, because in the associated photon spectrum only one single x-ray line is observed stemming from the decay of the $1s(2s^2)$ state.

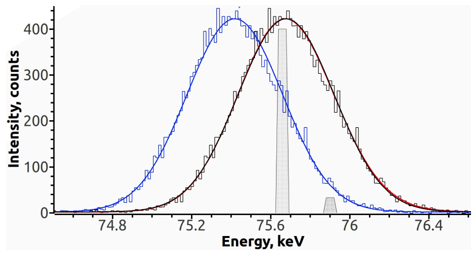

Figure 2: Preliminary analysed ionization spectrum peak; blue steps / blue line: the peak position defined by radiative sources calibration/ the corresponding fitting curve; black steps / black line: the peak position obtained by the calibration based on the theoretical Kα1 and Kα2 lines / the corresponding fitting curve; grey boxes: theoretical predictions for the TEOP (left) and M1 (right) transitions with the widths corresponding to the theoretical uncertainties; red line: convolution of the theoretical predictions [3].

The energy separation between the two transitions of interest, TEOP[$1s(2s^2) \rightarrow (1s)^2 2p_{1/2}$] and M1[$1s(2s^2) \rightarrow (1s)^2 2s_{1/2}$], is close to 250 eV in the emitter frame. Due to the lack of high resolution x-ray detectors within the current investigation, the goal of the current data analysis is to determine M1/TEOP branching ratio, i.e. the contamination of the TEOP by the M1 decay, using an accurate line centroid determination of the observed x-ray line. Apart from a conventional method utilising an accurate calibration of the detector with radioactive sources, a complementary calibration method was used based on corresponding energies of the Kα1- and Kα2-lines, produced by excitation (Fig. 1:Excitation), as an energy reference. The latter provides an important cross-check for the Doppler corrections to be applied. This, however, is based on the assumption that K-shell excitation of the Be-like ions occurs to the $1s(2s)^2 p_{3/2}$ and $1s(2s)^2 p_{1/2}$ levels exclusively. Preliminary results are presented in the Fig. 2, suggesting a dominance of the TEOP over the M1 transition. The data analysis is in progress.

References

[1] J. Rzadkiewicz et al., Phys. Rev. A 74, 012511 (2006)

[2] C. Z. Dong et al., J. Phys. B: At. M. Op. Ph. 39, 3121 (2006).

[3] A. Volotka and Y. Kozhedub, Private communication.

QED IN EXTREME FIELDS BY X RAYS FROM HIGH-Z IONS *

H.F. Beyer[1], *D. Banaś*[2], *K.-H. Blumenhagen*[8], *F. Bosch*[1], *C. Brandau*[4], *W. Chen*[1], *Chr. Dimopoulou*[1], *E. Förster*[3,8], *T. Gaßner*[1], *A. Gumberidze*[4], *S. Hagmann*[1,5], *R. Heß*[4], *P.-M. Hillenbrand*[1], *P. Indelicato*[6], *P. Jagodzinski*[2], *T. Kämpfer*[8], *Chr. Kozhuharov*[1], *M. Lestinsky*[1], *D. Liesen*[1], *Yu.A. Litvinov*[1], *R. Loetzsch*[8], *B. Manil*[7], *R. Märtin*[8], *F. Nolden*[1], *N. Petridis*[4,5], *M.S. Sanjari*[1], *K.S. Schulze*[8], *M. Schwemlein*[1], *A. Simionovici*[10], *U. Spillmann*[1], *M. Steck*[1], *Th. Stöhlker*[1,8], *C.I. Szabo*[6], *M. Trassinelli*[10], *S. Trotsenko*[8], *I. Uschmann*[3,8], *G. Weber*[8], *O. Wehrhan*[3,8], *N. Winckler*[1], *D. Winters*[1], *N. Winters*[1], *and E. Ziegler*[11]

[1]GSI Helmholtzzentrum, Darmstadt, Germany; [2]Institute of Physics, Swietokrzyska Academy, Kielce, Poland; [3]Inst. für Optik und Quantenelektronik, F. Schiller-Universität, Jena, Germany; [4]Extreme Matter Institute, EMMI, GSI Helmholtzzentrum, Darmstadt, Germany; [5]Institut für Kernphysik, Goethe-Universität, Frankfurt am Main, Germany; [6]Lab. Kastler Brossel, Université P. et M. Curie, Paris, France; [7]Laboratoire de Physique des Lasers (LPL) UMR 7538 CNRS - Université Paris 13, Villetaneuse, France; [8]Helmholtz-Institut Jena, Jena, Germany; [9]LGIT, Observatoire des Sciences de l'Univers de Grenoble, Grenoble, France; [10]Institut des Nanosciences de Paris, Université Pierre et Marie Curie-Paris 6 and CNRS-UMR 7588, Paris, France; [11]ESRF, Grenoble, France

The ground-state electron in a heavy hydrogen-like ion is exposed to the extraordinarily strong electric field of the nucleus providing the testing ground for bound-state quantum electrodynamics (QED) in extreme fields. The QED contribution to the 1s binding energy is accessible via accurate spectroscopy of the hard x rays comprising the Lyman spectrum.

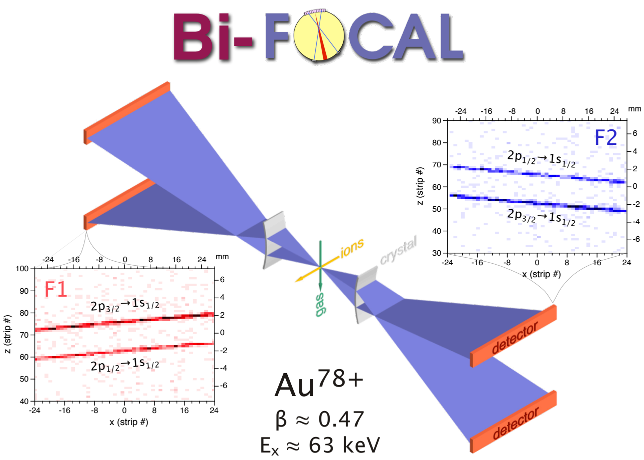

Figure 1: Two crystal-spectrometers, Bi-FOCAL, symmetrically arranged around the ion beam at the ESR gas jet. The Lyman-α spectra of Au^{78+} appear as slanted lines in the position-sensitive x-ray detectors.

A twin crystal-spectrometer assembly, Bi-FOCAL, operated in the **FO**cusing **C**ompensated **A**symmetric **L**aue geometry has been arranged for accurate x-ray spectroscopy at the ESR gas jet as schematically depicted in figure 1 [1]. The spectrometer system equipped with two 2D position-sensitive Ge strip detectors was operated for the first time in a beam time of three weeks.

It could be demonstrated that the newly developed crystal optics in concert with the position sensitive detectors can cope with the low count-rates of only about 6 events per hour encountered. Background could be effectively reduced by proper shielding facilitated by the existence of a polychromatic focus and by making use of the time and energy resolving capabilities of our detectors applied in particle – x-ray coincidences. As a result, the Lyman spectra of hydrogen-like Au^{78+}, as seen in the insets of figure 1 and as a projected spectrum in figure 2, reveal an impressively low background.

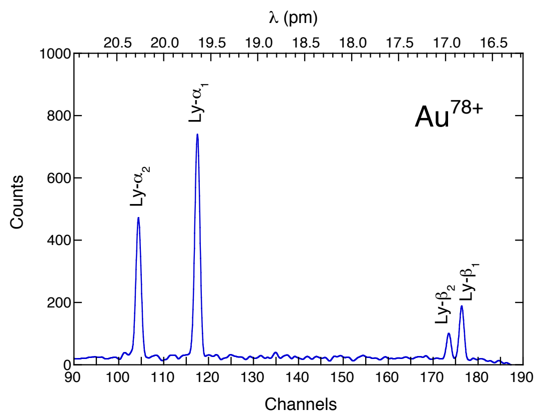

Figure 2: The Lyman-α and -β doublets of Au^{78+} obtained by projection of the 2D intensity distribution.

The slanted lines observed in figure 1 are in accordance with the underlying x-ray-optical design. This way spectral resolving power can be retained also for fast moving sources. Coming in pairs the x-ray optics provide Doppler cancellation capabilities. In the experiment the Lyman-α_1 line was Doppler tuned to the position of the 63.1-keV gamma-ray line emitted from a radioactive sample of ^{169}Yb used as a calibration source. From a detailed analysis of the line positions will be extracted an accurate value of the 1s binding energy and thus of the 1s Lamb shift.

We thank the Institut für Kernchemie of the Johannes Gutenberg-Universität, Mainz, for the preparation of our calibration sources.

[1] H.F. Beyer *et al.*, Spectroch.Acta Part B **64** (2009) 736.

* Work supported by EU and EURONS contract No. 506065. D. Banas acknowledges the support by the Polish Ministry of Science and Higher Education under Grant No. N N202 46353.

CYLINDRICALLY BENT GERMANIUM CRYSTALS FOR SPECTROSCOPY OF INTRA-SHELL TRANSITIONS IN U^{90+}

O. Wehrhan[1,2], *I. Uschmann*[1,2], *H. Marschner*[2], *E. Förster*[1,2], *and H.F. Beyer*[3]

[1]Helmholtz-Institut Jena, Jena, Germany; [2]Institut für Optik und Quantenelektronik, Friedrich-Schiller-Universität, Jena, Germany; [3]GSI Helmholtzzentrum, Darmstadt, Germany

Quantum electrodynamic and relativistic effects in the strong field of a very heavy nucleus can be studied in highly charged two-electron ions by an accurate spectroscopy of the respective n=2→2 transitions. For U^{90+} the wavelength of the corresponding x rays is near 2.7 Å and can be accomodated by a Ge (220) crystal employed in a Johann spectrometer. A preliminary experiment of this type has already been conducted using stored highly charged uranium ions in the ESR storage ring at GSI [1]. The accuracy of the experiment was limited by an asymmetry observed in the x-ray line shape. A culprit for that could be imperfections of the analyzer crystal used. Indeed the x-ray topography taken of the crystal after the experiment revealed strong inhomogeneities. Therefore a continuation of the experiment is only meaningful with much improved crystals.

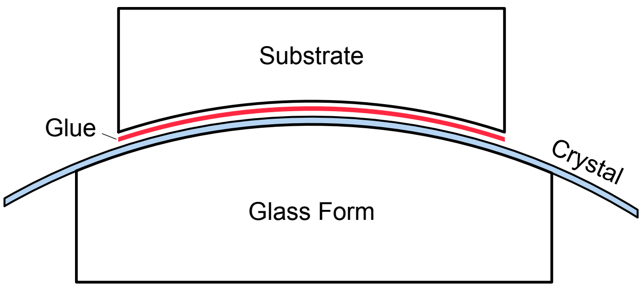

Figure 1: Method of bending a crystal to a cylindrical form. The polished crystal is wrung to a cylindrical glass form of high-quality finish which predetermines the geometrical form. After gluing the crystal with its rear side to another glass form the front glass form is detached.

Consequently, a total of four high-quality cylindrically bent crystals of dimension $50 \times 25 \times 0.12$ mm^3 and a radius of curvature of 2 m have been produced and characterized. The method of bending employed, is schematically illustrated in figure 1. The prepared and polished crystal slab is wrung to a cylindrical glass body with a highly accurate cylindrical finish that defines the geometrical shape of the crystal. After gluing the crystal with it's rear side to another glass substrate, the crystal is shaped to the required size of it's large surface and thereafter detached from the front glass form.

There is still one degree of freedom, that is the choice of the crystal's azimuthal rotation. The latter has been optimized such as to minimize possible influences of Umweg excitations. For that purpose calculations of multiple diffractions have been carried out with the aid of the XOP software [2]. It turned out that in the interesting region of Bragg angles Umweg excitation can be widely avoided. Only when in use with the calibration source in second order of diffraction it can not be totally diminished.

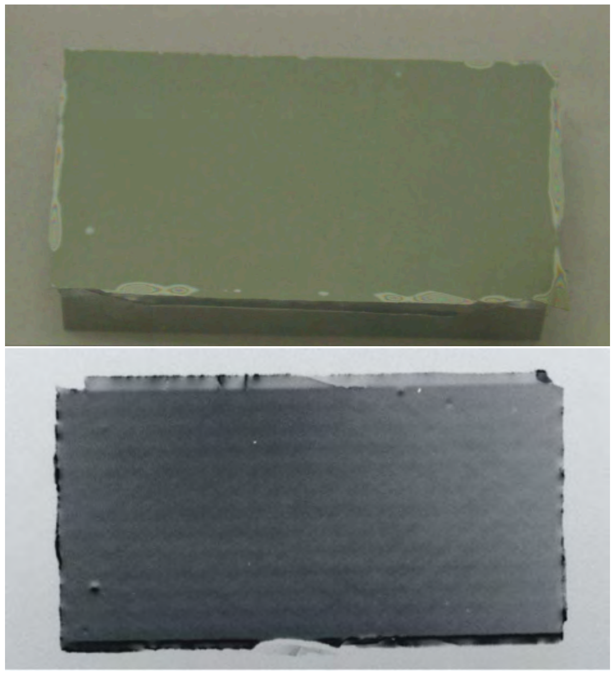

Figure 2: One of the crystal specimens shown as an optical photography (top) and as an x-ray topography (bottom) obtained with Cu-Kα radiation in a von-Hàmos geometry.

As a final quality test x-ray topographies were taken with Cu-Kα radiation in a von-Hàmos and in a Rowland geometry. In figure 2 both, an optical photography and the result of a von-Hàmos topography is displayed revealing a single spot in the lower left corner of the crystal due to an isolated adhesive imperfection. Otherwise the crystal is free of distortions in the central part that is going to be used in the spectrometer. The curved Ge crystals are mounted and prealigned in crystal modules which will be part of the crystal spectrometers to be assembled. Subsequently, a number of test measurements with prototype spectrometers will be performed.

References

[1] M. Trassinelli *et al.*, European Physics Letters **87** (2009) 63001.

[2] M. Sanchez del Rio: XOP, X-ray Oriented Programs, ESRF Grenoble.

Characterization of a novel setup for hard x-ray spectroscopy and polarimetry at very high fluxes

G. Weber[*1,2], *C. Hahn*[1,3], *A. Paz*[1,3], *and R. Märtin*[1,2]

[1]HI-Jena, Jena, Germany; [2]GSI, Darmstadt, Germany; [3]IOQ, FSU, Jena, Germany

X-ray spectroscopy is a powerful tool for the diagnosis of plasmas being produced in fusion devices, celestial objects and in the interaction of high-power lasers or ion beams with matter. It is also known that radiative processes like bremsstrahlung, radiative recombination and characteristic transitions occurring in plasmas may exhibit distinct anisotropic and polarization features. In general, an anisotropic plasma tends to produce polarized radiation, and by photon polarimetry and/or angular resolved measurements one can investigate the anisotropic, and thus non-thermal features of the plasma [1, 2].
While single photon spectroscopy up to roughly 20 keV can be performed using standard x-ray CCD cameras, precise studies in the hard x-ray regime are often hampered by the lack of adequate detector technology. This is due to extremely high fluxes in combination with low repetition rates being typically found at plasma sources which generate x-rays up to the MeV regime, e. g. high-power laser facilities. Here, the operation of standard unsegmented, large-volume detectors leads to photon pile-up in the detector or requires unrealistic long acquisition times in order to obtain single photon spectra. Thus, state-of-art studies of hard x-ray spectra originating from plasmas still rely on low-precision techniques like stacks of several filter materials in front of an image plate [3]. However, with the recent development of pixelated CdTe sensors equipped with the Timepix readout chip [4, 5], energy-resolving detectors have become available that combine a high granularity comparable to x-ray CCDs with the high-stopping power of a high-Z detector material.

In this report, we present a setup optimized for Compton spectroscopy and linear polarimetry of incident x-rays up to a few hundred keV based on such detector systems, see Fig. 1. Here, two 1 mm thick CdTe detectors with up to 256×256 pixels record the radiation which is Compton scattered within a low-Z target. Compton spectroscopy aims for the reconstruction of the incident x-ray spectrum from the spectral distribution of the scattered photons and is in particular well-suited for fluxes being too high to expose the detector directly to the incident radiation [6]. As for photon energies below about 1 MeV the Compton cross section varies only slightly, the efficiency and consequently the amount of flux reduction of the scattering setup is mainly determined by geometry, namely the solid angle covered by the CdTe detectors. Similarly, the spectral broadening due to the dependence of the scattered photon energy on the longitudinal Compton scattering angle ϑ can be adjusted.

* g.weber@gsi.de

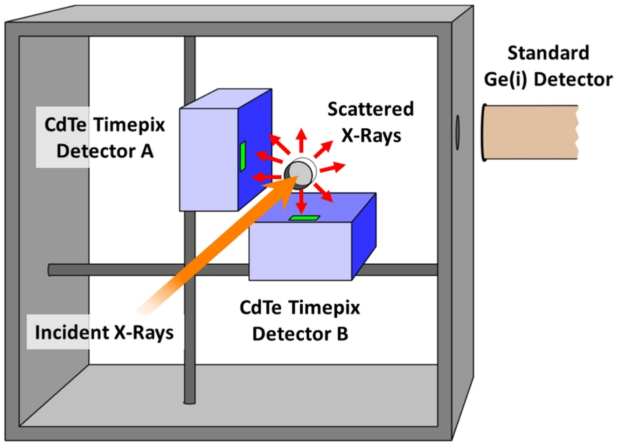

Figure 1: Setup for Compton spectroscopy and polarimetry consisting of two pixelated CdTe detectors and a scatter target, as it was used in the test measurement at DESY.

Moreover, the degree of linear polarization P_L of the incident radiation can be obtained by means of Compton polarimetry, which is based on the asymmetry of the scattered photon emission pattern with respect to the azimuthal scattering angle φ, see [7]. Assuming that the CdTe detectors are located at 0° and 90° with respect to the incident photon electric field vector, the linear polarization is given by $P_L = M(N_{0^\circ} - N_{90^\circ})/(N_{0^\circ} + N_{90^\circ})$, with M denoting the modulation factor depending on the photon energy and the experimental setup. If the orientation of the polarization is unknown, this quantity can also be obtained by rotation the detectors around the scattering target.
Recently the setup from Fig. 1 was used in a test measurement at the PETRA III synchrotron facility at DESY where high-intensity, highly polarized photon beams between 50 and a few hundred keV were impinging on the scatter target. The analysis of the obtained data is still ongoing.

References

[1] D. Giulietti and L. A. Gizzi, La Rivista del Nuovo Cimento **21**, 1 (1998).

[2] *Plasma polarization spectroscopy* edited by T. Fujimoto and A. Iwamae, Springer (2008).

[3] B. R. Maddox et al., Rev. Sci. Instrum. **82**, 023111 (2011).

[4] X. Llopart et al., NIM A **581**, 485 (2007).

[5] P. Cermak et al., NSS '08. IEEE, 444 (2008).

[6] H. I. Amols et al., NIM A **227**, 373 (1984).

[7] F. Lei et al., Space Sci. Rev. **82**, 309 (1997).

Energy Calibration of Pixelated CdTe Detectors Based on the Timepix Chip

C. Hahn[1,2], *A. Paz*[1,2], *and G. Weber*[1,3]
[1]Helmholtz Institute Jena, Germany; [2]FSU, Jena, Germany; [3]GSI, Darmstadt, Germany

Spatially- and energy-resolved imaging of hard X-ray radiation with active detector systems has gained growing importance in recent years. When operated with high-Z detector materials, the Medipix2 family of ASIC readout chips, in particular its Timepix derivative, constitutes a comparatively small and versatile member of this detector class [1, 2]. Two $1\ \mathrm{mm}$ thick CdTe sensors equipped with Timepix readout chips, manufactured at FMF, Freiburg, are being employed at HI-Jena. The detectors have $128 \times\ 128$ pixels with a size of $55\ \mu\mathrm{m}$, and $256 \times\ 256$ pixels with a size of $110\ \mu\mathrm{m}$, respectively. As each pixel features its own amplifier and output circuitry, variations in the response of different pixels occur. The devices are capable of performing measurements of either arrival time, event counting, or deposited energy, depending on the selected mode of operation. However, efficient use of their energy measurement function requires energy calibration of each pixel [3].

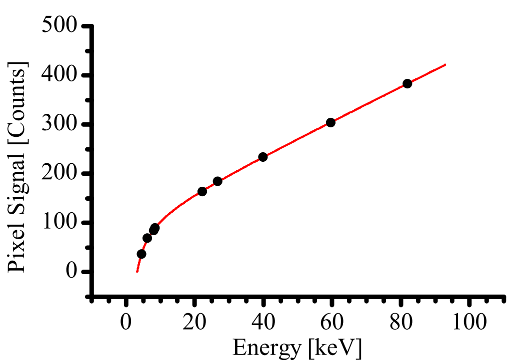

Figure 1: Energy–signal dependence of a sample Timepix pixel, derived from fitting the marked measuring points.

The general dependence of a pixel's signal on the detected energy is outlined in Figure 1. Note its deviation from linear behavior near the threshold. The mathematical relationship between signal and energy follows the equation [3]

$$f(E) = a \cdot E + b - \frac{c}{E - t}$$

and may be inverted for energies greater than the low-energy threshold t, providing a way to deduce the energy detected in a pixel from its signal as long as its characteristic parameters a, b, c and t are known.

We therefore performed a series of calibration measurements to obtain a reliable estimate of each pixel's signal when irradiated with a given energy, using the K_α lines of various materials and the γ lines of Americium and Barium.

Subsequent calculations and analysis algorithms were implemented using the MATLAB environment [5], which offers numerous appropriate high-level functions as well as excellent array operation capabilities. For every pixel we compiled spectra of its signal, with the restriction that we disregarded events of adjacent pixels also returning a signal, thus eliminating some of the cases where the incident photons were absorbed incompletely in the pixel of interest.

Using a program derived from O'Haver's peak fitting routine [4], the corresponding peak position for every radiation source was localized in each pixel's spectrum. Adjusting the above-noted mathematical relationship to these measuring points, the corresponding set of which is marked for the example pixel used in Figure 1, yielded the parameters needed for an energy calibration curve of each pixel. Figure 2 exemplifies this by juxtaposing ^{241}Am γ ray spectra as measured with a Timepix device before and after calibration. The need for pixel-wise calibration is illustrated by the non-overlapping peaks of single- and double-pixel events in the uncalibrated spectrum, both being combined in a single peak after calibration.

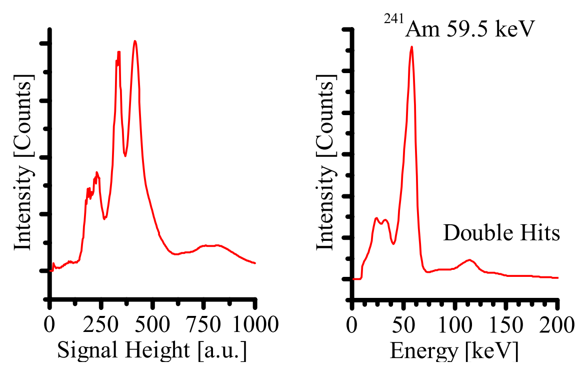

Figure 2: ^{241}Am γ ray spectra, measured with a Timepix device, before (left) and after calibration (right).

References

[1] X. Llopart, M. Campbell, R. Dinapoli, D. San Segundo and E. Pernigotti, IEEE Trans. Nucl. Sci. **49** (2002) 2279

[2] X. Llopart, R. Ballabriga, M. Campbell, L. Tlustos and W. Wong, Nucl. Instr. and Meth. A **581** (2007) 485

[3] J. Jakůbek, Nucl. Instr. and Meth. A **633** (2011) S262

[4] T. O'Haver, http://terpconnect.umd.edu/˜toh/spectrum/

[5] MATLAB Release 2010b, The MathWorks, Inc., Natick, Massachusetts, United States

Monte Carlo simulations of novel Compton polarimeter systems based on semiconductor and calorimeter technology

K.-H. Blumenhagen[*1,2,3], *A. Fleischmann*[4], *R. Märtin*[1,2], *G. Weber*[1,2], *and Th. Stöhlker*[1,2,3]

[1]GSI, Darmstadt, Germany; [2]HI-Jena, Germany; [3]IOQ, University of Jena, Germany; [4]KIP, University of Heidelberg, Germany

Compton polarimetry has proven to be a powerful tool to measure the linear polarization of hard x-rays. In the GSI atomic physics department, several polarization measurements have been carried out using a lithium-drifted silicon (Si(Li)) double-sided strip detector (DSSD) [1,2,3,4]. This detector system works efficient in a photon energy range of about 60 keV a few 100 keV. An extension to higher energies can be achieved by using a heavier detector material, providing a higher Compton cross section and also a higher stopping power. For the low-energy region of about 20 keV to 80 keV, an entirely new concept for Compton polarimetry is proposed: the polarimeter consists of a low-Z cylindrical scatterer and - around it - a ring of high-Z absorber plates. Both the scatter target and the absorbers will work as high-resolution microcalorimeters which are a novel development of the "Magnetic Calorimeters" group in Heidelberg [5]. In this work, the efficiencies of both polarimeter systems have been investigated in Monte Carlo simulations using EGS5 [6]. A Ge(i) DSSD, that can cover higher x-ray energies, was studied using simulation techniques as presented in [7]. For the microcalorimeter-polarimeter, an entirely new EGS5 code was written.

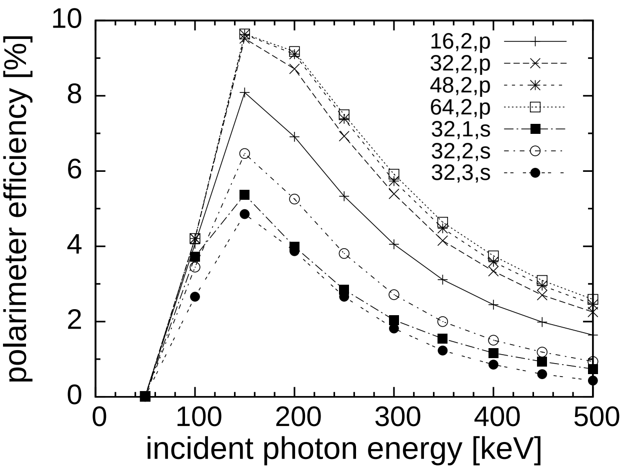

Figure 1: DSSD results. Legend format: number of strips, detector thickness [cm], incidence spread (p=no, s=yes).

The Ge(i) detector consists of a single crystal segmented into n_x vertical and n_y horizontal 1 mm wide strips resulting in a quadratic pseudo-pixel structure of 1 mm^2 size. The parameters varied n_x (always $n_y = n_x$) and the detector thickness (z-direction). First, results were obtained for a point-like (p) incidence in the center of the detector, then the incoming photons were spread over the detector area (s). Results are shown in figure 1.

For the microcalorimeter polarimeter, the following geometry has been considered: the scattering cylinder had a diameter and length of 1 mm. The area of the absorber plates (here: gold) facing the scatterer was 1 mm by 1 mm, their thickness 0.2 mm. The radius of the absorber ring was dervied from the requirement that one absorber covers the longitudinal scatter angle range of $\theta = 90^\circ \pm \Delta\theta$. The angular acceptance $\Delta\theta$ was choosen here according the number of absorbers to minimize the gaps between them. So far, three configurations have been simulated: 40 absorbers and $\Delta\theta = 3.5^\circ$ with (1) a beryllium and (2) a carbon scatterer, and (3) 31 absorbers and $\Delta\theta = 5.8^\circ$ with a carbon scatterer. Figure 2 shows the microcalorimeter simulation results.

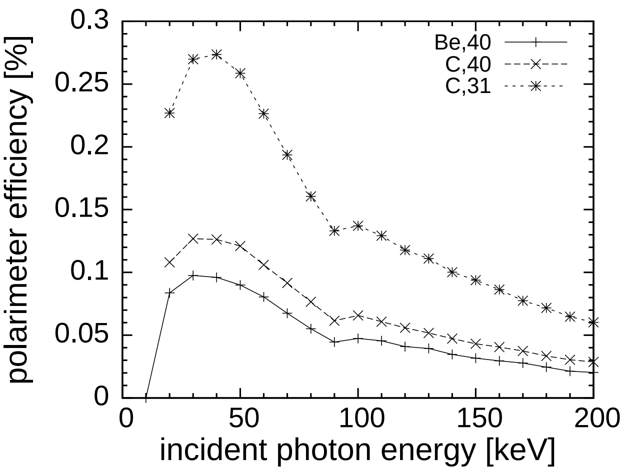

Figure 2: Microcalorimeter results. Legend format: scatterer material, number of absorbers.

* k.-h.blumenhagen@gsi.de

References

[1] H. Bräuning et al., AIP Conference Proceedings, 1099, 117-120 (2009).

[2] G. Weber et al., PRL 105, 243002 (2010).

[3] G. Weber et al., JINST 5, C07010 (2010).

[4] R. Märtin et. al, PRL 108, 264801 (2012).

[5] C. Pies et al., Journal of Low Temperature Physics, 167, 3-4, 269-279 (2012).

[6] H. Hirayama et al. (2005), `http://rcwww.kek.jp/research/egs/egs5_manual/slac730-070620.pdf`.

[7] G. Weber et al., Physica Scripta, T144, 014034 (2011).

Characterization of a Si(Li) Compton polarimeter for the hard x-ray regime, using synchrotron radiation.*

M. Schwemlein[1,2,3], K.-H. Blumenhagen[4,5], A. Gumberidze[1,6], R. Märtin[4,5], N. Schell[7], U. Spillmann[8], G. Weber[4,5], and Th. Stöhlker[4,5,8]

[1]ExtreMe Matter Institute EMMI and Research Division, Darmstadt, Germany, [2]PI, Universität Heidelberg, Germany, [3]Staatliches Seminar für Didaktik und Lehrerbildung, Heidelberg, Germany, [4]Helmholtz-Institut Jena, Germany, [5]IOQ, Universität Jena, Germany, [6]Frankfurt Institute for Advanced Studies, Frankfurt, Germany, [7]Helmholtzzentrum Geesthacht, Germany, [8]GSI, Darmstadt, Germany

Novel highly-segmented semiconductor detectors which combine a good detection efficiency, energy and time resolution, together with millimetre to sub-millimetre position sensitivity, represent a versatile tool for Compton polarimetry in the hard x-ray regime [1]. Such detection systems have recently been introduced for the investigation of radiative processes involving high-Z ions in collisions with gaseous matter at the storage ring ESR [2,3,4] as well as in electron-atom collisions at the TU Darmstadt [5].

In the present experiment, a novel Si(Li) Compton polarimeter [6], which was developed for experiments at the international FAIR facility, has been tested at the DESY PETRA III beamline P07-EH1. For this purpose, the detector was exposed to the synchrotron radiation. Since the synchrotron radiation is nearly 100% linearly polarized, we were able to test the detector performance as an x-ray polarimeter for photons in the hard x-ray regime.

Figure 1 shows the Si(Li) detector response to the incident synchrotron radiation. The monochromator of the beamline was set to 57.3 keV. The clearly visible line at 161.1 keV could be identified as the third harmonic. The broad structures at lower energies belong to recoil electrons of the Compton-scattered photons.

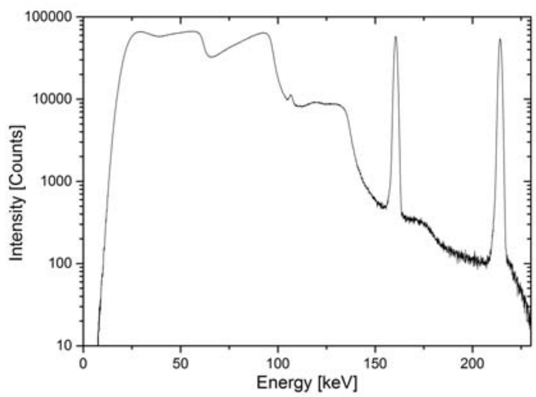

Figure 1: Si(Li) detector response to the incident synchrotron radiation.

Figure 2 shows the position distribution of Compton scattered photons inside the Si(Li) detector crystal. In this case, only the 161.1 keV incident photons of Figure 1 and only polar scattering angles of 90°+-10° are taken into account. The incoming x-ray beam was centred on the centre of the detector. Compton recoil electrons (spot in the centre of Figure 2) have been detected in coincidence with the corresponding Compton scattered photons. To reconstruct the whole kinematic process, each pair of Compton-electron and Compton-photon has been quantified in position and energy.

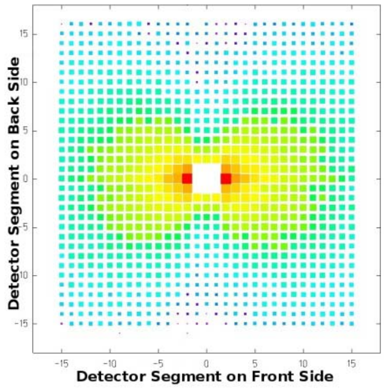

Figure 2: The position distribution of Compton scattered photons inside the Si(Li) detector crystal for 161.1 keV incident photons. The strong anisotropy indicates the high degree of linear polarization of the incident synchrotron radiation.

According to Klein-Nishina equation, the photons are scattered mostly perpendicular to the incident photon electric field vector (polarization axis). This is clearly reflected in the strong azimuthal anisotropy of Figure 2, which indicates a very high degree of linear polarization, typical for synchrotron radiation facilities. The degree of linear polarization as well as the polarization orientation of the incident radiation can be reconstructed apllying a least-squares adjustment to the azimuthal scattering distribution [7].

We have acquired the Compton scattering data for different x-ray energies as well as different detector orientations. The evaluation is currently under way.

References

[1] U. Spillmann et al., Rev. Sci. Instr. **79**, 083101 (2008).
[2] S. Tashenov et al., PRL **97**, 223202 (2006).
[3] S. Hess et al., J. Phys.: Conf. Ser. **163,** 012072 (2009)
[4] G. Weber et al., PRL **105**, 243002 (2010).
[5] R. Märtin et al., PRL **108**, 264801 (2012).
[6] G. Weber et al., JINST **5**, C07010 (2010)
[7] F. Lei et al., Space Sci. Rev.**82**, 309 (1997)

* Work supported by Helmholtz Alliance EMMI.

RECENT IMPROVEMENTS OF A CRYOGENIC CURRENT COMPARATOR (CCC) FOR FAIR

R. Geithner, R. Neubert*, W. Vodel, and P. Seidel*
*Friedrich-Schiller-University Jena, Helmholtzweg 5, 07743 Jena

A non-intercepting detection of high brightness, high intensity primary ion beams as well as low intensities of rare isotope beams is required for the high-energy transport beam lines at FAIR [1]. The expected beam currents in these beam lines are in the range of few nA up to several µA. The CCC optimally fulfils the requirements for the FAIR beam parameters [2].

The total intrinsic noise of the complete CCC is composed by the intrinsic noise of the SQUID itself and its electronics as well as the magnetization noise of the embedded coils. The current spectral density $\langle I^2 \rangle$ of a coil at a temperature T could be calculated with the Fluctuation-Dissipation-Theorem (FDT) and the measured frequency dependent serial inductance L_S (ν) respectively serial resistance R_S (ν) in the equivalent circuit diagram of a real coil, whereas R_S (ν) represents the total losses:

$$\langle I^2 \rangle = 4k_B T \int \frac{R_S(\upsilon)}{\left(2\pi\upsilon\left(L_{SQUID} + L_S(\upsilon)\right)\right)^2 + \left(R_S(\upsilon)\right)^2} d\upsilon \quad (1)$$

Based on the results of preliminary investigations cores of nanocrystalline ferromagnetic Nanoperm M764-01 [3] with an outer diameter of 260 mm, an inner diameter of 205 mm and a width of 97 mm were ordered. After welding the single-turn toroidal niobium winding the coil was characterized at 4.2 K in a customized wide-neck cryostat.

Noise measurements were performed using a SQUID System *"SQUID Control 5.3"* of Jena University. The output voltage noise density of the SQUID electronics was measured by an HP 35670A dynamic signal analyzer. The Nanoperm pick-up coil was shielded against external magnetic fields using two niobium pots fitted into each other. The DESY-CCC pick-up coil was already enclosed into the meander-shaped shielding during the noise measurements.

The measured current noise density of the Nanoperm pick-up coil (see (a) in Fig. 1) is lower by a factor of 2 - 5 than the current noise density of the DESY-CCC pick-up coil with an amorphous core of Vitrovac 6025F [4] (see (d) in Fig. 1).

The noise was decreased to 35 pA/Hz$^{1/2}$ compared to 110 pA/Hz$^{1/2}$ at 7 Hz and to 2.7 pA/Hz$^{1/2}$ compared to 13.3 pA/Hz$^{1/2}$ at 10 kHz. The total noise of the Nanoperm coil is calculated to be 1.2 nA in the frequency range from 0.2 Hz to 10 kHz. In the case of the DESY-CCC pick-up coil the predictions from the FDT (see (e) in Fig. 1) matches very well to the noise measurements.

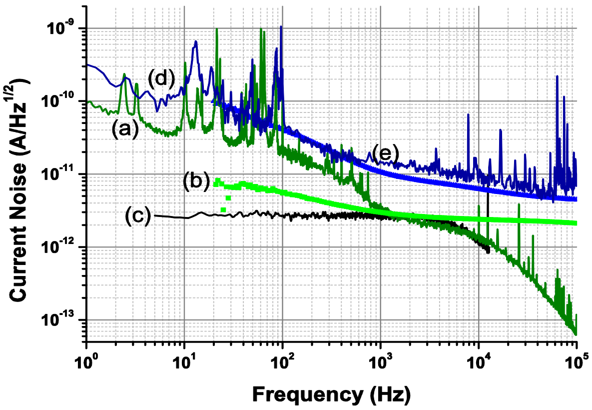

Fig. **1**: Measured (a) and calculated (b) current noise of the welded pick-up coil with Nanoperm M-764-01 core as well as the measured current noise of the SQUID sensor **(**c) compared with the measured (d) and calculated current noise of DESY-CCC with Vitrovac 6025 F.

The CCC has shown its capability as beam monitor for high energy ions as well as electrons. With the usage of the presented material Nanoperm M-764-01 the current noise density of the pick-up coil was reduced by a factor of two to five. With the increased attenuation factor of the meander-shaped shielding a further noise reduction in the low frequency range up to 1 kHz should be possible. This would allow the detection of beam currents below 1 nA.

[1] "FAIR", Conceptual Design Report, Darmstadt, 2000, http://www.gsi.de/GSI-Future/cdr

[2] R. Geithner, R. Neubert, W. Vodel, P. Seidel, K. Knaack, S. Vilcins, K. Wittenburg, O. Kugeler, and J. Knobloch, Rev. Sci. Instrum. 82 (2011) 013302

[3] MAGNETEC GmbH, Industriestrasse 7, D-63505 Langenselbold, Germany

[4] VACUUMSCHMELZE GmbH & Co. KG, Grüner Weg 37,D-63450 Hanau, Germany

The S-EBIT for precision experiments at HITRAP within the FAIR/SPARC collaboration

S. Trotsenko[1,2], *G. Vorobjev*[2], *W. Enders*[2], *D. Racano*[2], *D. Hoff*[1,3], *Y. Ke*[4,5], *T. Mohamed*[4], *A. Gumberidze*[6], *F. Herfurth*[2], *Th. Stöhlker*[1,2,3], *and R. Schuch*[4]

[1]Helmholtz-Institut Jena, Jena, Germany; [2]GSI Helmholtzzentrum, Darmstadt, Germany; [3]Inst. für Optik und Quantenelektronik, F. Schiller-Universität, Jena, Germany; [4]Fysikum, Stockholm University, AlbaNova, Stockholm, Sweden; [5]Shanghai EBIT Laboratory, Institute of Modern Physics, Fudan University, Shanghai 200433, China; [6]ExtreMe Matter Institute, EMMI, GSI Helmholtzzentrum, Darmstadt, Germany

The high voltage electron beam ion trap S-EBIT [1] shall provide highly charged ions - ultimately fully stripped heaviest ions up to uranium - for precision experiments and also serve as a development platform for SPARC experiments at the future FAIR facility [2].

According to an agreement between Stockholm University and Helmholtz Institute Jena, the S-EBIT should be transferred for a series of experiments over an extended period of time, to start with for 5 years with the option to extend for a longer time period, to the Helmholtz Institute at Jena within the framework of the FAIR/SPARC collaboration.

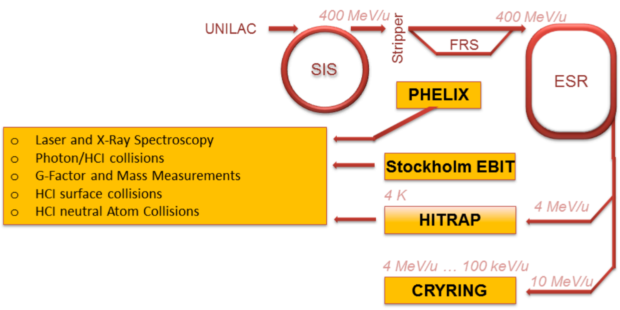

Figure 1: Schematic of experimental arrangements related to the HITRAP along with the main physics topics (for description compare text).

The S-EBIT will be installed and commissioned at the experiment platform of the HITRAP facility [3], where it will not only be used as a standalone device but also serve as a source of highly charged heavy ions for HITRAP (Fig. 1 and Fig. 2). This is of particular importance for the FAIR related shutdown period (2014 through 2017), where virtually no beam time will be provided for SIS18/ESR and consequently for the HITRAP facility.

The S-EBIT will provide extracted medium Z ions up to about Z=66 with sufficient intensities, allowing to perform a unique physics program and to make use of the available experimental infrastructure of HITRAP as well as of the novel instrumentation provided by the HI-Jena [4]. In addition, the important R&D projects related to FAIR, such as tests of spectrometers, position sensitive detectors operating in UHV environment and so on can be conducted which are of particular relevance for the first available facility of the FAIR project, the CRYRING@ESR [5]. Moreover, first experiments with highly-charged ions in intense laser fields can be carried out (PHELIX) at the HITRAP location.

Along with the S-EBIT, a high current plasma source CHORDIS will be built up, which would provide isotope clean singly charged ions for further charge breeding in the EBIT. For that a sophisticated extraction scheme with a charge cleaning magnet and a time-of-flight section for charge breeding diagnostics will be build up.

For the operation of the source and the whole beam extraction and transport system, the control system is being upgraded/developed based on the CS3.1. The control system will continuously monitor the temperature of the superconducting coils, the vacuum, the emission and collector current, the anode current and the power consumption of the high voltage power supply. Besides that, the control system will allow coupling with the data taking in S-EBIT experiments, which ultimately would allow implementation of an event-by-event mode.

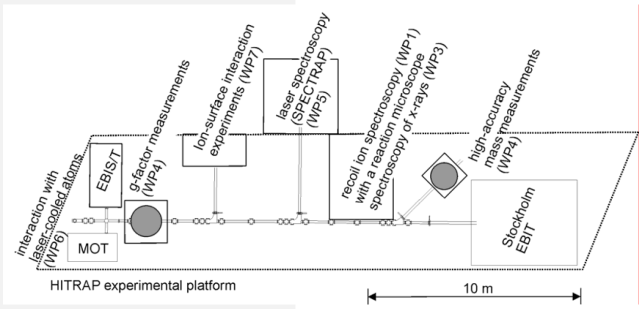

Figure 2: Available and upcoming experimental setups, dedicated to slow highly-charged heavy-ions as provided by the HITRAP and the S-EBIT.

All available components of the S-EBIT have been shipped by now to GSI and the assembling of the machine at the HITRAP platform is on-going.

References

[1] R. Schuch et al., JINST 5, C12018 (2010).

[2] The international FAIR Project, http://www.fair-center.de/; The SPARC collaboration, http://www.gsi.de/sparc.

[3] T. Beier et al., Adv. in Quant. Chem., Vol 53, 83-98 (2008).

[4] M. Vogel et al., Nucl. Inst. Meth. B 285, 65 (2012).

[5] M. Lestinsky et al., CRYRING@ESR: A study group report, (2012).

The CRYRING@ESR Project

F. Herfurth[1], M. Lestinsky[1], R. Bär[1], A. Bräuning-Demian[1], S. Litvinov[1], O. Dolinskii[1], W. Enders[1], M. Engström[2], B. Franzke[1], O. Gorda[1], A. Källberg[2], Y. Litvinov[1], A. Simonsson[2], J. Sjöholm[2], M. Steck[1], Th. Stöhlker[1,3,4], G. Vorobjev[1], N. Winckler[1]

[1]GSI, Darmstadt, Germany; [2]MSL, Stockholm University, Stockholm, Sweden; [3]HI-Jena, Germany; [4]IOQ, University of Jena, Germany

The low energy storage ring LSR shall provide low energy, highly-charged ions and antiprotons at FAIR used by two collaborations, SPARC and FLAIR, for precision experiments. The LSR is a Swedish in-kind contribution to the FAIR facility in Darmstadt,

The LSR [1] evolves from the heavy-ion storage ring CRYRING, which has been operated at the Manne Siegbahn Laboratory in Stockholm until 2010. Instead of warehousing the ring components until installation at the Facility for Antiproton and Ion Research, FAIR, the immediate installation behind the existing Experimental Storage Ring, ESR, has been proposed and worked out in detail by a Swedish-German working group. The estimated efforts for installation and operation of CRYRING at the ESR have been summarized in a report [2] published by that working group in 2012.

A schematic overview of the storage ring and its facilities is shown in fig. 1. CRYRING can decelerate, cool and store heavy, highly-charged ions down to a few 100 keV/nucleon. It provides a high performance electron cooler in combination with a gas jet target. It is equipped with it's own injector and ion source, to allow for standalone commissioning.

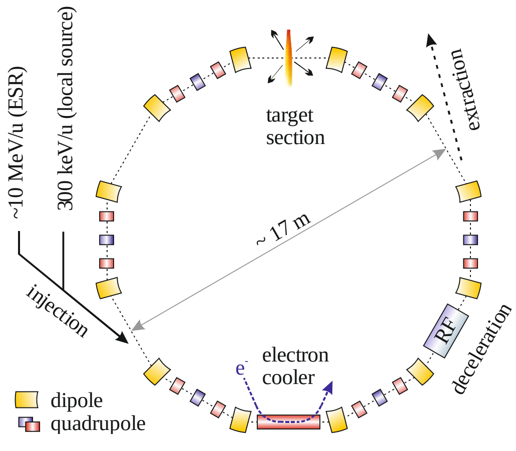

Figure 1: CRYRING at ESR.

The ions are kept in orbit by twelve 30° magnetic dipoles and a number of magnetic quadrupoles and sextupoles (not shown in the figure) in six of the twelve straight sections. The other six sections house an injection and an extraction system, the deceleration and acceleration drift, and the electron cooler. One section is used for experimental installations as for instance a gas target.

The storage ring is capable of accelerating ions with mass to charge ratio below four injected at only 300 keV/nucleon from the off-line ion source to the maximum rigidity of 1.44 Tm. It also decelerates ions injected at the maximal rigidity down to the lower rigidity limit of 0.054 Tm. The magnets are conceived for fast ramping, such that the whole decelerating (accelerating) process could be done in only 150 ms.

One of the key features is an electron cooler with adiabatic expansion of the electron beam. This yields about 100 times lower transversal electron temperature than in the ESR and yields directly higher resolution in recombination spectroscopy with merged ion – electron beams.

The proposed installation behind the ESR in combination with its own injector makes CRYRING@ESR the perfect machine for FAIR related tests of diagnostics, software and concepts on one side, and atomic physics experiments with heavy, highly charged ions stored at low energy on the other side. The new, FAIR type, control system will be implemented for the first time in a machine that delivers beam and hence will be the perfect occasion to test not only the cooperation of the design concepts but also the stability of the system. Since the ring can be operated any time it is the perfect training ground for operators on the new control system and this allows for valuable feedback on the operational concept well in advance before the commissioning of FAIR's key machines.

Physics applications range from "classical" atomic physics experiments like the determination of the lamb shift using X-ray spectroscopy, but with increased resolution, over measurements at the borderline of atomic and nuclear physics for instance to determine the charge radius to a yet unexplored energy regime for astrophysical interesting nuclear reactions. The details of planned experiments are laid down in the "Physics book" that is close to completion [2].

Most components have been shipped by now to GSI and on-site tests are ongoing. CRYRING@ESR will be installed in Cave B and the necessary reconstruction work has been started.

References

[1] H. Danared, et al. (2011) "LSR - Low-energy Storage Ring, Technical design report", Manne-Siegbahn Laboratory, Stockholm University, version 1.3.

[2] M. Lestinsky, et al. (2013) "Physics Book: CRYRING@ESR", in preparation.

[3] M. Lestinsky, et al. (2012) "CRYRING@ESR: A study group report", Project study, GSI, Darmstadt, https://www.gsi.de/fileadmin/SPARC/documents/Cryring/ReportCryring_40ESR.PDF

STRONG-FIELD PHYSICS USING LASERS AND RELATIVISTIC HEAVY IONS AT THE HIGH-ENERGY STORAGE RING HESR AT FAIR

T. Kühl, [1,2,3] V. Bagnoud, [1,3], T. Stöhlker, [1,3,6], Y. Litvinov, [1] D.F.A. Winters, [1] B. Zielbauer,[1,3] H. Backe,[2] C. Spielmann,[3,6] J. Seres,[3,6] J. Limpert [3,6] A. Tünnermann,[3,6] P.Neumayer,[4,5] B. Aurand, [7] S. Namba,[8] H.Y. Zhao [9]

[1] GSI Helmholtzzentrum für Schwerionenforschung GmbH, Darmstadt, Germany
[2] Johannes-Gutenberg-Universität, Mainz, Germany
[3] Helmholtz Institut Jena, Germany
[4] Extreme Matter Institute (EMMI), Darmstadt, Germany
[5] Goethe-Universität Frankfurt am Main, Germany
[6] Friedrich-Schiller-Universität Jena, Germany
[7] Lund University, Sweden
[8] Hiroshima University, Japan
[9] IMP-CAS Lanzhou, China

In the current FAIR planning, the High-Energy Storage Ring (HESR) will be available for storing ionic species accelerated by the SIS [1].This opens the way for a far reaching expansion of present laser experiments using stored heavy-ion beams[2].The large SPARC community, mainly centering on Atomic Physics and bound state QED has gathered a strong physics case for experiments with stored, cooled particles.As a novel and unique possibility for research in ultra-high field science the HESR will provide brilliant intense stored ion pulses at relativistic velocities of ($\gamma = 6$). For the interaction with laser pulses, the interaction frame will see a Doppler shift of the laser frequency by more than one order of magnitude. In addition, the relativistic Doppler effect will shorten a contra-propagating laser pulse, in total boosting the relevant parameters by more than 2 orders of magnitude. Changes in the ionic charge can be detected on a single particle level. Interaction with lasers and x-ray laser sources will be possible in the straight sections, or just before the 180° arcs.

Novel laser sources given by e.g. the PHELIX laser [3], and laser driven x-ray sources [4,5] can be used in this context. The most developed source is the plasma x-ray laser. Upcoming new approaches are Thomson laser scattering from medium energy electron beams, high harmonics generation, and betatron emission [5] in laser driven plasmas.

Exploiting the unique combination of a large Doppler shift and the excellent beam quality, novel spectroscopy approaches for studies not only in the ionic states, but also in nuclear excitations and pair-creation processes are accessible. For this purpose an experimental station has to be created, where laser and ion beams can be merged in counter propagating direction. This is possible at several locations within the HESR.

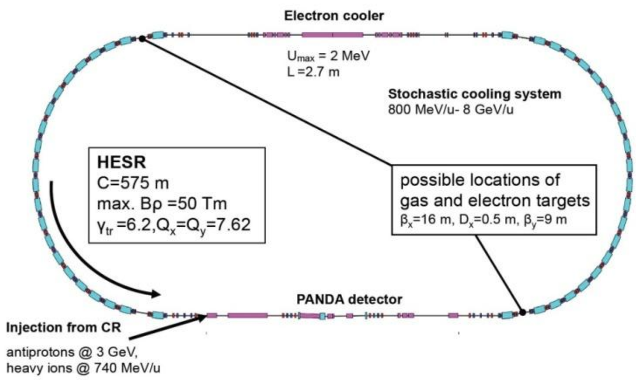

Figure 1. Layout of the HESR at FAIR The ions are injected from the bottom-left and circulate the ring in an anti-clockwise direction.

References

[1] M. Steck et al. **2012**, Proceedings of IPAC2012
[2] S. Reinhard et al. **2010**, Proc. Laser Spectroscopy 2012, 10.1142/9789814282345_0027, 297
[3] V. Bagnoud et al., **2010**, Appl. Phys. **B100** (1), 137
[4] B. Ecker et al. **2012**, Opt. Express **20** (23), 25391
[5] M. Schnell et al. **2012**, Phys. Rev. Lett. 108, 075001

Theory

Influence of the hot electron energy spectrum on the TNSA process

T. Kiefer[*1] *and T. Schlegel* [2,3]

[1]Friedrich-Schiller Universität, Jena, Germany; [2]Helmholtz-Institut Jena, Jena, Germany; [3]GSI, Darmstadt, Germany

We investigated the ion acceleration mechanism in the Target Normal Sheath Acceleration (TNSA) scheme analytically as well as numerically. A sophisticated computer code was developed, which is based on a kinetic treatment of the particles. In contrast to common Particle-in-Cell (PIC) methods, the electrons are assumed to remain in a stationary distribution with the electrical potential (see, e.g., Refs. [1, 2]). This concept is inspired by the small electron mass in comparison to ion masses and allows to simulate the corresponding ion acceleration phenomena at arbitrary electron dynamics, which permits a remarkable reduction of numerical efforts and simulation time.

In a previous study [3], we deduced the self-consistent form of the electron energy spectrum when the adiabatic expansion of the hot electron gas is described hydrodynamically. In this case, we found a step-like distribution function. This approach provides energy conservation ab initio. In the present Report, we describe essential consequences of such a so-called waterbag energy distribution function for the TNSA process, in contrast to theories commonly assuming a Maxwellian hot electron spectrum (e.g., in Refs. [1, 2]).

A self-similar solution for the plasma expansion process can be derived,

$$\phi_{\rm ss} = \frac{T_{\rm e,0}}{e}\left[\frac{\kappa-1}{(\kappa+1)^2}\left(\frac{x}{c_{\rm s}\,t}\right)^2 - \frac{4\sqrt{\kappa}}{(\kappa+1)^2}\,\frac{x}{c_{\rm s}\,t} - \frac{\kappa\cdot(\kappa+3)}{(\kappa+1)^2}\right], \tag{1a}$$

$$v_{\rm i,ss} = \frac{2\,c_{\rm s}}{1+\kappa}\left(\frac{x}{c_{\rm s}\,t}+\sqrt{\kappa}\right), \tag{1b}$$

$$Z_{\rm i}\,n_{\rm i,ss} = n_{\rm e,0}\cdot\left[\frac{2}{\kappa+1}\left(1-\frac{\kappa-1}{2\sqrt{\kappa}}\,\frac{x}{c_{\rm s}\,t}\right)\right]^{2/(\kappa-1)}, \tag{1c}$$

which depends on the adiabatic index κ (details are given in [4]). Equations (1) include the self-similar solution [1] assuming Maxwellian electrons as a limiting case ($\kappa \to 1$). Moreover, an empirical expression for the electric field strength at the ion front can be obtained,

$$E(t) \approx \frac{E(t=0)}{[1+C(\kappa)(\omega_{\rm pi}\,t)^2]^{\kappa/2}}, \tag{2}$$

which generalizes the result of Mora [2], which was deduced for isothermal Maxwellian electrons. Starting from Eq. (2), one can immediately calculate the velocity, position and kinetic energy of the ion front. For the final maximum ion energy $\varepsilon_{\rm max}$ per nucleon $Z_{\rm i}$ at a given mean electron energy $T_{\rm e,0}$ one gets the approximate expression

$$\varepsilon_{\rm max}/Z_{\rm i} \approx T_{\rm e,0}\,\frac{1.36312+4.58725\,T_{\rm e,0}/\mathrm{MeV}}{0.750591+T_{\rm e,0}/\mathrm{MeV}}. \tag{3}$$

It becomes apparent that this energy is lower by almost one order of magnitude in comparison to the numbers extracted in cases with Maxwellian electrons (see Fig. 1), despite of comparable macroscopic variables such as the characteristic electron energy and density.

Our analysis emphasizes the role of the detailed shape of the electron energy distribution function in the TNSA process, which may account for remarkable differences in the final ion energy values. At the same time, the study motivates further efforts to get a deeper understanding of hot electron generation and transport in this ion acceleration scheme.

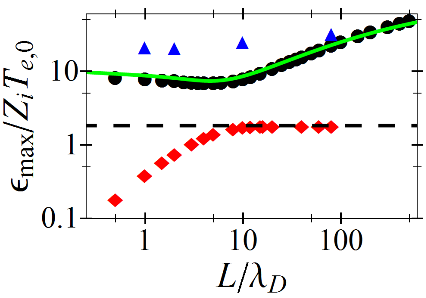

Figure 1: Maximum ion energy as a function of the normalized target thickness. Red diamonds correspond to step-like distributed electrons. For initially Maxwell-like electrons, two different approaches concerning the temporal evolution of the electron distribution were considered. While the black dots depict the case of electrons with an unchanged Maxwell distribution ("adiabatic Maxwellian model"), the blue triangles represent the "kinetic Maxwellian model", where the initial Maxwell distribution may evolve arbitrarily. The black dashed and the green solid lines illustrate our analytic results for step-like distributed electrons and the adiabatic Maxwellian model, respectively.

References

[1] A. V. Gurevich, L. V. Pariiskaya, and L. P. Pitaevskii, Sov. Phys. JETP **22**, 449 (1966).

[2] P. Mora, Phys. Rev. Lett. **90**, 185002 (2003).

[3] T. Kiefer and T. Schlegel, Phys. Plasmas **19**, 102101 (2012).

[4] T. Kiefer, T. Schlegel, and M. C. Kaluza, Phys. Rev. E **87**, 043110 (2013).

* kiefer.thomas@gmail.de

Comparison of model calculations assuming different hot electron distribution functions with TNSA experiments *

T. Kiefer †[1], *T. Schlegel* [2,3], *and M.C. Kaluza*[1,2]

[1]Friedrich-Schiller Universität, Jena, Germany; [2]Helmholtz-Institut Jena, Jena, Germany; [3]GSI, Darmstadt, Germany

In a second step of our recent study [1], we applied the analytical estimates to the published results of numerous experimental campaigns. First of all, we analyzed the maximum proton energy (see Fig. 1) as well as at the proton energy spectrum (Fig. 2). In agreement with previous research (e.g., Ref. [2]), we confirmed the existence of different scaling laws for the maximum ion energy $\varepsilon_{\max}$ in dependence on laser intensity $I_{\rm L}\,\lambda_{\rm L}^2$ at interactions with ultrashort pulse durations $\tau_{\rm L} \leq 80$fs and for experiments using relatively long laser pulses, $\tau_{\rm L} \geq 300$fs. This remarkable influence of the laser pulse duration also shows up in the corresponding ion spectra.

Concerning the ion energies in long-pulse experiments, the observed data are in good agreement with model calculations assuming isothermal Maxwellian electrons [3], in contrast to the ultrashort pulse regime. In the latter case, the laser heating time will be shorter than the effective acceleration time of the ions, so that the adiabatic cooling of hot electrons becomes relevant. However, our analysis showed that also adiabatic expansion models assuming Maxwellian electrons [4, 5] cannot explain the corresponding observation data. In the opposite, a rather good coincidence between the experimental data and the estimates from the model assuming a step-like electron energy distribution, was found. Although this fact is not a unique evidence for the presence of such a hot electron spectrum in ultrashort pulse experiments, we interpret it as a clear hint for non-Maxwellian electron energy distributions in such TNSA interactions. But, more efforts are required to finally answer the question how the hot electron energy distribution function evolves and effects the acceleration process.

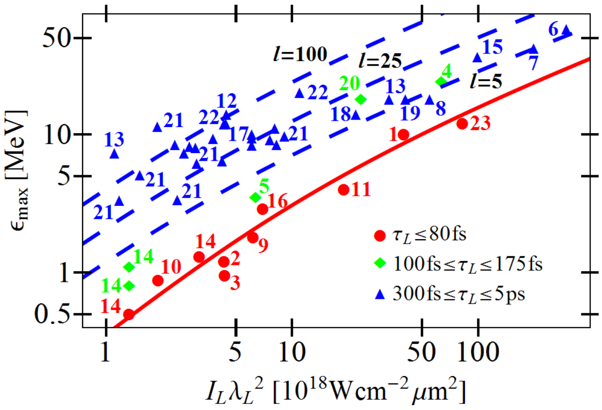

Figure 1: Experimentally observed maximum proton energies as a function of the laser intensity. Obviously, there is a different scaling for experiments with ultrashort pulse durations $\tau_{\rm L} \leq 80$fs and relatively long laser pulses $\tau_{\rm L} \geq 300$fs. Moreover, the scaling predicted by the analytical model with a step-like electron energy distribution (red solid line) fits well to the numbers from ultrashort pulse experiments, while we observe a discrepancy in case of Maxwellian electrons (blue dashed lines). More details see in Ref. [1].

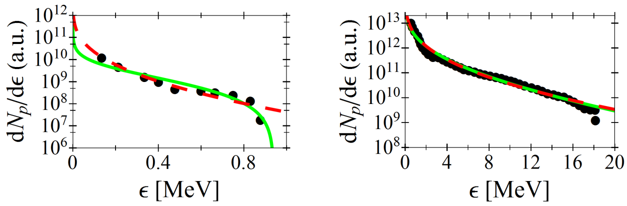

(a) (b)

Figure 2: Experimental data (black dots) for the proton spectrum. While (a) corresponds to an ultrashort pulse experiment ($\tau_{\rm L} = 70$fs), (b) concerns an experiment with relatively long laser pulses ($\tau_{\rm L} = 350$fs). The best fit for the theoretical ion spectrum assuming Maxwellian electrons is depicted by red dashed lines. The corresponding fit assuming step-like electrons is shown by green solid curves. Obviously, there is a good agreement between the short-pulse experimental result and the prediction of the model assuming step-like electrons, in contrast to the estimates based on Maxwellian electrons. In (b), both fit results are quite similar.

References

[1] Thomas Kiefer, Theodor Schlegel, and Malte C. Kaluza, Phys. Rev. E **87**, 043110 (2013).

[2] J. Fuchs, P. Audebert, M. Borghesi, H. Pépin, and O. Willi, C. R. Phys. **10**, 176 (2009).

[3] J. Fuchs, P. Antici, E. D'Humières, E. Lefebvre, M. Borghesi, E. Brambrink, C. A. Cecchetti, M. Kaluza, V. Malka, M. Manclossi, S. Meyroneinc, P. Mora, J. Schreiber, T. Toncian, H. Pépin, and P. Audebert, Nature Phys. **2**, 48 (2006).

[4] P. Mora, Phys. Rev. E **72**, 056401 ,(2005).

[5] T. Grismayer, P. Mora, J. C. Adam, and A. Héron, Phys. Rev. E **77**, 066407 (2008).

* Work supported by BMBF (03ZIK445 and 03Z1H531) and by DFG (TR18)

† kiefer.thomas@gmail.de

Nonlinear Thomson scattering at ultraintense laser hole boring *

T. Schlegel† [1,2] *and V. T. Tikhonchuk*[3]

[1]Helmholtz-Institut Jena, Jena, Germany; [2]GSI, Darmstadt, Germany; [3]University Bordeaux 1 - CNRS - CEA, CELIA, UMR 5107, F-33400 Talence, France

The electron dynamics in strong electromagnetic fields behind a quasistationary laser piston at essential radiation damping is reported. The mechanism of ponderomotive ion acceleration in an overdense plasma bulk was found in Particle-in-Cell (PIC) simulations [1], [2] and contemplated also analytically [3]. Most efficiently it works for circular laser polarization because of minimum electron heating. Furthermore, PIC simulations at laser intensities exceeding $10^{22}\,\mathrm{Wcm}^{-2}$ and including the radiation friction term in the equation of relativistic electron motion, have shown remarkable deceleration of electrons with energies of hundreds of MeV after the propagation over several laser wavelengths, previously escaping the piston region in the direction towards the incident laser wave (see Fig. 1). This damping effect will support the formation of a stable piston.

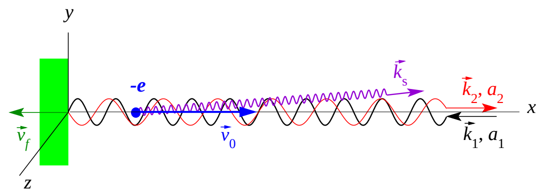

Figure 1: Interaction scheme: A relativistic classical electron escapes the quasistationary laser piston, which is pushed by an ultraintense plane laser wave (amplitude a_1, wave vector $\vec{k}_1$, carrier frequency $\omega_1 = k_1\, c$) with the velocity $\vec{v}_f$. The electron has the initial velocity $\vec{v}_0$ and interacts with the fields of the incident $\vec{k}_1$ and reflected $\vec{k}_2$ laser waves. Thereby, high-energy photons are transmitted due to nonlinear Thomson scattering as well as due to selfemission by the electron.

In our classical approach, the equation of relativistic electron motion with the friction term in the Landau-Lifshitz approximation [4] was solved numerically for the superposition of an incoming plane laser wave with circular polarization and its reflection from the moving plasma surface [5]. The obtained electron velocity components allowed the calculation of the high-energy photon emission spectra. The piston reflection coefficient was taken from a PIC simulation with the corresponding incident laser intensity and homogeneous plasma density. A typical result is demonstrated in Fig. 2, where the piston case is compared to the motion in a standing wave (resting mirror) with the same normalized incident vector potential a_1. The decrease in the electron energy due to radiation damping transforms the Doppler-upshifted line spectrum to a quasi-continuum with reduced spectral intensities.

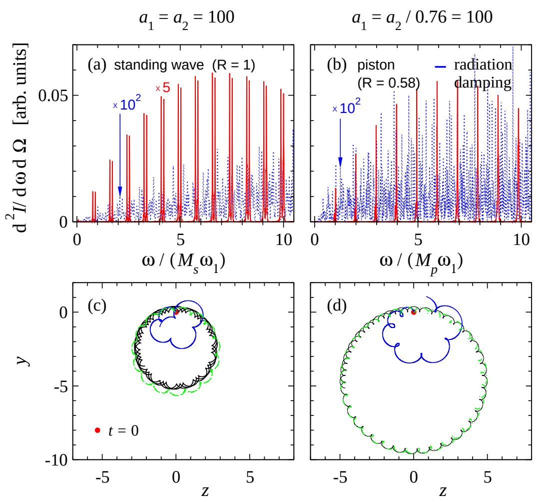

Figure 2: Electron motion in the ultrastrong field of a standing wave (a, c) or behind a stationary laser piston (b, d). Spectral intensities of the radiation emitted in the direction of the electron drift motion ($\theta = 0$) without the radiation damping effect (red lines) and with the account for this effect (blue dotted curves) are plotted in the upper panels (a) and (b), the transverse projections of the electron trajectories with radiation damping (blue curves) and without it (black curves) are depicted in the lower panels (c, d). The initial electron energy is $\gamma_0 = 300$, the laser field strenghts are given in the panel titels. Frequencies are normalized with the Doppler upshift factors M_i, which were estimated analytically, the spatial coordinates are related to the wavelength of the incident light. In comparison with numerical data, the dashed green curves display analytical estimates, which were derived in the moving frame of the electron at neglected radiation friction.

References

[1] A. P. L. Robinson, P. Gibbon, M. Zepf, S. Kar, R. G. Evans, C. Bellei, Plasma Phys. Control. Fusion **51**, 024004 (2009).

[2] N. Naumova, T. Schlegel, V. T. Tikhonchuk, C. Labaune, I. V. Sokolov, G. Mourou, Phys. Rev. Lett. **102**, 025002 (2009).

[3] T. Schlegel, N. Naumova, V. T. Tikhonchuk, C. Labaune, I. V. Sokolov, G. Mourou, Phys. Plasmas **16**, 083103 (2009).

[4] L. D. Landau, E. M. Lifshitz, *The Classical Theory of Fields* (New York, Pergamon, 1994).

[5] T. Schlegel and V. T. Tikhonchuk, New J. Phys. **14**, 073034 (2012).

* Work supported by Region Aquitaine, project No. 34293, and by the European Marie Curie IRSES project # 230777

† t.schlegel@gsi.de

Magnetic interactions and retardation in the electron emission from highly-charged ions

S. Fritzsche[1,2,3]*, A. Surzhykov*[1,2,4]*, A. Gumberidze*[1,5,6]*, and T. Stöhlker*[1,2,3]

[1]GSI, Darmstadt, Germany; [2]Helmholtz Institute Jena, Germany; [3]University of Jena, Germany; [4]University of Heidelberg, Germany; [5]FIAS, Frankfurt, Germany; [6]EMMI, Darmstadt, Germany

X-ray studies from multiple and highly charged ions have been found a unique tool for exploring the electron-electron (e-e) and electron-photon interactions in the presence of strong fields [1]. The x-ray spectroscopy of such systems have demonstrated for a long time that accurate energies and cross sections are obtained only if, apart from the static Coulomb repulsion among the electrons, the magnetic interactions and retardation as well as leading quantum-electrodynamical effects are taken into account. In contrast to the spectrocopy of hard x-rays, however, much less is known how relativistic interactions among the electrons affect their emission and, hence, the dynamics of electrons in strong fields.

To obtain further insight into the strong-field dynamics of electrons, we re-analyzed the excitation and autoionization of highly charged ions with the goal to separate the magnetic and retardation contributions to the e-e interaction from the static Coulomb repulsion. A remarkable change in the electron angular distribution due to the relativistic terms in the e-e interaction was found especially for the autoionization of (initially) beryllium-like projectiles, following a $1s \rightarrow 2p_{3/2}$ Coulomb excitation in collision with some target nuclei. In this process, the angular distribution of the emitted electron is given by

$$W(\theta) \propto 1 + \sum_{k=2,4,...} \mathcal{A}_k(\alpha_r J_r)\, f_k(\alpha_r J_r, \alpha_f J_f)\, P_k(\cos\theta),$$

where $\mathcal{A}_k(\alpha_r J_r)$ characterizes the alignment of the intermediate state after the excitation, θ is the polar angle with regard to the beam direction and where the $f_k(\alpha_r J_r, \alpha_f J_f)$ are characteristic functions that describe the dynamics of the autoionization. The function f_k in this distribution merely depends on the (reduced) matrix elements of the (frequency-dependent) e-e interaction

$$V \;=\; V^{\mathrm{Coulomb}} + V^{\mathrm{Breit}}$$

that comprises both, the instantaneous Coloumb repulsion and the (so-called) Breit interaction, i.e. the magnetic and retardation contributions.

For the excitation-autoionization process via the $1s2s^2 2p_{3/2}\ ^3P_2$ resonance, a diminished (electron) emission in forward direction as well as oscillations in the electron angular distribution due to the magnetic and retarded interactions are predicted especially for the electron emission into the $1s^2 2s\ ^2S_{1/2}$ ground and $1s^2 2p\ ^2P_{1/2}$ excited levels of the finally lithium-like ions. This emission pattern is in strong contrast to a pure Coulomb repulsion between the bound and the outgoing electrons. For example, Figure 1 displays the angular distribution of electrons

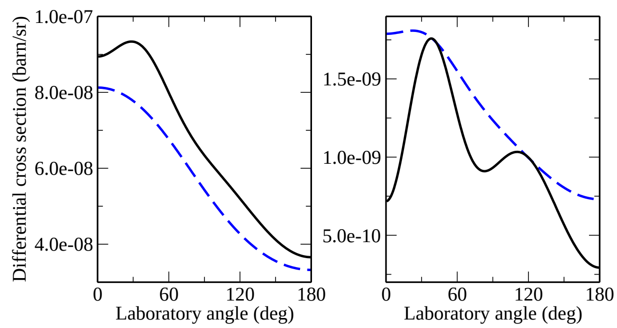

Figure 1: Angular distribution of electrons emitted in the $1s2s^2 2p_{3/2}\ ^3P_2 - 1s^2 2s\ ^2S_{1/2}$ (left panel) and $1s2s^2 2p_{3/2}\ ^3P_2 - 1s^2 2p\ ^2P_{1/2}$ (right panel) autoionization of U^{88+} projectiles with energy T_p = 5 MeV/u.

emitted in the $1s2s^2 2p_{3/2}\ ^3P_2 - 1s^2 2s\ ^2S_{1/2}$ (left panel) and $1s2s^2 2p_{3/2}\ ^3P_2 - 1s^2 2p\ ^2P_{1/2}$ (right panel) autoionization of U^{88+} projectiles with energy T_p = 5 MeV/u. Results are shown in the laboratory frame and by incorporating only the Coulomb repulsion into the Auger amplitude (blue dashed lines) as well as for a full account of the e-e interaction (black solid lines). The lowering of the electron emission in forward direction ($\theta \approx 0^o$) is significant and enhanced in the laboratory frame due to the Lorentz transformation of the energetic electrons

In conclusion, the proposed excitation-autoionization process can be observed at existing storage rings and will provide novel insight into the dynamics of electrons in strong fields. The most simple signatures of the relativistic contributions to the e-e interaction in high-Z ions is the reduced electron emission in forward direction ($\theta < 5^o$) as well as the double-peak structure in the expected angular distribution; these signatures arise especially at low projectile energies < 10 MeV/u and for beryllium-like ions with nuclear charge $Z > 70$. The electron angular distribution from such projectiles can be analyzed with present-day electron spectrometers and provide complementary information about the electron dynamics in strong fields that is not accessible from x-ray spectra alone.

References

[1] S. Fritzsche, P. Indelicato and T. Stöhlker, J. Phys. B 38, S707 (2005).

[2] S. Fritzsche et al., New J. Phys. 14, 083018 (2012).

Two-photon absorption of few-electron heavy ions *

S. Fritzsche[1,2], P. Indelicato[3], J. P. Santos[4], P. Amaro[4,5], and A. Surzhykov[1,2,5]

[1]GSI, Darmstadt, Germany; [2]Helmholtz Institute Jena, Germany; [3]Laboratoire Kastler Brossel, Paris, France; [4]Departamento de Física, Universidade Nova de Lisboa, Portugal; [5]Physikalisches Institut Heidelberg, Germany

The recent progress in developing coherent light sources have opened new avenues for studying two- and multi-photon transitions in ions, atoms and molecules. For example, the $ns \to n's$ and $ns \to n'd$ two-photon excitation of atomic hydrogen and deuterium has been explored in great during recent years and and helped determine the *fundamental* constants with unprecendented accuracy [1]. Less attention, however, has been paid until now to *induced* two-photon absorption processes in multiple and high-Z atoms and ions, though they are exptected to provide new insights into relativistic, many-body and QED phenomena in strong electromagnetic fields and, hence, may serve as a valuable alternative to x-ray absorption (XAS) spectroscopy and related techniques [2]. Moreover, induced two-photon excitations have been proposed as a promising tool for studying parity-violating interactions in high-Z ions [3].

To explore and better understand the two-photon absorption in strong fields, we have recently worked out a (unified) relativistic formalism that enables one to describe the (spatial and polarization) properties of light in a consistent manner [4]. Using second-order perturbation theory and Dirac's relativistic equation, expressions were derived for the two-photon excitation cross sections and decay rates, including the important many-electron effects as well as all (higher) multipoles in the expansion of the electron-photon interaction. For the absorption of a photon, arriving from the direction $\hat{\boldsymbol{k}} = (\theta, \phi)$ with regard to the quantization (z) axis, such an expansion of the electron-photon operator $\hat{\mathcal{R}} = \sum_m \boldsymbol{A}_m(\boldsymbol{k}, \boldsymbol{\epsilon})$ into spherical tensors reads as [5]

$$\boldsymbol{A}_m(\boldsymbol{k}, \boldsymbol{\epsilon}) = 4\pi \sum_{pLM} i^{L-|p|} \left(\boldsymbol{\epsilon} \cdot \boldsymbol{Y}^{(p)*}_{LM}(\hat{\boldsymbol{k}}) \right) \boldsymbol{a}^p_{LM,m}(k) \,,$$

where $\boldsymbol{Y}^{(p)}_{LM}(\hat{\boldsymbol{k}})$ is a vector spherical harmonics and the index p describes either the electric (p = 1), magnetic (p = 0), or longitudinal (p = –1) component of the electromagnetic field. In this formalism, in addition, the properties of the incident light are described conveniently by means of the (so-called) *angular-polarization* tensor, and which is known to contain the complete information about the direction and polarization states of the incident photons in the two-photon absorption process.

While our derived expressions are general and independent of the particular shell structure of the ion, detailed computations have been carried out for the two-photon absorption of hydrogen-, helium-, and beryllium-like ions, and they are compared with the available theoretical and experimental data [4]. Figure 1, for example, displays the (reduced) cross section $\alpha_0 = \sigma_{2\gamma}/g(\omega)G^{(2)}$ for the $1s \to 2s$ and $1s \to 2p_{1/2}$ absorption of hydrogen-like ions. Here, $G^{(2)}$ is the two-photon statistical factor and $g(\omega)$ is the line-shape function. As seen from the figure, the relativistic contraction of the wave functions toward the nucleus as well as the nondipole effects in the electron-photon interaction lead to a faster decrease of the cross sections than predicted by the non-relativistic $\alpha_0(1s \to 2s) \sim Z^6$ and $\alpha_0(1s \to 2p) \sim Z^4$ scalings. Further computations have been performed for the (excitation) probabilities of the two-photon induced $1s2p\ {}^3P_0 \to 1s2s\ {}^1S_0$ and $1s^2 2s^2\ {}^1S_0 \to 1s^2 2s2p\ {}^3P_0$ transitions of helium-like and beryllium-like ions.

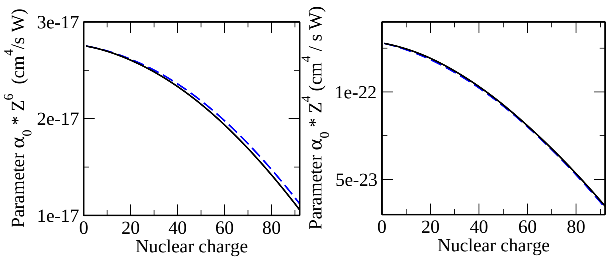

Figure 1: The parameter α_0 for the two–photon $1s \to 2s$ (left panel) and $1s \to 2p_{1/2}$ (right panel) absorption of hydrogen–like ions. Predictions have been obtained within the electric dipole (dashed line) approximation as well as by taking the higher terms into account (solid line).

In conclusion, our studies demonstrate the importance of relativistic and higher-multipole effects upon the two-photon absorption and emission rates. Reliable theoretical rates are however required to plan and prepare future experiments on the parity violation in high-Z ions as they will be performed at the future Facility for Antiproton and Ion Research (FAIR) in Darmstadt. A new generation of such two-photon absorption experiments with helium-like ions is currently being planned at the GSI facility in Darmstadt and the Helmholtz Institute in Jena.

References

[1] B. de Beauvoir et al., Eur. Phys. J. D 12, 61 (2000).

[2] C. Szymanowski et al., Europhys. Lett. 37, 391 (1997).

[3] M. Maul et al., J. Phys. B 31, 2725 (1998).

[4] A. Surzhykov et al., Phys. Rev. A84, 022511 (2011). P. Amaro et al., Phys. Rev. A86, 042509 (2012)

[5] S.P. Goldman and G.W.F. Drake, PRA 24, 183 (1981).

* Work supported the Helmholtz Gemeinschaft and GSI (Nachwuchsgruppe VH-NG-421).

Hyperfine–interaction effects on the linear polarization of Kα_1 transition *

A. Surzhykov[1], *Y. Litvinov*[2], *Th. Stöhlker*[2,3], *and S. Fritzsche*[2,3]

[1]Helmholtz Institute Jena; [2]GSI Helmholtzzentrum für Schwerionenforschung, Darmstadt;
[3]Friedrich–Schiller–University of Jena

During the recent years, a large number of experiments have been performed to investigate the angular and polarization properties of the characteristic photon emission from highly–charged ions. These measurements have revealed important information on the many–body, relativistic and even quantum electrodynamics (QED) effects in heavy atomic systems [1]. Most of the angular– and polarization–resolved studies have dealt, however, with the ions having *zero* nuclear spin. Much less attention both in experiment and theory was paid up to now to the ions with $I \neq 0$, whose electronic structure may be significantly affected by the hyperfine–interaction effects. Since these effects are expected to manifest themselves in the properties of the characteristic lines, the accurate analysis of the linear polarization of the decay radiation can serve as a valuable tool for probing not only the details of electron–nuclear magnetic coupling but also the nuclear spin and moments.

In order to inquire the potential application of the x–ray polarimetry to the analysis of hyperfine–interaction phenomena, a theoretical study of characteristic transitions in few–electron ions with non-zero nuclear spin have been recently performed [2]. A general formalism was laid down which accounts for both, the many–electron effects and the higher–order multipoles of the radiation field, including hyperfine–induced channels. While the developed formalism can be applied to any ion, independent of its shell structure, special attention was paid to the $1s2p_{3/2}\,{}^3P_2 \to 1s^2\,{}^1S_0$ decay of helium–like heavy species. The polarization properties of such a Kα_1 radiation are currently available for experimental investigations at storage rings where the projectiles in the excited $1s\,2p_{3/2}$ states can be *prepared* by means of the radiative electron capture [1]. Moreover, because of the hyperfine interaction, which *mixes* the excited $1s2p\ {}^3P_2$ state with the short–lived $1s2p\ {}^{1,3}P_1$ levels, the $2\,{}^3P_2 \to 1\,{}^1S_0$ decay can proceed also via the hyperfine–induced electric–dipole $E1$ decay in addition to the leading magnetic–quadrupole $M2$ transition. The interference between the $E1$ and $M2$ amplitudes may affect the polarization properties of the characteristic Kα_1 emission and can be utilized as a tool for probing the nuclear spins and dipole magnetic moments.

To illustrate the $E1$–$M2$ *multipole mixing*, the degree of the $2\,{}^3P_2 \to 1\,{}^1S_0$ polarization is displayed in Fig. 1 as a function of photon emission angle and for the decay of helium–like ^{205}Tl^{79+} ($I = 1/2$, $\mu_I = 1.638\,\mu_N$) and lead ^{207}Pb^{80+} ($I = 1/2$, $\mu_I = 0.593\,\mu_N$) ions following REC. Calculations have been performed for the projectile

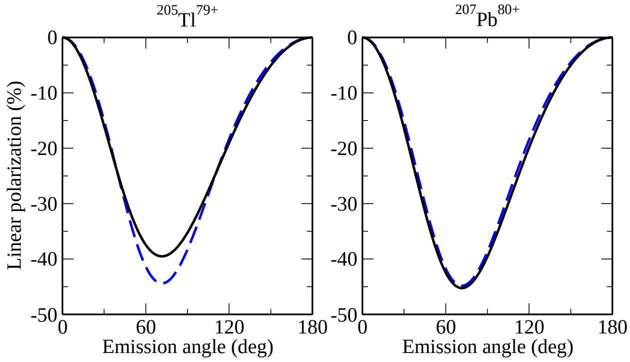

Figure 1: Degree of linear polarization of the $1s2p_{3/2}\,{}^3P_2 \to 1s^2\,{}^1S_0$ fine–structure transition following radiative electron capture into $1s2p_{3/2}\,{}^3P_2$ state of finally helium–like thallium ^{205}Tl^{79+} and lead ^{207}Pb^{80+} ions with projectile energy T_p = 50 MeV/u. Calculations are performed within the magnetic–quadrupole approximation (dashed line) and by taking the $E1$–$M2$ mixing into account (solid line).

ion energy $T_p = 50$ MeV/u and within two approximations. That is, predictions of the rigorous relativistic treatment (solid line) are compared with those obtained within the pure magnetic–quadrupole $M2$ approximation (dashed line), i.e. when the quenched $E1$ transition is neglected. Even though thallium ^{205}Tl^{79+} and lead ^{207}Pb^{80+} have the same nuclear spin, I = 1/2, and their charges Z differ just by *one* unit, the surprisingly significant difference between the magnitude of the $E1$–$M2$ interference effect is observed for these two ions. Namely while the multipole mixing results in a 15% reduction of the linear polarization for thallium ions and large emission angles $\theta \approx 60°$ (cf. left panel of Fig. 1), it has almost no influence on the decay properties of lead. Above all, such a difference should be attributed to the fact that the magnetic moment of ^{205}Tl isotope is about three times larger than that of ^{209}Pb.

Polarization–resolved studies of characteristic emission from ions with non–zero spin can be performed now at heavy–ion storage rings, like, e.g., the experimental storage ring ESR at GSI, Darmstadt, where the in–flight separated beams of highly–charged radionuclides of all chemical elements up to uranium can be stored for envisioned experiments.

References

[1] J. Eichler and Th. Stöhlker, Phys. Rep. **439**, 1 (2007).

[2] A. Surzhykov et al., submitted to Phys. Rev. A.

* Work supported the Helmholtz Gemeinschaft and GSI (Nachwuchsgruppe VH-NG-421).

Parity–nonconservation in the radiative recombination of hydrogen–like ions *

J. Gunst[1]*, A. Surzhykov*[2]*, Th. Stöhlker*[2,3,4]*, A. Artemyev*[2,5]*, S. Tashenov*[5]*, and S. Fritzsche*[2,4]

[1]Max–Planck Institute for Nuclear Physics, Heidelberg; [2]Helmholtz Institute Jena; [3]GSI Helmholtzzentrum für Schwerionenforschung, Darmstadt; [4]Friedrich–Schiller–University of Jena; [5]Physics Institute, University of Heidelberg

Measurements of the parity–violation (PV) effects in atomic systems attract considerable attention as a valuable tool for testing the Standard Model in the low–energy regime. In the past, the PV studies have mainly dealt with the valence–shell transitions in neutral atoms. Even though the results of these studies have revealed unique information on the Weinberg angle and the nuclear anapole moment, their interpretation was often hindered by the precision of atomic–structure calculations. This difficulty can, to a large extent, be overcome by the use of highly–charged, heavy ions. During the recent years a number of proposals have been made to perform PV–experiments with these heavy few–electron species (see eg. Ref. [1]). Many of these proposals, however, require application of spin–polarized ion beams and/or performing *circular* polarization x–ray measurements; the experimental tasks which can not be easily accomplished today.

An alternative approach to explore PV phenomena in heavy, highly–charged ions was recently pursued by Maiorova and co–workers [2] who considered the radiative recombination of a free electron into excited states of (finally) helium–like ions. It was shown that the angle–differential cross section of this process might be sensitive to the parity violation effects if only photons of a particular *linear* polarization are recorded by x–ray detectors. In this contribution, we lay out an extension of the method of Ref. [2] which is based on the analysis of the *rotation* of the linear polarization of RR photons. Owing to the recent advances in energy– and position–sensitive solid state detectors, such a rotation is likely to be detected in the near future with a sub–degree accuracy opening, thus, a new route to the PV studies with heavy ions.

Similarly to the scenario from Ref. [2], we consider the recombination of unpolarized electrons into the $1s2p_{1/2}\,{}^3P_0$ state of (finally) helium–like ions. Due to a significant PV–mixing between the 2^3P_0 state and the opposite–parity $1s2s_{1/2}\,{}^1S_0$ level, the direction of the RR linear polarization is slightly tilted with respect to the parity–conserved (i.e. purely electromagnetic) case. That is, based on the density matrix approach we found that the angle of the linear polarization is given [3]:

$$\Delta\chi_{\rm PNC} \equiv \chi_0 \quad \chi_0^{\rm em} = \frac{\xi}{2}\,\mathcal{F}(Z, T_p, \theta) + \mathcal{O}(\xi^3)\,. \quad (1)$$

where ξ represents the weak mixing coefficient, $\chi_0^{\rm em}$ defines the angle of the RR linear polarization if a parity is preserved ($\chi_0^{\rm em}$ = 0° or 90° if both incident ions and electrons are unpolarized), and $\mathcal{F}$ is the function which depends only on the collision parameters. To understand this effect qualitatively we recall that the weak interaction processes prefer emission (or absorption) of electrons with the particular helicity. For the case of the radiative recombination such an asymmetry results in a dependence of the capture cross section on the projection of the electron spin and, hence, in the rotation of the RR linear polarization.

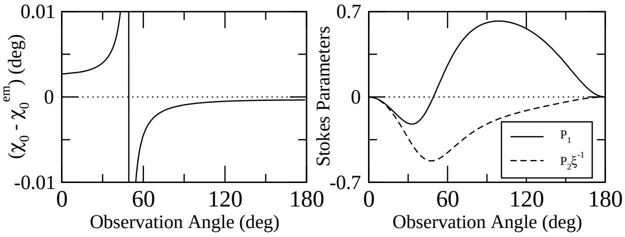

Figure 1: The rotation angle (left) and the Stokes parameters (right) of the linear polarization of the photons emitted due to the radiative recombination of electrons into $1s2p_{1/2}\,{}^3P_0$ state of finally helium–like gadolinium ions with a projectile energy of 300 MeV/u.

In order to estimate the size of the PV effect on the rotation angle χ_0 calculations have been performed for the electron capture by (initially unpolarized) gadolinium ions with projectile energy T_p = 300 MeV/u. For this energy we displayed in the left panel of Fig. 1 the difference between the polarization rotation angles as obtained with and without account for the parity mixing between the $2\,{}^3P_0$ and $2\,{}^1S_0$ states. In the right panel, the Stokes parameters that characterize (apart from the angle) the degree of RR polarization are displayed. As seen from the figure, the PV–induced tilt may reach the value of 0.01° in the angular region where the degree of the polarization is large enough to be detected by present–day polariemeters.

Together with the high–precision measurements of the RR tilt angle, the practical realization of the proposed scenario requires distinction between the electron capture into $2\,{}^3P_0$ and almost degenerate $2\,{}^1S_0$ state. This can be achieved by the analysis of the subsequent characteristic emission and by employing the significant difference between the lifetimes of both excited states.

References

[1] A. Bondarevskaya et al., Phys. Rep. **507** 1 (2011).

[2] A. V. Maiorova et al., J. Phys. B **42** 205002 (2009).

[3] J. Gunst et al., Phys. Rev. A **87**, 032714 (2013).

* Work supported the Helmholtz Gemeinschaft and GSI (Nachwuchsgruppe VH-NG-421).

Parity–violating transitions in beryllium–like ions*

A. Surzhykov† [1,2,3], *S. Fritzsche* [3,4], *A. V. Maiorova* [5], *V. M. Shabaev* [5], *and Th. Stöhlker* [1,3,4]
[1]GSI, Darmstadt, Germany; [2]University of Heidelberg, Germany; [3]Helmholtz Institute Jena, Germany; [4]University of Jena, Germany; [5]St. Petersburg State University, Russia

Parity–violation (PV) phenomena in highly–charged ions currently attract much attention (see e.g. [1, 2]). In particular, many studies are focused on the mixing between opposite–parity atomic levels caused by the weak electron–nucleus interaction. A number of proposals have been made to detect such a mixing and, hence, to explore the basic parameters of the electroweak theory. Most of theses proposals have dealt up to now with the near–degenerate $1s2s$ and $1s2p_{1/2}$ states of helium–like *heavy* ions for which the PV effects are significantly enhanced. In the high–Z domain, however, the lifetimes of such singly–excited states are shorter than $\tau \sim 10^{-10}$ seconds which makes the observation of the parity–violating phenomena in two–electron systems rather challenging. During the recent years, therefore, particular interest has been given to other few–electron species whose *long–lived* levels might be mixed by the weak interaction.

Owing to their shell structure, beryllium–like heavy ions may provide an alternative and promising tool for studying atomic PV phenomena. For the case of *zero* nuclear spin, the first excited state of these ions, $1s^2\,2s\,2p\ ^3P_0$, can decay to the $1s^2\,2s^2\ ^1S_0$ ground level solely by the strongly suppressed two–photon $E1M1$ emission and, hence, has a lifetime of the order of seconds. Moreover, the energy splitting between these two levels does not exceed 260 eV even for the heaviest ions, thus leading to a rather remarkable $^1S_0$–$^3P_0$ parity–violating mixing [3]. To observe such a mixing, we have recently proposed to utilize the source of the coherent extreme ultraviolet (EUV) radiation and to induce a single–photon transition between the metastable $1s^2\,2s\,2p\ ^3P_0$ and short–lived $1s^2\,2s\,2p\ ^3P_1$ levels [4]. Since the $^3P_0$ state has a small PV–admixture of the ground one, such an absorption can proceed not only via the allowed $M1$ but also the parity–violating $E1$ channel (see Fig. 1).

The interference between the $M1$ and PV–$E1$ excitation channels becomes “visible” if the $1s^2\,2s\,2p\ ^3P_0 \rightarrow 1s^2\,2s\,2p\ ^3P_1$ transition is induced by the circularly polarized light. In this case the photoexcitation cross section reads as [4]:

$$\sigma_\lambda = \sigma_{M1}\,(1 + \lambda\epsilon)\ , \qquad (1)$$

where $\lambda = \pm 1$ for the right– and left–hand polarization, σ_{M1} describes the leading, parity–preserved $^3P_0 \rightarrow\ ^3P_1$ magnetic dipole channel, and the so–called asymmetry coefficient ϵ is given by:

$$\epsilon = -2\,\eta_{PV}\,\frac{\langle 1s^2 2s 2p\ ^3P_1\,\|E1\|\,1s^2 2s^2\ ^1S_0\rangle}{\langle 1s^2 2s 2p\ ^3P_1\,\|M1\|\,1s^2 2s 2p\ ^3P_0\rangle}\,. \qquad (2)$$

* Work supported by Helmholtz Association under the project VH–NG–421.
† surz@physi.uni-heidelberg.de

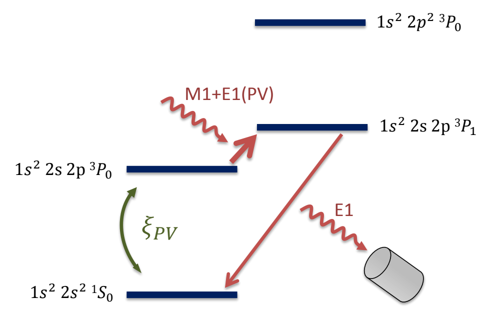

Figure 1: Proposed scheme for measuring the PV–mixing between the ground $1s^2\,2s^2\ ^1S_0$ and the first excited $1s^2\,2s\,2p\ ^3P_0$ states of beryllium–like heavy ions. For the case of U^{88+}, the energies $E_{^3P_0}$ and $E_{^3P_1}$ if defined relative to the ground state energy are 258.3 and 298.2 eV, correspondingly. From Ref. [4].

In this expression, $\langle ...\,\|E1, M1\|\,...\rangle$ are the reduced matrix elements for the $^1S_0 \rightarrow^3 P_1$ ($E1$) and $^3P_0 \rightarrow^3 P_1$ ($M1$) transitions, and the parameter η_{PV} describes the PV–mixing between the $^1S_0$ and $^3P_0$ states.

The asymmetry parameter ϵ is the physical observable in the proposed experiment. It can be determined by inducing the $1s^2\,2s\,2p\ ^3P_0 \rightarrow 1s^2\,2s\,2p\ ^3P_1$ transition separately with left– and right– circularly polarized light and by recording then the intensity difference of the x–rays from the decay of the $^3P_1$ state. Since these intensities are proportional to the photo–excitation cross sections (1), $I_\lambda(^3P_1 \rightarrow^1 S_0) \sim \sigma_\lambda$, we can find:

$$\epsilon = \frac{I_+ - I_-}{I_+ + I_-}\,. \qquad (3)$$

In order to provide an estimate of this asymmetry parameter, detailed calculations have been performed within the framework of the multi–configuration Dirac–Fock (MCDF) approach [4]. Based on these calculations, we argue that the most suitable candidate for the experimental realization of the proposed scheme is beryllium–like uranium U^{88+}. For this ion, the PV–mixing between the $1s^2\,2s\,2p\ ^3P_0$ and $1s^2\,2s^2\ ^1S_0$ states gives rise to $\eta_{PV} = -1.0 \times 10^{-8}$ and the asymmetry parameter $\epsilon = 3.1 \times 10^{-7}$.

References

[1] V. M. Shabaev *et al.*, Phys. Rev. A 81 (2010) 052102.
[2] A. Bondarevskaya *et al.*, Phys. Rep. 507 (2011) 1.
[3] M. Maul *et al.*, J. Phys. B: At. Mol. Phys. 31 (1998) 2725.
[4] A. Surzhykov *et al.*, Phys. Scr. (2013), accepted.

Minicharged Particles Search in a Dedicated Laboratory Experiment

B. Döbrich[1,2], *H. Gies*[1,2], *N. Neitz*[†2], *and F. Karbstein*[1,2]

[1]Helmholtz-Institut Jena; [2]Theoretisch-Physikalisches Institut, Friedrich-Schiller-Universität Jena

We propose a dedicated laboratory experiment of the light-shining-through-walls (LSW) type to search for a particular class of beyond-the-standard-model particles, namely Dirac fermionic minicharged particles (MCPs).

Dirac fermionic MCPs resemble electrons/positrons but differ in their charge and mass. While they are expected to carry only a tiny fraction ϵ of the electron charge e – and thus couple only very weakly to ordinary matter –, their mass m_ϵ is a priori unconstrained. Based on a recently proposed genuinely quantum field theoretic tunneling mechanism [1], depicted schematically in Fig. 1, we propose a LSW experiment particularly suited to search for MCPs with masses in and below the meV regime [2]. We have specified a realistic experimental setup and explicitly worked out the transition rates for state of the art experimental parameters [3]. To be specific we mainly use parameters of the ALPS experiment at DESY [4].

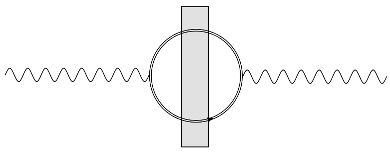

Figure 1: Tunneling of photons through an opaque barrier mediated by virtual minicharged particle–antiparticle fluctuations in a magnetic field.

As in ALPS-I, we consider light of a frequency doubled standard laser light source, $\lambda = 532\text{nm}$, which is fed into an optical resonator cavity of length $L = 8.6\text{m}$ to increase the light power available for MCP production. The resonator uses a plano-concave design with one plane mirror and a curved one with radius of curvature $R = 15\text{m}$. The incident laser light is coupled into the resonator via the curved mirror and is directed towards the plane mirror, mounted right in front of the barrier. In this way, a stable resonator mode is built up in between the two mirrors [5].

As a suitable magnet we have identified a presently unused ZEUS compensation solenoid [6] available at DESY. It features a bore of 0.28m diameter and 1.20m length and provides a field strength of $B = 5\text{T}$. The field points along the bore, and is assumed to be adequately aligned on the solenoid's axis. The field strength near the center of the solenoid is expected to be sufficiently homogeneous at least over a typical extent of the order of the bore's diameter. The wall with a width of $\mathcal{O}(\text{cm})$ is installed in the center of the bore and the back end of the cavity extends into the bore. The angle $\theta = \sphericalangle(\vec{k}, \vec{B})$ between the photon wave vector and the magnetic field is adjusted by tilting the entire optics assembly relative to the solenoid's axis. The length scale over which the field can be considered as approximately homogeneous should be comparable to or larger than the Compton wavelength of the MCP [2, 3]. Thus, with the ZEUS compensation solenoid, access to MCP masses down to $m_\epsilon \gtrsim 7\times10^{-7}\text{eV}$ – corresponding to a Compton wavelength of 0.28m – is granted.

The smallest resolvable MCP mass is also limited by the threshold for the production of real MCP pairs: $\omega \sin\theta = 2m_\epsilon$, with ω the frequency of the incident laser light (cf. Fig. 2). Through this relation the smallest resolvable MCP mass is directly constrained by the smallest experimentally realizable angle θ. Given a precise alignment of the magnetic field lines within a diameter of $\mathcal{O}(\text{mm})$ about the solenoid's axis, the uncertainty in the adjustment of θ is expected to be dominated by the maximum angular deviation from the optical axis in the resonator $\Delta\theta$. For $D = 0.6\text{m}$, i.e., half the length of the ZEUS compensation solid, we obtain $\Delta\theta \approx 0.0007°$. Given this small uncertainty in the alignment, angles down to $\theta = 0.001°$ should be experimentally feasible. Our results are depicted schematically in Fig. 2.

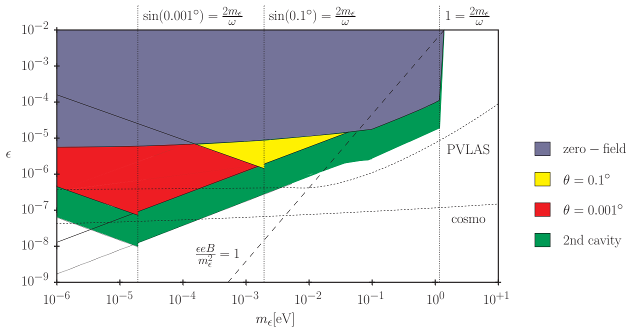

Figure 2: Cartoon of the accessible minicharged particle parameter space based on our LSW scenario. Our setup has the potential to exclude the colored parameter regimes.

References

[1] H. Gies and J. Jaeckel, JHEP **0908**, 063 (2009).

[2] B. Döbrich, H. Gies, N. Neitz and F. Karbstein, Phys. Rev. Lett. **109**, 131802 (2012).

[3] B. Döbrich, H. Gies, N. Neitz and F. Karbstein, Phys. Rev. D **87**, 025022 (2013).

[4] K. Ehret *et al.*, Phys. Lett. B **689**, 149 (2010).

[5] K. Ehret *et al.* [ALPS Collaboration], Nucl. Instrum. Meth. **A612**, 83-96 (2009).

[6] O. Dormicchi *et al.*, IEEE Trans. Magnetics **27**, 1958 (1991).

* Now at: DESY, Hamburg.

† Now at: MPI für Kernphysik, Heidelberg.

Renormalization Flow of Axion Electrodynamics

Astrid Eichhorn[2,3], *Holger Gies*[1,2], *and Dietrich Roscher*[2]

[1]Helmholtz Institut Jena, Fröbelstieg 1, D-07743 Jena, Germany; [2]Theoretisch-Physikalisches Institut, Friedrich-Schiller-Universität Jena, Max-Wien-Platz 1, D-07743 Jena, Germany; [3]Perimeter Institute for Theoretical Physics, 31 Caroline Street N, Waterloo, N2L 2Y5, Ontario, Canada

We discover a non-renormalization property of axion-electrodynamics, serving as an effective field theory for the interactions of light with fundamental pseudo-scalar particles, as tested in optical and strong-field experiments. As a consequence, renormalized couplings remain finite even in the deep infrared in the presence of massless photon fluctuations and even for massless axions. This result supports the foundations of optical searches for axion-like particles (ALP).

The existence of a fundamental pseudoscalar particle is strongly motivated by the Peccei-Quinn solution to the strong CP problem [1]. The resulting effective theory, axion electrodynamics, actually has a wide range of applications and forms the basis of optical and strong-field experiments actively searching for axion-like particles over a wide range of scales. As this theory involves massless or light degrees of freedom (photons and axions) with an interaction term $\mathcal{L}_{\rm int} \sim \bar{g} a F_{\mu\nu} \widetilde{F}^{\mu\nu}$, fluctuations could in principle lead to strong renormalization effects for the axion mass $\bar{m}$ or the coupling $\bar{g}$ in the long-range limit, possibly affecting the interpretation of current experiments.

In [2], we have performed a first non-perturbative study of the renormalization flow of axion electrodynamics using the functional renormalization group (RG). We discovered a non-renormalization property of the bare quantities $\partial_t \bar{m}^2 = 0$, $\partial_t \bar{g} = 0$, where t denotes a logarithmic RG scale, implying that the only renormalization effects can arise from the wave function renormalizations of the axion and the photon field. As an example, let us mention the running of the (dimensionful) renormalized coupling in the large mass and small coupling regime,

$$g_{\rm R}^2(k) = \frac{g_{\rm R}^2(\Lambda)}{1 + \frac{1}{6(4\pi)^2}(\Lambda^2 - k^2) g_{\rm R}^2(\Lambda)}, \qquad (1)$$

where $g_{\rm R}^2(\Lambda)$ denotes the initial coupling value at the UV cutoff. We observe that the photon-axion coupling undergoes a finite renormalization even in the deep infrared (IR) limit, despite the fact that massless photonic fluctuations never strictly decouple. The photons still *effectively* decouple, as their low-momentum contributions to the flow vanish according to the powerlaw $\sim k^2 g_{\rm R}^2(\Lambda)$ for $k \to 0$. A similar conclusion holds for the axion mass. Axion electrodynamics therefore exhibits a remarkable IR stability. Quantitatively, both the coupling as well as the axion mass run to slightly smaller values towards the infrared in the present limit.

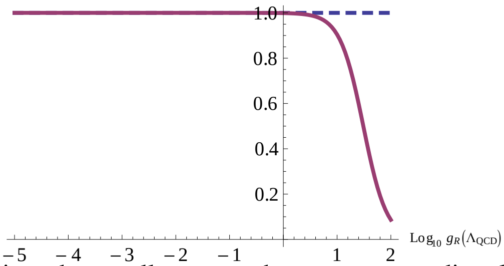

While the effective theory parameters are typically considered in terms of the microscopic couplings at the scale Λ, optical experiments or astrophysical/cosmological observations do actually not test these parameters directly, but typically at much lower scales $k_{\rm obs}$, ranging down to to $\sim \mu$eV scales in light-shining-through walls experiments. In the figure, the renormalized ratio $g_{\rm R}(k_{\rm obs})/m_{\rm R}(k_{\rm obs})$ (blue/dashed line) as well as the ratio of the product $g_{\rm R}(k_{\rm obs}) m_{\rm R}(k_{\rm obs})$ (purple/solid line) are shown, both curves are normalized to the corresponding initial condition at Λ taken as the QCD scale $\Lambda_{\rm QCD}$ for the QCD axion. For small couplings, the renormalization of both coupling and mass remain unobservably small implying that both ratios are close to unity. Only for larger couplings, the renormalization of both towards smaller values becomes visible, implying a significant decrease of the product. Most importantly, the proportionality between mass and coupling remains essentially unaffected. Numerically, the ratio of the parameters changes only on the 10^{-5} level.

We conclude that exclusion bounds derived from the non-observation of axion effects are not modified by renormalization effects of axion electrodynamics along the lines of constant $g_{\rm R}/m_{\rm R}$. As the physically relevant parameter space for the QCD axion lies below $g_{\rm R} \lesssim 10^{-9}({\rm GeV})^{-1}$, we conclude from the figure that the renormalization effects within the effective theory of axion electrodynamics do not affect optical and strong-field experiments. For more general axion-like particles, our results imply a generic upper bound on possible values of the axion-photon coupling. Our RG study [2] demonstrates that couplings are in fact bounded by $g_{\rm R} \lesssim \mathcal{O}(10)/\Lambda$ due to renormalization effects in the axion-photon sector. In view of the rather unconstrained ALP parameter space at large masses and comparatively large couplings (see, e.g., the compilation in [3]), our bound could become of relevance for ALP searches at hadron colliders above $m_{\rm R} \gtrsim 1$GeV and couplings above $g_{\rm R} \gtrsim 10^{-3}/({\rm GeV})^{-1}$.

References

[1] R. D. Peccei and H. R. Quinn, Phys. Rev. Lett. **38**, 1440 (1977).

[2] A. Eichhorn, H. Gies and D. Roscher, Phys. Rev. D **86**, 125014 (2012) [arXiv:1208.0014 [hep-ph]].

[3] J. L. Hewett, *et al.*, arXiv:1205.2671 [hep-ex].

Thermally-induced vacuum instability in a single plane wave

Ben King[3,4], *Holger Gies*[1,2], *and Antonino Di Piazza*[3]

[1]Helmholtz Institut Jena, Fröbelstieg 1, D-07743 Jena, Germany; [2]Theoretisch-Physikalisches Institut, FSU Jena, Max-Wien-Platz 1, D-07743 Jena, Germany; [3]Max-Planck-Institut für Kernphysik, Saupfercheckweg 1, D-69117 Heidelberg, Germany ; [4]Ludwig-Maximilians-Universität, Theresienstraße 37, 80333 München, Germany

A unanimously accepted statement in QED is that the vacuum is stable in the presence of an electromagnetic plane wave. However, we show that this statement is not rigorously valid in a real situation, where thermal effects are present. We show that the thermal vacuum, in the presence of a single plane-wave field, even in the limit of zero frequency, decays into electron-positron pairs. Interestingly, the pair-production rate is found to depend nonperturbatively on both the amplitude of the constant crossed field and on the temperature.

An inevitable consequence of Dirac's theory of the electron is that in regions of sufficiently high energy density, the quantum vacuum can break down in a spontaneous generation of electron-positron pairs. In a seminal work, Schwinger [1] derived a central result of strong-field quantum electrodynamics: the rate of pair creation in a constant and uniform electric field of strength E. To leading order, the rate exhibits a nonperturbative exponential dependence, $\sim \exp(-\pi E_{\mathrm{cr}}/E)$, for field strengths smaller than the "critical" electric field $E_{\mathrm{cr}} = m^2c^3/e\hbar = 1.3 \times 10^{16}$ Vcm^{-1}. However, it has long been accepted that pair creation can never occur in single plane waves, as encapsulated in Schwinger's famous statement "there are no nonlinear vacuum phenomena for a single plane wave, of arbitrary strength and spectral composition" [1]. The physical reason for this is that all photons in a plane wave propagate in the same direction and so cannot interact with each other.

In [2], we have demonstrated how the inevitable presence of background heat radiation in all real scenarios can serve as a seed for pair creation in a plane wave. This is the case even if the frequency of the plane wave tends to zero (the so-called constant crossed field configuration).

By considering the existence of a thermal background, we have derived an expression for the rate of real pair creation with two different methods: first, by averaging the polarization tensor in a crossed field over a thermal photon ensemble, and second, by extracting the imaginary part of the 2-loop effective action in a crossed field at finite temperature. The result is nonperturbative in both the field strength E and the background temperature T, in both prefactor and exponent,

$$\rho_{\mathrm{th}}(T,E) \simeq \frac{3^{3/4}\alpha}{4\pi^{3/2}}\, m^4 \left(\frac{T}{m}\right)^2 \delta^{1/4} \mathrm{e}^{-\frac{4}{\sqrt{3\delta}}}, \quad \delta = \frac{T}{m}\frac{E}{E_{\mathrm{cr}}},$$

in the limit $\sqrt{\delta} \ll 1$. Apart from the conceptual advance, our result can be of relevance to the description of relativistic plasmas, heavy-ion collisions and for a full understanding of the pair-production processes near neutron stars.

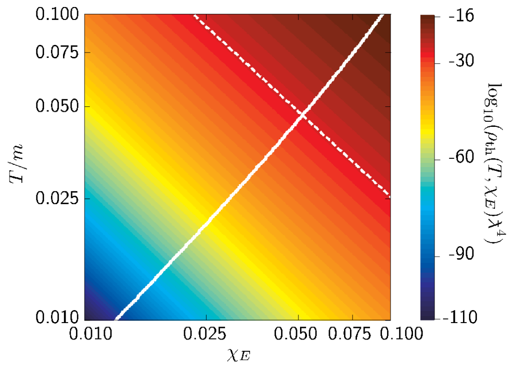

Figure 1: Logarithm of the expected number of pairs generated in a constant crossed field $\chi_E = E/E_{\mathrm{cr}}$ for the parameters specified in the text.

In Fig. 1, the log of the rate $\rho_{\mathrm{th}}(T,E)$ times the four-dimensional volume $\lambda^4 = 1/m^4 = 7.4 \times 10^{-53}$ cm^3 s. In the region above the dashed line, the number of pairs created in a typical optical strong laser beam four-volume $\Omega_l = \tau_l V_l$, where $\tau_l = 10$ fs, $V_l = \pi \times (0.8\,\mu\mathrm{m})^2 \times c\tau_l = 6 \times 10^{-12}$ cm^3 (where we temporarily recover the speed of light, c), is larger than one. Upon inspection of Fig. 1, we notice that for high enough temperatures, even with $E = 0.025$, an exponential number of pairs can be produced in a typical optical laser pulse. This should be compared to the case of zero temperature, for which the expected number of pairs is identically zero. The solid line shows the significance of the background process of pure thermal pair creation, which dominates for large T/m and small E/E_{cr}. Our results also confirm the tendency observed for Schwinger pair production that the thermal contribution exceeds the zero temperature contribution in the limit of weak fields. Here, this is particularly evident, as the production rate at zero temperature in crossed fields is exactly zero.

We have shown how a thermal background can seed the creation of particles in a constant crossed field. This conclusion also applies to single plane waves in the tunneling regime. The probability for this new process is distinct from other analytical results for pair creation by external fields. The unavoidable presence of thermal photons in all physically realistic scenarios will trigger electron-positron pair production even in a single plane wave.

References

[1] J. Schwinger, Phys. Rev. **82**, 664 (1951).

[2] B. King, H. Gies and A. Di Piazza, Phys. Rev. D **86**, 125007 (2012); 069905(E) (2013) [arXiv:1204.2442 [hep-ph]].

Publications 2012

B. Aurand, C. Rödel, H. Zhao, S. Kuschel, M. Wünsche, O. Jäckel, M. Heyer, F. Wunderlich, M. C. Kaluza, G. G. Paulus and T. Kühl
A large aperture four-mirror reflective wave-plate for high-intensity short-pulse laser experiments
Rev. Sci. Instrum. **83**, 036104 (2012).

M. Baumgartl, M. Chemnitz, C. Jauregui, T. Meyer, B. Dietzek, J. Popp, J. Limpert and A. Tünnermann
All-fiber laser source for CARS microscopy based on fiber optical parametric frequency conversion
Optical Express **20**, 4484 (2012).

M. Baumgartl, C. Lecaplain, A. Hideur, J. Limpert and A. Tünnermann
66 W average power from a microjoule-class sub-100 fs fiber oscillator
Optics Letters **37**, 1640 (2012).

M. Baumgartl, B. Ortac, J. Limpert and A. Tünnermann
Impact of dispersion on pulse dynamics in chirped-pulse fiber lasers
Applied Phys. B **107**, 263 (2012).

J. Bierbach, C. Rödel, M. Yeung, B. Dromey, T. Hahn, A. Galestian Pour, S. Fuchs, A. E. Paz, S. Herzer, S. Kuschel, O. Jäckel, M. C. Kaluza, G. Pretzler, M. Zepf and G. G. Paulus
Generation of 10 μW relativistic surface high-harmonic radiation at a repetition rate of 10 Hz
New J. Phys. **14**, 065005 (2012).

S. Breitkopf, A. Klenke, T. Gottschall, H.-J. Otto, C. Jauregui, J. Limpert and A. Tünnermann
58 mJ burst comprising ultrashort pulses with homogenous energy level from an Yb-doped fiber amplifier
Optics Letters **37**, 5169 (2012).

R. A. Costa Fraga, A. Kalinin, M. Kühnel, D. C. Hochhaus, A. Schottelius, J. Polz, M. C. Kaluza, P. Neumayer and R. E. Grisenti
Compact cryogenic source of periodic hydrogen and argon droplet beams for relativistic laser-plasma generation
Rev. Sci. Instrum. **83**, 025102 (2012).

S. Demmler, J. Rothhardt, S. Hädrich, J. Bromage, J. Limpert and A. Tünnermann
Control of nonlinear spectral phase induced by ultra-broadband optical parametric amplification
Optics Letters **37**, 3933 (2012).

B. Dobrich and A. Eichhorn
Can we see quantum gravity? Photons in the asymptotic-safety scenario
J. High Energy Phys. **1206**, 156 (2012).

B. Dobrich, H. Gies, N. Neitz and F. Karbstein
Magnetically amplified tunneling of the 3rd kind as a probe of minicharged particles
Phys. Rev. Lett. **109**, 131802 (2012).

B. Dromey, S. Rykovanov, M. Yeung, R. HØrlein, D. Jung, D. C. Gautier, T. Dzelzainis, D. Kiefer, S. Palaniyppan, R. Shah, J. Schreiber, H. Ruhl, J. C. Fernandez, C. L. S. Lewis, M. Zepf and B. M. Hegelich
Coherent synchrotron emission from electron nanobunches formed in relativistic laser-plasma interactions
Nature Phys. **8**, 804 (2012).

A. Eichhorn, H. Gies and D. Roscher
Renormalization flow of axion electrodynamics
Phys. Rev. D **86**, 125014 (2012).

S. Eyring, C. Kern, M. Zuerch and C. Spielmann
Improving high-order harmonic yield using wavefront-controlled ultrashort laser pulses
Optics Express **20**, 5601 (2012).

S. Fritzsche, A. Surzhykov, A. Gumberidze and T. Stöhlker
Electron emission from highly charged ions: Signatures of magnetic interactions and retardation in strong fields
New J. Phys. **14**, 083018 (2012).

S. Fuchs, A. Blinne, C. Rödel, U. Zastrau, V. Hilbert, M. Wünsche, J. Bierbach, E. Frumker, E. Förster and G. G. Paulus
Optical coherence tomography using broad-bandwidth XUV and soft x-ray radiation
Applied Phys. B **106**, 789 (2012).

A. Gopal, T. May, S. Herzer, A. Reinhard, S. Minardi, M. Schubert, U. Dillner, B. Pradarutti, J. Polz, T. Gaumnitz, M. Kaluza, O. Jäckel, S. Riehemann, W. Ziegler, H.-P. Gemuend, H.-G. Meyer and G. G. Paulus
High energy T-ray pulses from table-top laser driven ion accelerators
New J. Phys. **14**, 083012 (2012).

T. Gottschall, M. Baumgartl, A. Sagnier, J. Rothhardt, C. Jauregui, J. Limpert and A. Tünnermann,
Fiber-based source for multiplex-CARS microscopy based on degenerate four-wave mixing
Optics Express **20**, 12004 (2012).

S. Hädrich, J. Rothhardt, M. Krebs, S. Demmler, J. Limpert and A. Tünnermann
Improving carrier-envelope phase stability in optical parametric chirped-pulse amplifiers by control of timing jitter
Optics Letters **37**, 4910 (2012).

M. Harmand, C. D. Murphy, C. R. D. Brown, M. Cammarata, T. Doeppner, S. Duesterer, D. Fritz, E. Förster, E. Galtier, J. Gaudin, S. H. Glenzer, S. Gode, G. Gregori, V. Hilbert, D. Hochhaus, T. Laarmann, H. J. Lee, H. Lemke, K.-H. Meiwes-Broer, A. Moinard, P. Neumayer, A. Przystawik, H. Redlin, M. Schulz, S. Skruszewicz, F. Tavella,T. Tschentscher, T. White, U. Zastrau and S. Toleikis
Plasma switch as a temporal overlap tool for pump-probe experiments at FEL facilities
J. Instrum. **7**, P08007 (2012).

K. Jansen *et al.* [ETM Collaboration]
$\Lambda_{\bar{M}S}$ from the static potential for QCD with $n_f = 2$ dynamical quark flavors
J. High Energy Phys. **1201**, 25 (2012).

F. Jansen, F. Stutzki, C. Jauregui, J. Limpert and A. Tünnermann
High-power very large mode-area thulium-doped fiber laser
Optics Letters **37**, 4546 (2012).

F. Jansen, F. Stutzki, H.-J. Otto, T. Eidam, A. Liem, C. Jauregui, J. Limpert and A. Tünnermann
Thermally induced waveguide changes in active fibers
Optics Express **20**, 3997 (2012).

C. Jauregui, T. Eidam, H.-J. Otto, F. Stutzki, F. Jansen, J. Limpert and A. Tünnermann
Temperature-induced index gratings and their impact on mode instabilities in high-power fiber laser systems
Optics Express **20**, 440 (2012).

C. Jauregui, T. Eidam, H.-J. Otto, F. Stutzki, F. Jansen, J. Limpert and A. Tünnermann
Physical origin of mode instabilities in high-power fiber laser systems
Optics Express **20**, 12912 (2012).

C. Jauregui, A. Steinmetz, J. Limpert, and A. Tünnermann
High-power efficient generation of visible and mid-infrared radiation exploiting four-wave-mixing in optical fibers
Optics Express **20**, 24957 (2012).

C. Jocher, T. Eidam, S. Hädrich, J. Limpert and A. Tünnermann
Sub 25 fs pulses from solid-core nonlinear compression stage at 250 W of average power
Optics Letters **37**, 4407 (2012).

S. Kar, K. F. Kakolee, B. Qiao, A. Macchi, M. Cerchez, D. Doria, M. Geissler, P. McKenna, D. Neely, J. Osterholz, R. Prasad, K. Quinn, B. Ramakrishna, G. Sarri, O. Willi, X. Y. Yuan, M. Zepf and M. Borghesi
Ion acceleration in multispecies targets driven by intense laser radiation pressure
Phys. Rev. Lett. **109**, 185006 (2012).

S. Keppler, M. Hornung, R. Bödefeld, M. Kahle, J. Hein and M. C. Kaluza
All-reflective, highly accurate polarization rotator for high-power short-pulse laser systems
Optics Express **20**, 20742 (2012).

T. Kiefer and T. Schlegel
Implications for the electron distribution from the stationary hydrodynamic model of a one-dimensional plasma expansion into vacuum
Phys. Plasmas **19**, 102101 (2012).

B. King, H. Gies and A. Di Piazza
Thermally-induced vacuum instability in a single plane wave
Phys. Rev. D **86**, 125007 (2012).

J. Körner, C. Vorholt, H. Liebetrau, M. Kahle, D. Klöpfel, R. Seifert, J. Hein and M. C. Kaluza
Measurement of temperature-dependent absorption and emission spectra of Yb:YAG, Yb:LuAG and Yb:CaF_2 between 20^o C and 200^o C and their effect on laser performance
J. Optical Soc. B **29**, 2493 (2012).

J. Limpert, F. Stutzki, F. Jansen, H.-J. Otto, T. Eidam, C. Jauregui and A. Tünnermann
Yb-doped large-pitch fibres: effective single-mode operation based on higher-order mode delocalisation
Light: Science & Applications **1**, e8 (2012).

R. Lötzsch, I Uschmann and E. Förster
Spatially resolved twin domain distribution and lattice parameter variations in the near-surface region of $SrTiO_3$ single crystals
Applied Phys. A **106**, 563 (2012).

R. Lötzsch, O. Jäckel, S. Höfer, T. Kämpfer, J. Polz, I. Uschmann, M. C. Kaluza, E. Förster, E. Stambulchik, E. Kroupp, and Y. Maron
K-shell spectroscopy of silicon ions in high electric fields
Rev. Sci. Instrum. **83**, 113507 (2012).

A. V. Maiorova, A. Surzhykov, S. Tashenov, V. M. Shabaev and T. Stöhlker
Production and diagnostics of spin-polarized heavy ions in sequential two-electron radiative recombination
Phys. Rev. A **86**, 032701 (2012).

R. Märtin, G. Weber, R. Barday, Y. Fritzsche, U. Spillmann, W. Chen, R. D. DuBois, J. Enders, M. Hegewald, S. Hess, A. Surzhykov, D. B. Thorn, S. Trotsenko, M. Wagner, D. F. A. Winters, V. A. Yerokhin and T. Stöhlker
Polarization transfer of bremsstrahlung arising from spin-polarized electrons
Phys. Rev. Lett. **108**, 264801 (2012).

P. Neumayer, B. Aurand, R. A. Costa Fraga, B. Ecker, R. E. Grisenti, A. Gumberidze, D. C. Hochhaus, A. Kalinin, M. C. Kaluza, T. Kühl, J. Polz, R. Reuschl, T. Stöhlker, D. Winters, N. Winters, Z. Yin
Evidence for ultra-fast heating in intense-laser irradiated reduced-mass targets
Phys. Plasmas **19**, 122708 (2012).

A. Paz, S. Kuschel, C. Rödel, M. Schnell, O. Jäckel, M. C. Kaluza and G. G. Paulus
Thomson backscattering from laser-generated, relativistically moving high-density electron layers
New J. Phys. **14**, 093018 (2012).

G. R. Plateau, C. G. R. Geddes, D. B. Thorn, M. Chen, C. Benedetti, E. Esarey, A. J. Gonsalves, N. H. Matlis, K. Nakamura, C. B. Schroeder, S. Shiraishi, T. Sokollik, J. van Tilborg, C. Toth, S. Trotsenko, T. S. Kim, M. Battaglia, T. Stöhlker and W. P. Leemans
Low-emittance electron bunches from a laser-plasma accelerator measured using single-shot x-ray spectroscopy
Phys. Rev. Lett. **109**, 064802 (2012).

A. Przystawik, A. Kickermann, A. Al-Shemmary, S. Duesterer, A. M. Ellis, K. von Haeften, M. Harmand, S. Ramakrishna, H. Redlin, L. Schroedter, M. Schulz, T. Seideman, N. Stojanovic, J. Szekely, F. Tavella, S. Toleikis and T. Laarmann
Generation of the simplest rotational wave packet in a diatomic molecule: Tracing a two-level superposition in the time domain
Phys. Rev. **85**, 052503 (2012).

C. Rödel, D. an der Brügge, J. Bierbach, M. Yeung, T. Hahn, B. Dromey, S. Herzer, S. Fuchs, A. Galestian Pour, E. Eckner, M. Behmke, M. Cerchez, O. Jäckel, D. Hemmers, T. Toncian, M.C. Kaluza, A. Belyanin, G. Pretzler, O. Willi, A. Pukhov, M. Zepf and G. G. Paulus
Harmonic generation from relativistic plasma surfaces in ultrasteep plasma density gradients
Phys. Rev. Lett. **109**, 125002 (2012).

J. Rothhardt, S. Demmler, S. Hädrich, J. Limpert and A. Tünnermann
Octave-spanning OPCPA system delivering CEP-stable few-cycle pulses and 22 W of average power at 1 MHz repetition rate
Optics Express **20**, 10870 (2012).

J. Rothhardt, A. M. Heidt, S. Hädrich, S. Demmler, J. Limpert and A. Tünnermann
High stability soliton frequency-shifting mechanisms for laser synchronization applications
J. Opt. Soc. Am. B **29**, 1257 (2012).

T. Schlegel and V. T. Tikhochuk
Classical radiation effects on relativistic electrons in ultraintense laser fields with circular polarization
New J. Phys. **14**, 073034 (2012).

M. Schnell, A. Sävert, B. Landgraf, M. Reuter, M. Nicolai, O. Jäckel, C. Peth, T. Thiele, O. Jansen, A. Pukhov, O. Willi, M. C. Kaluza and C. Spielmann
Deducing the electron-beam diameter in a laser-plasma accelerator using x-ray betatron radiation
Phys. Rev. Lett. **108**, 075001 (2012).

M. Schulz, R. Riedel, A. Willner, S. Duesterer, M. J. Prandolini, J. Feldhaus, B. Faatz, J. Rossbach, M. Drescher and F. Tavella,
Pulsed operation of a high average power Yb:YAG thin-disk multipass amplifier
Optics Express **20**, 5038 (2012).

J. Seres, E. Seres and C. Spielmann
Classical model of strong-field parametric amplification of soft x rays
Phys. Rev. A **86**, 013822 (2012).

E. Seres, J. Seres and C. Spielmann
Extreme ultraviolet light source based on intracavity high harmonic generation in a mode locked Ti:sapphire oscillator with 9.4 MHz repetition rate
Optics Express **20**, 6185 (2012).

E. Siminos, M. Grech, S. Skupin, T. Schlegel and V. T. Tikhonchuk
Effect of electron heating on self-induced transparency in relativistic-intensity laser-plasma interactions
Phys. Rev. E **86**, 056404 (2012).

F. Stutzki, F. Jansen, A. Liem, C. Jauregui, J. Limpert and A. Tünnermann
26 mJ, 130 W Q-switched fiber-laser system with near-diffraction-limited beam quality
Optics Letters **37**, 1073 (2012).

N. A. Tahir, V. Kim, E. Lamour, I. V. Lomonosov, A. R. Piriz, J. P. Rozet, T. Stöhlker, V. Sultanov and D. Vernhet
Two-dimensional thermal simulations of an aluminum beam stripper for experiments at SPIRAL-2
Nucl. Instrum. Meth. B **276**, 66 (2012).

I. I. Tupitsyn, Y. S. Kozhedub, V. M. Shabaev, A. I. Bondarev, G. B. Deyneka, I. A. Maltsev, S. Hagmann, G. Plunien, and T. Stöhlker
Relativistic calculations of the K-K charge transfer and K-vacancy production probabilities in low-energy ion-atom collisions
Phys. Rev. A **85**, 032712 (2012).

M. Vogel, W. Quint, G. G. Paulus and T. Stöhlker
A Penning trap for advanced studies with particles in extreme laser fields
Nucl. Instrum. Meth. B **285**, 65 (2012).

G. Vorobjev, A. Sokolov, A. Thorn, F. Herfurth, O. Kester, W. Quint, T. Stöhlker and G. Zschornack
Demonstration of charge breeding in a compact room temperature electron beam ion trap
Rev. Sci. Instrum. **83**, 11 (2012).

G. Weber, R. Märtin, A. Surzhykov, M. Yasuda, V. A. Yerokhin and T. Stöhlker
PEBSI - A Monte Carlo simulator for bremsstrahlung arising from electrons colliding with thin solid-state targets
Nucl. Instrum. Meth. B **279**, 155 (2012).

A. Willner, S. Hage, R. Riedel, I. Grguras, A. Simoncig, M. Schulz, T. Dzelzainis, H. Hoeppner, S. Huber, M. J. Prandolini, B. Dromey, M. Zepf, A. L. Cavalieri and F. Tavella
Coherent spectral enhancement of carrier-envelope-phase stable continua with dual-gas high harmonic generation
Optics Letters **37**, 3672 (2012).

M. Zuerch, C. Kern, P. Hansinger, A. Dreischuh and C. Spielmann
Strong-field physics with singular light beams
Nature Phys. **8**, 743 (2012).